RELAXATION STUDIES IN Nd^{3+} AND Dy^{3+} DOPED SINGLE CRYSTALS USING NITROGEN LASER

By

HARATI JAGANNATH

DEPARTMENT OF PHYSICS

INDIAN INSTITUTE OF TECHNOLOGY KANPUR

JANUARY, 1977

RELAXATION STUDIES IN Nd^{3+} AND Dy^{3+} DOPED SINGLE CRYSTALS USING NITROGEN LASER

A Thesis Submitted
In Partial Fulfilment of the Requirements
for the Degree of

DOCTOR OF PHILOSOPHY

By

HARATI JAGANNATH

to the

DEPARTMENT OF PHYSICS

INDIAN INSTITUTE OF TECHNOLOGY KANPUR

JANUARY, 1977

Certificate

This is to certify that the work presented in this thesis is the original work of Mr. H. Jagannath done under our joint supervision, and it is not submitted elsewhere for a degree.

D. Ramachandra Rao
Professor of Physics
I.I.T., Kanpur

Putcha Venkateswarlu
Professor of Physics
I.I.T., Kanpur

ACKNOWLEDGEMENTS

I am most indebted to Professor P. Venkateswarlu and Professor D. Ramachandra Rao for their guidance and constant encouragement. The interest they have shown in my work is gratefully acknowledged.

The Lanthanum fluoride crystals used in this work were loaned to us by Professor H.P. Broida, University of California, Santa Barbara. I am very thankful to him.

The calcium fluoride crystals were grown at Bhabha Atomic Research Centre, Bombay with the help of my colleague Mr. A. Sivaram. We are extremely thankful to Dr. S. Muralidhara Rao, Health Physics Division for his help in growing the crystals in their vacuum furnace. We are also thankful to Dr. S.D. Soman, Head, Health Physics Division and Dr. A.K. Ganguly, Director, Chemistry Division for their interest in our work.

It is a great pleasure to acknowledge the cooperation and assistance extended by my colleagues Dr. U.V. Kumar, Mr. A. Sivaram, Mr. D. Narayana Rao, Mr. Bansilal and Dr. D. Madhavan. I am very thankful to Dr. G. Chakrapani who has helped me in the fabrication of the nitrogen laser.

I am extremely thankful to Mr. D.S. Rawat, Mr. G. Satyanarayana, Mr. V.V.N. Murthy and Mr. N.V.G. Swamy for their help in the laboratory and to Mr. Kuldip Singh Ubhey, Mr. Bahadur Singh and Mr. J.P. Srivastava for their help in machining the different components of nitrogen laser. Thanks are also due to the staff of the Glass-blowing shop - specially to Mr. C.M. Sharma and Mr. J.N. Sharma, the Central Precision workshop and the Physics Electronics shop for the cooperation shown by them.

I am very thankful to Mrs. B. Rukmini Devi for her neat and patient typing. Thanks are also due to Mr. H.K. Panda for the cyclostyling of the stencils.

The financial assistance from the Council of Scientific and Industrial Research, India and the National Bureau of Standards, U.S.A, is gratefully acknowledged.

HARATI JAGANNATH

CONTENTS

LIST OF FIGURES

TABLES

SYNOPSIS

The study of the optical properties of impurity ions in crystalline solids has been a subject of wide interest for many decades. The quenching and sensitisation of fluorescence in inorganic solids are known for a long time. The interest in these studies has been renewed with the discovery of lasing action in impurity ions embedded in solids. The possibility of obtaining high power lasers and new materials for lasers has necessitated a detailed study of the excitation and deexcitation mechanisms of the impurity ions. More elegant and simpler experimental techniques are now possible for the study of relaxation processes with the availability of pulsed lasers. The rare earth ions when embedded in solids, are known to be good laser hosts. The thesis represents an attempt to study the relaxation mechanisms of the excited rare earth ions in LaF_3 crystals. A pulsed nitrogen laser has been fabricated in the laboratory for the excitation of the ions. The observed decay rates of the excited stark multiplets are explained in terms of the different relaxation mechanisms - radiative and nonradiative - that are operative.

The first chapter of the thesis deals with the general introduction to the subject of relaxation processes. The relaxation processes can be divided broadly into two categories, radiative and nonradiative. The electric and magnetic multipole transitions between the levels of the ion contribute to the radiative relaxation. The nonradiative transitions are due to the energy transfer between the impurity ions and/or the lattice through inter ion or ion lattice interaction. The different relaxation processes that are operative in the relaxation of the excited rare earth ions are discussed.

The various theoretical models proposed to explain the different relaxation processes are presented in Chapter 2. A brief outline of the theoretical calculations of the relaxation rates, based on these models, is given. The Judd-Ofelt's theory for calculation of radiative transition probabilities is discussed. The Kiel's and Feng's models for the treatment of ion lattice interaction which lead to multi-phonon transitions are given. The discussion is limited to the treatment of ion pair transitions in the case of ion-ion interaction relaxation.

Chapter 3 deals with the theory and details of the fabrication of the pulsed nitrogen laser and the experimental set up for the decay time measurements. The laser output has a pulse width of 7.5 nsec. The output power has not been measured but is sufficient to pump organic dyes to superradiance. The theory, the design criteria and the fabrication details of the laser are presented. This laser has been used for the excitation of fluorescence of the rare earth ions in LaF_3. The fluorescence output is collected in a direction perpendicular to the direction of the incident beam and is passed through a 0.25 m Jarrell Ash monochromator before detection with a photomultiplier tube. The output of the detector is displayed on an oscilloscope for measurement. With this set up, decay times as low as 10 nsec have been measured.

The decay times of fluorescence of $LaF_3:Nd^{3+}$ (2% by wt); $LaF_3:Dy^{3+}$ (1% by wt) and of Nd^{3+} in the system $LaF_3:Dy^{3+}$ in which it occurs as an additional impurity in small proportion ($\sim$ 0.02% by wt) have been measured at six different temperatures between liquid nitrogen temperature and room temperature. The levels studied are L, K and R of Nd^{3+} and level $^4F_{9/2}$ of Dy^{3+}. The results are presented in Chapter 4 and are discussed in Chapter 5.

The rate of decay of the fluorescence of the level L of Nd^{3+} is dependent on the temperature and the concentration. The decay function is a single exponential at low concentration ($\sim$0.02% of Nd^{3+} by wt) and is nonexponential in the 2% LaF_3:Nd^{3+} system. This suggests the possibility of the relaxation being predominantly due to radiative and multiphonon transitions at low concentration while the ion pair transitions contributing significantly at higher concentrations. The other two levels K and R also relax by all the three processes though the rate of multiphonon transitions from level R is negligible in comparison to the total decay rate.

The radiative decay rates are now calculated for all the three levels using Judd-Ofelt's theory. The estimated rates of multiphonon transitions are obtained from emperical relation between the transition rate and the energy gap established for LaF_3 by Riseberg and Moos. The total calculated decay rate (multiphonon transition rate + radiative transition rate) for the levels L and R are in agreement with the reported/observed values. The decay rates for the K level have not been reported/measured for the low concentration of the impurity ion. The temperature dependence of the decay rate of level L has been explained in terms of the multiphonon emission. Unlike in other systems, the contribution to the relaxation due to the low energy phonons appears to be significant.

The ion-ion interaction contributes significantly to the relaxation of all the three levels, L, K and R in LaF_3:Nd^{3+}. The ion pair transitions from level L occur mostly through dipole-dipole interaction. The nature of the interaction has not been determined for the transitions from the other levels K and R. The rate of diffusion of the excitation energy of the level R has

been reported to be very large resulting in the averaging of different ion pair interactions and the decay is a single exponential. An indirect evidence of the ion pair transitions from the level L has been obtained by the study of the decay functions of the levels K and R. Information about the pumping mechanism of these levels and also of the relaxation mechanism of the upper levels is provided by these studies.

Decay times of level $^4F_{9/2}$ of Dy^{3+} have been measured at different temperatures. The rates of decay have not varied much with temperature. The level relaxes by radiative and ion pair transitions. The fluorescence mechanism of the level is not well understood.

The work on the fluorescence spectrum of $CaF_2:Dy^{3+}$ at liquid nitrogen temperature is presented in Chapter 6. The nitrogen laser excited fluorescence has been observed in $CaF_2:Dy^{3+}$ in the region 4700Å-9000Å. The observed spectrum is mostly due to tetragonal sites and coincides with the spectrum observed earlier in the region 4700Å-6000Å. The spectrum is analyzed in terms of the energy level diagram proposed by Luks et.al. Tentative assignment of the Stark multiplets has been made for the levels $^6H_{11/2}$,($^6H_{9/2}$, $^6F_{11/2}$),and ($^6H_{7/2}$, $^6F_{9/2}$).

In conclusion, the results of the studies on the different mechanisms, by which the excited rare earth ions Nd^{3+} and Dy^{3+} relax in the lattice LaF_3, have been presented in the thesis. The radiative transition rates required for the interpretation of the results, have been calculated using Judd-Ofelt's theory. The pulsed nitrogen laser with its short pulse width, has been found to be very useful in these studies. A complete understanding of the nature of the relaxation processes is possible by the measurement of the rates of decay of fluorescence with different concentrations of impurity ion ranging from 0.01% to 20% and over a wider range of temperatures from liquid helium temperature to

CHAPTER I

INTRODUCTION

1.1 General

The study of the properties of impurity ions in crystalline solids has been a subject of wide interest for many decades. Numerous investigations have been carried out on the optical properties of solids - infrared absorption optical absorption and luminescence. Information about the crystal symmetry, the lattice phonons, the impurity ion energy levels and their lifetimes are obtained from these. The interest in these studies has been renewed with the discovery of lasing action in impurity ions embedded in solids. The possibilit of obtaining high power lasers and new materials for lasers has necessitated a complete understanding of the excitation and de-excitation mechanisms of the impurity ions. The availability of pulsed lasers has facilitated the study of a wide range of de-excitation mechanisms, the rate of relaxation being any where between $\sim$0 to 10^9 sec^{-1}. The thesis represents an effort in building a pulsed Nitrogen laser and using it for the study of the energy transfer processes of ions in solids.

The energy levels of an ion in the crystalline lattice are not the same as in the 'free' state. The ion, which enters the lattice substitutionally or interstitially is subjected to electric and/or magnetic fields due to the host ions. The spherical symmetry of the 'free ion' is reduced to the symmetry of the site in the lattice. If the oxidation state of the ion is more than the oxidation state of the site in which it enters, ions of opposite charge are required to compensate for the excess charge. This results in a local symmetry which is different from the symmetry of the site. The 'free ion' levels thus split, the amount of splitting being dependent on the strength of the crystal field interaction and the number of the components depend on the symmetry of the site. In addition, the ions are coupled to the lattice through lattice phonons. This enables the lattice and the ion to exchange energy by exchanging lattice phonons. Specifically, an excited ion relaxes to a lower level by radiative and/or nonradiative transitions. Of the nonradiative relaxation processes the multiphonon relaxation and the phonon - assisted ion pair relaxation are due to the energy exchange between the lattice and the ion[18]. A study of the relaxation rate of an excited ion reveals the nature of different relaxation processes.

In the present thesis an attempt is made to study the relaxation process of some of the rare earth ions in LaF_3 host lattice. The rare earth ions in crystalline lattice are known to be laser materials. Much of the current interest in these ions is for this reason. The free ion levels of the Re^{3+}(Re-rare earth) are well known and extensively studied. In the ground configuration of 4f the outermost electrons are in the 4f orbital. This orbital is shielded by the

$5s^2 5p^6$ orbitals resulting in a weak interaction with the lattice in a crystal. The energy level splittings due to the crystalline field are thus small compared to the level separations. The 'free ion' character of the ion is preserved to some extent resulting in sharp spectra. The relative spacings of the centers of gravity of Stark levels of different J levels is about the same as between the different J levels of 'free ion'. The 'free ion' wavefunctions are used to explain the spectral intensities and oscillator strengths with considerable success.

Another advantage with the 'free ion' character of the rare earth ions is that, different J levels can be selectively excited and the corresponding different relaxation processes can be studied. This selective excitation is not difficult with the advent of tunable lasers. The nitrogen laser pumped dye laser is one of the most suitable sources of pumping to study the relaxation processes. The pulse width of the laser is $\sim$ 10 nsec. which makes it possible to study the relaxation processes whose rate does not exceed $\sim 10^8$ sec^{-1}.

A pulsed nitrogen laser (3371Å) has been fabricated using flat plate transmission lines. The power output, though not measured, is expected to be about $\sim$ 200 KW. The pulse width is $\sim$ 8 nsec. Most of the rare earth ions fluoresce on exciting with this laser. The observed fluorescence decay timesof two of the ions Nd^{3+} and Dy^{3+} in LaF_3 have been studied and discussed here. The radiative relaxation rates are also calculated for $LaF_3:Nd^{3+}$. The L level of Nd^{3+} [54] is observed to decay nonexponentially. This has been explained in terms of the possible resonant ion pair transitions. The multiphonon process is found to be the dominant relaxation mechanism at higher temperature. Relaxation mechanisms of the other two levels - K and R are also discussed.

1.2 Relaxation Processes

Relaxation processes play an important role in the luminescence of rare earth ions in crystalline solids. It has been observed that if two spin-orbit levels of the ion are sufficiently close in energy, the upper level normally does not fluoresce. Quenching of fluorescence with increasing temperature and with increasing concentration are well known phenomena.

An excited multiplet of a rare earth ion in a crystal can relax to the ground multiplet radiatively or nonradiatively. There are a number of ways in which nonradiative relaxation can take place. The ion interacts with the lattice and relaxes to the lower level by spontaneous emission of phonons in the multiphonon relaxation process. In the ion-ion interaction relaxation process, the energy transfer takes place between the excited ion and the surrounding ground level ions through multipole interactions (dipole-dipole, quadrupole-dipole etc. or exchange interactions with or without the assistance of the lattice phonons. Another well known process is the migration of the excitation energy among the rare earth ions until a quenching center is encountered.

The observed lifetime of an excited multiplet is the inverse of the sum of the probabilities for all possible transitions (radiative and nonradiative) to all the lower multiplets. Contributions from different processes to the decay rate can be separated by studying the variation of lifetime with concentration and temperature. At low concentrations, the observed rate of decay is the sum of the rates of multiphonon and radiative transitions. As the concentration of the impurity ion is increased, the contributions due to ion-ion interactions and energy migration increase.

1.2a Radiative Relaxation

The radiative transition probability is obtained by calculating the total spontaneous emission probability or, from the combined measurements of the relative and absolute intensities in absorption and fluorescence spectra. The radiative transitions in the rare earth ions are mostly electric and magnetic in nature. In the ground configuration of $4f^n$, the magnetic dipole transitions are parity allowed. Electric dipole transitions, on the other hand, require an admixture of opposite parity states from the higher configurations into $4f^n$ and the ab initio calculations are difficult. Judd[1] and Ofelt[2] have shown that under certain simplifying assumptions, the probabilities for an electric dipole transition can be expressed as a sum of three terms involving parameters which contain the strength of configuration interaction. These parameters, are usually evaluated from the absolute intensity of the observed spectra. Using this theory, many authors have explained the observed spectral intensities of rare earth ions in different solids and liquids[3-6]. Radiative lifetimes have also been calculated for many systems and good agreement between experimental observations and the calculated values has been obtained. Given below is a list of some systems studied[7-12].

Pr^{3+}, Er^{3+}, Ho^{3+} in LaF_3[7,9,11] : Pr^{3+}, Nd^{3+}, Eu^{3+}, Er^{3+}, In^{3+} in Y_2O_3[8], Nd^{3+}, Ho^{3+} in $YAlO_3$[11,10].

1.2b Multiphonon Relaxation

Of all the nonradiative processes, the multiphonon relaxation has been extensively investigated. It was established as early as in 1942, by Hellwege[13] that the probability of nonradiative decay in rare earth salts is related to the energy separation between the excited level and the next lowest level (energy gap). A semiquantitative confirmation was provided, later, by the measurement of excited state lifetimes by many workers and an emperical relation between the energy gap and the relaxation rate was obtained[8,14-18]. The multiphonon relaxation rate is found to depend exponentially on the energy gap.

In the early theoretical treatment of the problem, Kiel[19] extended the existing theories for orbit-lattice relaxation in the frame work of the first order perturbation theory to higher orders to arrive at the processes involving simultaneous emission of many phonons. Increase in the relaxation rate with temperature was explained as due to the emission of stimulated phonons from phonon modes which become thermally populated. The phonon mode whose frequency is close to the cut-off frequency of the phonon spectrum of the lattice has been found to play a dominant role in the relaxation process.

A different approach has been used by Fong et.al[20-25]. Using Kubo's tim correlation function representation for the rate constant, they have calculated the relaxation rate in the frame work of the first order perturbation theory assuming adiabatic approximation. It has been shown that phonon scattering pro cesses resulting from the nonadiabatic part of the electron-phonon coupling ari sing from the kinetic energy operator of the ions contribute to the relaxation

The dominant phonon mode is the phonon mode with maximum energy. This mode plays a dual role of promoting the nonradiative transitions and accepting the scattered energy from the phonon scattering processes. The scattering processes involve in quantum changes $\Delta\nu$ of 0, $\pm$ 1, $\pm$ 2 in the promoting phonon mode. Processes in which the quantum change in the phonon mode is positive, the excitation of phonons in the lower level occurs simultaneously with the relaxation of the upper level, thereby reducing the effective energy gap. In the negative $\Delta\nu$ processes, relaxation is accompanied by the emission of phonons from the lower level with the result that the effective energy gap is increased and the relaxation is hindered. The processes in which $\Delta\nu$ = +1, +2 have been found to contribute significantly to the total relaxation rate. Good agreement between theoretical and experimental values has been obtained.

1.2c Ion-Ion Interaction Relaxation

Nonradiative relaxation through ion-ion interaction can occur in number of ways. Two of the well known processes are the ion pair energy transfer and the energy migration. In ion pair interactions the excited ions(donors) transfer part of their energy to ions in the ground state (acceptors) and excite them to intermediate levels through multipolar (dipole-dipole, dipole-quadrupole etc.) interactions or exchange interactions. Both of the interactions are strongly dependent on the separation between the donor and acceptor ions. Overlap of the donor emission and acceptor absorption spectra is essential from the energy conservation consideration. The decay of fluorescence of donor ions is nonexponential which is characterized by a rapid decrease in intensity in the

beginning followed by a slow decay which approaches the intrinsic decay rate (radiative and multiphonon) for large time. The initial rapid fall in the intensity of fluorescence is due to the energy transfer between the donors and surrounding acceptors. The population of the unexcited acceptors close to the donor ions is reduced rapidly with time. In time the fluorescence originates mostly from the donor ions which are well separated from the acceptor ions. The increase in the separation between the donor and acceptor ions reduces the rate of ion pair transitions and the decay rate approaches the intrinsic decay[26-

Even in systems in which the overlap of the donor emission and acceptor absorption spectrum is negligible, the ion-ion interactions have been found to play a significant role. Such nonresonant processes require absorption or emission of lattice phonons or of photons. The rate of relaxation depends on temperature - the functional form being similar to the dependence of multiphonon transition rate on temperature[32].

The theory for the resonant ion pair transitions was developed initially by Forster[33,34] and Dexter[35] for multipolar interaction which was later extended to the exchange interactions by Inokute and Hirayana[36]. The problem of nonresonant ion pair transitions was treated theoretically by Miyakawa and Dexter[37].

The migration of energy among the donor ions explains the concentration quenching of fluorescence when matching energy levels for ion pair transitions are not present[38-41]. The excitation energy is transferred between the donor ions in a random walk manner until a quenching center is encountered. This model was proposed by Botden[42] and the theory was developed by Dexter and Schulman[43]. Yokoto and Tanimoto[44] have obtained a general solution for the

donor decay function including the diffusion within the donor system and donor-acceptor energy transfer via dipole-dipole coupling.

In addition to these, processes like cooperative energy transfer have been observed which involve more than two ions[45,46]. Multiion interactions do contribute to the relaxation for large concentrations.

1.3 Reported Literature on the Nd^{3+} and Dy^{3+} in Lanthanum Halides

The relaxation of the R level of Nd^{3+} has been extensively investigated in a number of hosts[31,39,48-53]. This level is separated from the next lower level $W(^4I_{15/2}^*)$ by about $\sim$ 5000 cm^{-1}. This separation is too large for efficient multiphonon relaxation. Concentration quenching of fluorescence has been observed[39] which has been explained as due to the ion pair transition - $R \longrightarrow W$ and $Z \longrightarrow W^*$. The fluorescence branching ratios and radiative probabilities have been calculated by using Judd-Ofelt's theory. Other levels of Nd^{3+} which have been investigated are S and A in $LaBr_3$[16,17]; S, D, C, W, X and Y in $LaCl_3$[14,38]

The relaxation rates of the following levels have been measured in the case of Dy^{3+}, Y, X, W, A, B, D and E in $LaCl_3$[15,38]; B, C and E in $LaBr_3$[16,17]. Calculated radiative transition probabilities have not been reported in any system.

---

* The notation $4 \longrightarrow 3$, $1 \longrightarrow 2$ stands for the ion pair transition in which ion A relaxes from level 4 to level 3 while ion B is excited to level 2 from level 1, the energies E of the levels being such that $E_1 < E_2 < E_3 < E_4$.

REFERENCES

1. Judd, B.R - Phys.Rev. 127, 150 (1962).
2. Ofelt, G.S - J. Chem. Phys.37, 511 (1962).
3. Carnall, W.T., Fields, P.R. and Wybourne, B.G. - J. Chem. Phys. 42, 3797 (1965).
4. Krupke, W.F. - Phys.Rev. 145, 325 (1966).
5. Krupke, W.F. - IEEEJ Quantum Electronics QE2, 698 (1966).
6. Gruber, J.B., Krupke, W.F., and Poindexter, J.M. - J. Chem. Phys. 41, 3363 (1964).
7. Weber, M.J. - Phys.Rev. 157, 262 (1967).
8. Weber, M.J. - Phys.Rev. 171, 283-291 (1968).
9. Weber, M.J. - J. Chem. Phys. 48, 4774 (1968).
10. Weber, M.J., and Varitimos, T.E. - J. App. Phys. 42, 4996 (1971).
11. Weber, M.J., Matsinger, B.H., Donlan, V.L. and Surratt, G.T. - J. Chem. Phys. 57, 562 (1972).
12. Weber, M.J., Varitimos, T.E., and Matsinger, B.H. - Phys.Rev. B8, 47 (1973).
13. Hellwege, K.H. - Ann. Phys. (Leipz) 40, 529 (1942).
14. Partlow, W.D., and Moss, H.W. - Phys.Rev. 157, 252 (1967).
15. Riseberg, L.A., and Gandrud, W.B., Moos, H.W. - Phys.Rev. 159, 262 (1967).
16. Riseberg, L.A., and Moos, H.W. - Phys.Rev. Lett. 19, 1423 (1967).
17. Riseberg, L.A., and Moos, H.W. - Phys. Rev. 174, 429 (1968).
18. Moos, H.W. - J. of Luminischence 1,2, 106 (1970).
19. Kiel, A. - Quantum Electronics, edited by P. Grivet and N.Bloembergen (Columbia Univ. Press), NY (1964), Vol. 1, p. 765.
20. Miller, M.M., and Fong, F.K. - Chem. Phys. Lett. 10, 408 (1971).

21. Fong, F.K., Naberhuis, S.L., and Miller, M.M. - J. Chem. Phys. 56, 4020 (1972).

22. Diestler, D.J., and Fong, F.K. - J. Chem. Phys. 57, 4953 (1972).

23. Wassam, W.A., and Fong, F.K. - J. Chem. Phys. 58, 956 (1973).

24. Lauer, H.V., and Fong, F.K. - J. Chem. Phys. 60, 274 (1974).

25. Fong, F.K., Lauer, H.V., and Chilver, C.R. - J. Chem. Phys. 63, 366 (1975).

26. Brown, M.R. - J. Chem. Phys. 43, 1 (1965).

27. Van Uitert, L.G., Bearborn, E.F., and Rubin, J.J. - J. Chem. Phys. 47, 3653 (1967).

28. Nakasawa, E., and Shionoya, S. - J. Chem. Phys. 47, 3211 (1967).

29. Asawa, C.K. - Phys. Rev. 155, 188 (1967).

30. Weber, M.J. - Phys. Rev. B4, 3153 (1971).

31. Krasutsky, N., and Moos, H.W. - Phys. Rev. B8, 1010 (1973).

32. Yamada, N., Shionoya, S., and Fushida, T. - J. Phys. Soc. Jap. 32, 1577 (1972).

33. Forster, Th. - Ann. Physik 2, 55 (1948).

34. Forster, Th. - Discussion, Farday Society 27, 7 (1959).

35. Dexter, D.L. - J. Chem. Phys. 21, 836 (1953).

36. Inokuti, M., and Hirayana, F. - J. Chem. Phys. 43, 1978 (1965).

37. Miyakawa, T., and Dexter, D.L. - Phys. Rev. B1, 2961 (1970).

38. Gandrud, M.B., and Moos, H.W. - J. Chem. Phys. 49, 2170 (1968).

39. Asawa, C.K., and Robinson, M. - Phys. Rev. 141, 251 (1966).

40. Weber, M.J. - Phys. Rev. B4, 2932 (1971).

41. Sharp, E.J., Miller, J.E. and Weber, M.J. - J. App. Phys. 44, 4098 (1973).

42. Botden, Th.P.S. - Phillips Research Reports 6, 425 (1951).

43. Dexter, D.L., and Shulman, H.H. - J. Chem. Phys. 42, 1063 (1954).

44. Yokota, M., and Tanimoto, O. - J. Phys. Soc. Jap. 22, 779 (1967).

45. Ostermayer, F.W., and Van Uitert, L.G. - Phys. Rev. B1, 4208 (1970).

46. Livanova, L.D., Saitkulov, I.G., and Stolov, A.L. - Soviet Physics Solid State 11, 750 (1969).

47. Wright, J.C. - (private communication).

48. Rapp, C.F., and Chrysochoos, J. - J. Phys. Chem. 77, 1016 (1973).

49. Hong, H.Y.P., and Dwight, K. - Mat. Res. Bull. 9, 1661 (1974).

50. Singh, S., Smith, R.G., and Van Uitert, L.G. - Phys. Rev. B10, 2566 (1974).

51. Chrysochoos, J. - J. Chem. Phys. 61, 4596 (1974).

52. Liao, P.F., and Weber, H.P. - J. App. Phys. 45, 2931 (1974).

53. Singh, S., Miller, D.C., Potopowics, J.R., and Shick, L.K. - J. App. Phys. 46, 1191 (1975).

54. Kumar, U.V., Jagannath, H., Ramachandra Rao, D., and Venkateswarlu, P. - Indian J. Phys. 50, 90 (1976).

CHAPTER II

RELAXATION THEORIES

2.1 Introduction

The relaxation processes of ions in solids have been investigated - theoretically and experimentally by many workers. Some of the earliest reports in the field of energy transfer processes have been due to Hellwege[1], Botden[2], Perrin[3], Forster[4] and Dexter[5]. The energy-transfer processes between molecules in solution havebeen theoretically interpreted by Perrin[3] and Forster[4]. This was later extended by Dexter to the energy-transfer processes between ions in solids via dipole-dipole coupling. Further extension to this theory is due to Inokuti and Hirayama[6] who have included the exchange coupling between the ions.

Kiel[7] was the first to treat the multiphonon relaxation processes theoretically. He established the possibility of emission of a number of phonons simultaneously during relaxation in accordance with the principle of conservation of energy. Later, Fong et.al[8] have extended the time correlation function

approach developed for the nonradiative relaxation of molecules by Fisher[9] to the rare earth ions in solids.

The radiative relaxation of the rare earth ions is mostly due to forced electric dipole transitions which are parity forbidden in the lowest electronic configuration $4f^n$. The mixing of states of opposite parity from higher configurations in the lowest configuration is, thus, essential for the forbidden electric dipole transitions to be allowed. The calculation of the transition probabilities for electric dipole transitions involves the sum over the states of a large number of higher configurations. Judd[10] and Ofelt[11] have shown that the electric dipole transition probability can be expressed in terms of a small number of intensity parameters which are characteristic of the host lattice. Following this, Krupke[12] and Weber[13] have calculated the oscillator strengths and radiative transition probabilities of a number of ions in different hosts. In most of the cases[12,13], good agreement between the observed and calculated values has been obtained.

A brief outline of the existing theories for the different relaxation processes is given below.

2.2 Radiative Relaxation

The treatment of Krupke[12] and Weber[13] is followed here. The Hamiltonian for an ion in a crystalline solid can be written as

$$H = H_o + V \qquad (2.1)$$

where H_o is the sum of the electrostatic and spin-orbit interactions of the free ion and V is the crystal field potential. Assuming a static field model, the crystal field potential V may be expanded in spherical harmonics as

$$V = \sum_{kq} A_k^q \sum_i r_i^k V_k^q (\Theta_i \varphi_i) \qquad (2.2)$$

Here r_i is the radial coordinate of the i^{th} electron, $V_k^q (\Theta_i \varphi_i)$ is the q^{th} component of the spherical harmonic of order k. A_k^q are the parameters which depend on the nature of the symmetry of the crystal field.

In the rare earth ions in crystals, the spectra arise due to the $4f^n$ electrons which are shielded by the outer shells $5s^2 5p^6$. The interaction with the environment is thus small. The spin-orbit interactions, on the other hand, are strong. The unperturbed wavefunctions can be written in terms of the basis states $|\alpha SLJ\rangle$ as

$$|(\alpha SL)J\rangle = |\psi_J\rangle = \sum_{\alpha SL} C(\alpha SL) \, | f^n \alpha SLJ\rangle \qquad (2.3)$$

where $C(\alpha SL)$ are the intermediate coupling coefficients.

The effect of crystalline field is to split each 'free ion' J level further. The splittings are small as the interaction is weak.

The line strength of transition between two levels ψ_J and $\psi_{J'}$ is defined as

$$S(J,J') = |\langle \psi_J | \underline{Q} | \psi_{J'} \rangle|^2 \qquad (2.4)$$

where $\underset{\sim}{Q}$ may be electric dipole or a magnetic dipole operator given by

$$\underset{\sim}{P} = -e \sum_i \underset{\sim}{r}_i \quad \text{and} \quad \underset{\sim}{M} = -\frac{e}{2mc} \sum_i \underset{\sim}{L}_i + 2\underset{\sim}{S}_i \tag{2.5}$$

respectively. Here e is the charge and m is the mass of the electron.

The transition probabilities are related to the line strength through Einstein coefficients A and B. If ν (in cm^{-1}) is the frequency of the transition between the levels J and J', the spontaneous emission coefficient is given by

$$A(J,J') = 64\pi^4 \nu^3 (3h)^{-1} \chi S(J,J') \tag{2.6}$$

and spontaneous absorption coefficient by

$$B(J,J') = 8 \pi^3 (3h^2c)^{-1} \chi S(J,J') \tag{2.7}$$

χ is the correction factor for the refractive index of the medium of the host lattice. For a well localized center in an isotropic medium of refractive index n

$$\chi = \begin{cases} n(n^2+2)^2/9 & \text{for electric dipole transitions} \\ n^3 & \text{for magnetic dipole transitions} \end{cases} \tag{2.8}$$

In a crystal field, each J level splits into a number of Stark components. The wavefunctions are no longer the same. The probabilities for a transition from Stark components of the upper level to the Stark components of the lower

level depend on the strength of the interaction. This necessitates a detailed knowledge of the crystal field parameters and wavefunctions. In the absence of such a knowledge, it is assumed that all the Stark components of the initial level have equal probability of transition to components of the lower level. With this assumption (2.6) and (2.7) become

$$A\,[(\alpha SL)J,\ (\alpha'S'L')J'] = 64\,\pi^4 \nu^3 (3h)^{-1} (2J+1)^{-1} \times S\,[(\alpha SL)J,\ (\alpha'S'L')J'] \qquad (2.9)$$

and

$$B\,[(\alpha SL)J,\ (\alpha'S'L')J'] = 8\,\pi^3 (3h^2 c)^{-1} (2J+1)^{-1} \times S\,[(\alpha SL)J,\ (\alpha'S'L')J'] \qquad (2.10)$$

2.2a Magnetic Dipole Transitions

The magnetic dipole transitions are allowed between states of the same parity. In the lowest configuration $4f^n$, all the levels of the rare earth ion are of the same parity. The selection rules for the transitions are $\Delta\alpha = 0$, $\Delta L = 0$, $\Delta J = 0, \pm 1$ $(0 \not\leftrightarrow 0)$ in Russel-Saunders limit.

The spontaneous emission probability for magnetic dipole transition is

$$A_{md}\,[(\alpha SL)J,\ (\alpha'S'L')J'] = 64\,\pi^4 \nu^3 (3h)^{-1} (2J+1)^{-1} \times_{md} \left| \sum_{\alpha SL,\ \alpha'S'L'} C(\alpha SL)\, C(\alpha'S'L') \times \langle f^n \alpha SLJ \| M \| f^n \alpha'S'L'J' \rangle \right|^2 \qquad (2.11)$$

where the magnetic dipole operator $\underset{\sim}{M}$ is given by

$$\underset{\sim}{M} = - \frac{e}{2mc} (\underset{\sim}{L} + 2\underset{\sim}{S}) \tag{2.12}$$

The matrix elements of $\underset{\sim}{M}$ between αSLJ states are:

$$\text{for } J' = J, \langle f^n \alpha SLJ || \underset{\sim}{M} || f^n \alpha' S'L'J \rangle = \delta(\alpha\alpha') \delta(SS') \delta(LL')$$

$$\times \beta [(2J+1)/4J(J+1)]^{\frac{1}{2}} [S(S+1) - L(L+1) + 3J(J+1)] \tag{2.13}$$

$$\text{for } J' = J-1, \langle f^n \alpha SLJ || \underset{\sim}{M} || f^n \alpha' S'L'J-1 \rangle = \delta(\alpha\alpha') \delta(SS') \delta(LL')$$

$$\times \beta \left\{ \frac{[(S+L+1)^2 - J^2][J^2 - (L-S)^2]}{4J} \right\}^{\frac{1}{2}} \tag{2.14}$$

$$\text{for } J' = J+1, \langle f^n \alpha SLJ || \underset{\sim}{M} || f^n \alpha' S'L'J+1 \rangle = \delta(\alpha\alpha') \delta(SS') \delta(LL')$$

$$\times \beta \left\{ \frac{[(S+L+1)^2 - (J+1)^2][(J+1)^2 - (L-S)^2]}{4(J+1)} \right\}^{\frac{1}{2}} \tag{2.15}$$

where $\beta = e\hbar/2mc$.

2.2b Electric Dipole Transitions

Electric dipole transitions are forbidden between states of the same parity, which is the case with the rare earth ions in the lowest configuration. If there is an admixture of opposite parity states from other configurations,

transitions are still possible. This can be brought about also by the vibrational interaction with the lattice phonons or through the noncentrosymmetric fields. Explicit calculation of these probabilities is very difficult as it involves a summing over a large number of states of excited configurations. In addition, a complete knowledge of crystal field parameters is required. Judd[10] and Ofelt[11] have shown independently that by assuming the states of the excited configuration $nf^{n-1}\ n'l'$ to be degenerate and ascribing an average value to them, summation over the states of excited configurations can be done. The line strength of an electric dipole transition can then be expressed as

$$S = e^2 \sum_{\lambda = 2, 4, 6} \Omega_\lambda \left\langle f^n (\alpha SL)J \| \underset{\sim}{U}^{\lambda} \| f^n(\alpha' S'L')J' \right\rangle^2 \qquad (2.16)$$

Here Ω_λ are the phenomenological parameters which include the integrals involving the radial wavefunctions of the excited configurations and their energies.

The matrix elements of the unit matrix $\underset{\sim}{U}^{\lambda}$ can be evaluated from the formula

$$\left\langle f^n \alpha SLJ \| \underset{\sim}{U}^{\lambda} \| f^n \alpha' S'L'J' \right\rangle = (-1)^{S+L'+J+\lambda} \delta(SS') (2J+1)^{\frac{1}{2}}$$

$$\times (2J'+1)^{\frac{1}{2}} \left\langle f^n \alpha SL \| \underset{\sim}{U}^{\lambda} \| f^n \alpha' S'L' \right\rangle$$

$$\times \begin{Bmatrix} J & J' & \lambda \\ L' & L & S \end{Bmatrix} \qquad (2.17)$$

The Ω_λ are related to the oscillator strength f. The relation is

$$f_{ed} = \frac{8\pi^2\nu m}{(2J+1)3h} \sum_\lambda \Omega_\lambda \langle f^n (\alpha SL)J \| U \| f^n(\alpha'S'L')J' \rangle^2 \qquad (2.18)$$

where ν is the mean frequency of transition.

The oscillator strength is derived from the measurements of the integrated absorption spectrum using the relationship,

$$f = \frac{mc}{\pi e^2 n} \int \mu d\nu \qquad (2.19)$$

μ being the absorption coefficient (in cm^{-1}) and n is the total number of active ions per unit volume.

The probability for the spontaneous emission is given by

$$A_{ed}\left[(\alpha SL)J, (\alpha'S'L')J'\right] = 64\pi^4 e^2 \nu^3 (3h)^{-1}(2J+1)^{-1}\chi_{ed} \qquad (2.20)$$

$$\times \sum_\lambda \Omega_\lambda \langle f^n(\alpha SL)J \| U^\lambda \| f^n(\alpha'S'L')J' \rangle^2$$

The transition probability for electric dipole transitions due to the mixing of states of opposite parity from higher configuration through lattice phonons has a similar form. Thus the experimentally determined parameters include contributions from static field and the vibrational crystal field induced transitions.

The total radiative decay from the excited state is the sum of the spontaneous emission probabilities due to electric dipole and magnetic dipole transitions to all the low lying states. The contributions from the higher multipolar transitions are negligible.

2.3 Probability of Nonradiative Transitions - Multiphonon Relaxation

The lifetime of an excited state is governed by a combination of all the radiative and nonradiative transitions to the lower states i.e.

$$\tau_i^{-1} = \sum_j W_{ij}^R + \sum_j W_{ij}^{NR} \qquad (2.21)$$

Here W_{ij}^R (W_{ij}^{NR}) is probability of radiative (nonradiative) transitions to state j. The nonradiative decay between the J multiplets arises from (1) emission of multiphonons or (2) exchange of energy with a neighbouring ion with or without the assistance of lattice phonons. The emission of multiphonons is due to the orbit - lattice interaction and is temperature dependent. At low temperature, there is a spontaneous emission of phonons to conserve the energy. As the temperature is increased, the stimulated emission of phonons also takes place. The energy transfer by resonant ion pair processes depends on the concentration of the ions and the energy mismatch. It is independent of temperature. But the phonon-assisted processes are temperature dependent and the dependence is similar to that of the multiphonon processes.

The temperature dependence of the multiphonon decay rate has been a subject of considerable interest. The first theoretical model is by Kiel[7].

He has shown that the first order term of the orbit-lattice interaction can lead to the multiphonon emission if higher order perturbation theory is used. His treatment is based on the crude Born-Oppenheimer (CBO) approximation. The unperturbed electronic states are the states due to the crystal-field Hamiltonian. These states do not depend on the nuclear normal mode coordinates. Displacement in the equilibrium positions of the potential surfaces of the various electronic states is assumed to be zero. Explicit calculations of the probability of spontaneous emission of phonons is difficult in this approach as a large number of vibrational modes and the combination of intermediate states may have to be considered.

A second approach to the problem is by using the adiabatic approximation method. In this, the multiphonon rate constant is calculated in the framework of the first order perturbation theory using the time correlation function representation. A broad outline of the theory is given below[8].

The electron-lattice Hamiltonian in the adiabatic approximation for rare earth ions in a host lattice can be written as

$$H = -\frac{\hbar^2}{2m}\sum_i \partial^2/\partial r_i^2 + V(\underset{\sim}{r}, \underset{\sim}{R}) - \tfrac{1}{2}\hbar^2 \sum_j \left(\partial^2/M_j \partial R_i^2\right) \quad (2.22)$$

where $\underset{\sim}{r}$, $\underset{\sim}{R}$ are the coordinates of the electrons and the lattice ions respectively and $V(\underset{\sim}{r}, \underset{\sim}{R})$ includes all the ion-ion and electron-ion interactions. The operator for the kinetic energy of the ions can be regarded as a small perturbation in adiabatic approximation. Hence to zeroth order the eigenstates of H are given by the solution of the Schrodinger equation

$$\left[-\left(\frac{\hbar^2}{2m}\right)\sum_i \partial^2/\partial r_i^2 + V(\underset{\sim}{r},\underset{\sim}{R})\right] |\alpha(\underset{\sim}{r},\underset{\sim}{R})\rangle = \varepsilon_\alpha(\underset{\sim}{R})\,|\alpha(\underset{\sim}{r},\underset{\sim}{R})\rangle \qquad (2.23)$$

for fixed values of $\underset{\sim}{R}$.

The Born-Oppenheimer eigenstates $|\alpha(\underset{\sim}{r},\underset{\sim}{R})\rangle$ and the eigenvalues $\varepsilon_\alpha(\underset{\sim}{R})$ depend parametrically on $\underset{\sim}{R}$. $\varepsilon_\alpha(\underset{\sim}{R})$ is used as the effective adiabatic potential for the ionic motion. It can be expanded in powers of the displacement ΔR_α^j about the equillibrium position R_o corresponding to the electronic ground state in the Harmonic approximation.

$$\varepsilon_\alpha(\underset{\sim}{R}) = \varepsilon_\alpha^{\circ}(\underset{\sim}{R}_o) + \sum_i \left[\partial\varepsilon_\alpha(\underset{\sim}{R})/\partial R_i\right]_{R_j=R_o^j} \Delta R_\alpha^j$$

$$+ \tfrac{1}{2}\sum_j \left[\partial^2\varepsilon_\alpha(\underset{\sim}{R})/\partial R_j^2\right]_{R_j=R_o^j} (\Delta R_\alpha^j)^2 \qquad (2.24)$$

The Born-Oppenheimer eigenstates $|\alpha(\underset{\sim}{r},\underset{\sim}{R}_o)\rangle$ are the crystal symmetrized states formed from the appropriate $|LSJM_J\rangle$ free ion states.

The Hamiltonian can be rewritten in terms of the creation and annihilation operators of the electrons a_i^+, a_i and phonons b_i^+, b_i after a canonical transformation as

$$\tilde{H} = \sum_\alpha \varepsilon_\alpha a_\alpha^+ a_\alpha + \sum_{\alpha,j} \hbar w_\alpha^j a_\alpha^+ a_\alpha b_j^+ b_j - \sum_{\substack{\alpha\neq\alpha' \\ j}} \hbar^2\left(\frac{w_j}{2M_j\hbar}\right)^{\frac{1}{2}}$$

$$\times \frac{\langle\alpha|(\partial V/\partial R_j)_{R_j=R_o^j}|\alpha'\rangle}{\left[\varepsilon_\alpha(R_j) - \varepsilon_{\alpha'}(R_j)\right]} a_\alpha^+ a_\alpha B_\alpha^+ B_\alpha (b_j - b_j^+) \qquad (2.25)$$

where w_α^j is the frequency of the j^{th} normal mod (2.30)
the electron is in the Born-Oppenheimer state $|\alpha\rangle$
above equation is the nonadiabatic part of the el
sing from the kinetic energy of the ions which gi
transitions between the different Born-Oppenheim

B_α^+ and ε_α are given by

$$B_\alpha^+ = \exp \sum_j \tfrac{1}{2} g_\alpha^j (b_j^+ - b_j) \quad \text{and} \quad \varepsilon_\alpha = \varepsilon_\alpha^o - \sum_j \tfrac{1}{2} g_\alpha^j \hbar w_\alpha^j \qquad (2.26)$$

where g_α^j is a dimensionless quantity

$$g_\alpha^j = (2M_j w_\alpha^j/\hbar)^{\frac{1}{2}} \Delta R_\alpha^j \qquad (2.27)$$

The rate constant $W_{\alpha\alpha'}$ for transitions between the states α and α' in the time correlation function representation is given by

$$W_{\alpha\alpha'} = (\beta \langle N_\alpha \rangle)^{-1} \int_0^\infty dt \int_0^\beta d\lambda \langle (d\tilde{N}_\alpha/dt)(-t-i\hbar\lambda)$$

$$\times (d\tilde{N}_\alpha/dt)(0) \rangle_{\bar{H}} \qquad (2.28)$$

where $\tilde{N}_\alpha$ is the number operator given by

$$d\tilde{N}_\alpha/dt = (i/\hbar)[\tilde{H}, \tilde{N}_\alpha] = -(i/\hbar) \sum_j C_{\alpha\alpha'}^j a_\alpha^+ a_\alpha B_\alpha^+ B_\alpha (b_j - b_j^+)$$

$$+ \text{h.c} \qquad (2.29)$$

and $$C^{j}_{\alpha\alpha'} = -\left(\frac{\hbar^3 w_j}{2M_j}\right)^{\frac{1}{2}} \times \frac{\langle\alpha|(\partial V/\partial R_j)_{R_j=R_o^j}|\alpha'\rangle}{\left[\varepsilon_\alpha(R_j) - \varepsilon_{\alpha'}(R_j)\right]} \qquad (2.30)$$

The brackets indicate the average over the density operator ρ given by

$$\rho = \exp(-\beta \tilde{H})/\mathrm{Tr}\exp(-\beta \tilde{H}) \qquad (2.31)$$

Equation (2.28) is valid to any arbitrary order in the nonadiabatic perturbation. It has been evaluated to the lowest order in the perturbation by the method of steepest descent by Fong et.al[8] with the following assumptions.

a. The adiabatic potentials are minimally distorted. Hence $w_\alpha \simeq w_{\alpha'}$,

b. There is only one dominant mode of coupling and the $\sum_j g_j^2$ can be replaced by $L_m g_m^2$ where L_m is an effective degeneracy of the mediating phonon mode m responsible for the radiationless process.

c. For rare earth ions in crystals $\varepsilon_\alpha - \varepsilon_{\alpha'} >> L_m g_m^2 \hbar w_\alpha^m$.

The final expression for $W_{\alpha\alpha'}$ is given by

$$W_{\alpha\alpha'} = \frac{(2\pi)^{\frac{1}{2}}}{\hbar^2} L_m |C^m_{\alpha\alpha'}|^2 w_m^{-1} \sum_{\nu=2}^{\nu=2} A_{q\nu} (p-q\nu)^{-\frac{1}{2}}$$

$$\times \exp\left(-\tfrac{1}{4} L_m g_m^2 (2n_m+1)\right) \exp\left(-(p-q\nu)\right.$$

$$\left.\times\left\{\ln\left(4(p-q\nu)/L_m g_m^2 (n_m+1)\right)-1\right\}\right) \qquad (2.32)$$

with the coefficients $\lambda_{\Delta\nu}$ given by

$$\lambda_0 = \tfrac{1}{4} L_m g_m^2 (6n_m(n_m+1)+1), \quad \lambda_1 = -\tfrac{1}{2} L_m g_m^2 (2n_m+1)(n_m+1)+n_m+1$$

$$\lambda_{-1} = -\tfrac{1}{2} L_m g_m^2 (2n_m+1)n_m+n_m , \quad \lambda_2 = \tfrac{1}{4} L_m g_m^2 (n_m+1)^2$$

$$\lambda_{-2} = \tfrac{1}{4} L_m g_m^2 n_m^2 \qquad \text{where} \quad n_m = (\exp(\hbar w_\alpha^m/kT)-1)^{-1} \tag{2.33}$$

In the above expression the positive $\Delta\nu$ indicate contributions to the rate by relaxation processes in which a simultaneous excitation of quanta in the mediating mode while in the negative $\Delta\nu$ processes, the electronic relaxation takes place with the simultaneous emission of phonons. The first one is an assisted process as the effective band gap is reduced because of the excitation of the phonons, while the latter is a hindered process, the effective band gap being more. Significant contributions to the radiationless transitions are made by $\Delta\nu = +1$, $\Delta\nu = +2$ processes only.

The radiationless relaxation rate of an excited multiplet of Stark levels to a lower multiplet is the thermal average of the individual rates. It is given by

$$\bar{W} = \frac{\sum_i W_i \exp(-\Delta_i/kT)}{\sum_i \exp(-\Delta_i/kT)} \tag{2.34}$$

where the summation is over all thermally accessible states and Δ_i is the energy difference between the i^{th} state and the lowest Stark component of the decaying multiplet.

The quantities $L_m g_m^2$, $L_m C_{\alpha\alpha}^{m^2}$, and $\hbar w_\alpha^m$ are determined from the experimental observations as the ab initio calculations are extremely difficult.

2.4 Ion-Ion Interaction Relaxation

Relaxation of the excited ion is possible by transfer of a part of its energy to a neighbouring ion of the same species or different species in ground state. The ion in the excited state is called the donor and the ion in the ground state is the acceptor. The rate of energy transfer depends on the separation between the donor and acceptor, the rate being higher for smaller separations and vice versa. Interaction between the ions is through multipolar or exchange coupling. Three ion interactions are also known to contribute significantly to the relaxation. More significant are the phonon-assisted ion-ion interaction relaxation processes where absorption or emission of lattice phonons is essential from energy conservation considerations.

In the case of the donor and acceptor ions of the same species a total transfer of energy from a donor ion to an acceptor ion is possible. This transfer of the excitation energy can take place between the ions in a random walk manner, resulting in energy diffusion in the lattice. The energy migration continues till an energy sink or a quenching center is encountered. Migration contributes significantly to relaxation where ion pair transitions are not possible.

Experimentally what is observed, is the rate of relaxation due to the ensemble average of all the possible donor-acceptor pairs. The electronic levels involved in the transfer and the number of donor and acceptor ions

present in the system have to be known for averaging. Various models have been proposed for the interaction. The ensemble averaging is done under some simplifying assumptions. Grant[15] has derived a general expression from first principles for the rate of energy transfer in order to show explicitly the assumptions that are inherent in these models.

In this section, the ion pair relaxation rate for resonant energy transfer is only dealt with. A broad outline of the theory is given. For most of the discussions the theoretical treatment given by Inokuti and Hirayana[6] is followed.

Consider a system of two different kinds of ions, energy donors and energy acceptors which are assumed to be randomly distributed in the medium. Both the acceptors and donors are assumed to have only one excited electronic state in the energy region of interest and that the energy migration rate is small compared to the donor-acceptor transfer rate. The probability $\varphi(\underset{\sim}{r},t)$ of finding a donor at $\underset{\sim}{r}$ in an excited state at time t, decays exponentially with the intrinsic time constant τ_o in the absence of acceptors. The presence of acceptors increases the rate of decay. Let $w(R)$ denote the probability of energy transfer to an acceptor at distance R, then

$$\varphi(\underset{\sim}{r},t) = \exp(-t/\tau_o) \prod_{1}^{N_a V} \exp(-W(R)t) \qquad (2.35)$$

where $N_a V$ is the number of acceptors in a volume V.

If $W(R)$ is the probability distribution of donor-acceptor distance R in a volume V, the statistical average of $\varphi(\underset{\sim}{r},t)$ over an infinitely large

number of donors can be written as

$$\Phi(t) = \exp(-t/\tau_o) \lim_{\substack{N\to\infty \\ V\to\infty}} \left\{ \int_V \exp(-w(R)t)\,\mathbb{W}(R)\,dV \right\}^N \qquad (2.36)$$

The volume V over which integration is carried out is chosen large enough to contain a macroscopically large number of acceptors and the limit $N \to \infty$, $V \to \infty$ is such that N/V is finite. For a random distribution of acceptors around a donor, $\mathbb{W}(R)$ is replaced by $4\pi R^2 dR/V$. Thus

$$\Phi(\underset{\sim}{r},t) = \exp(-t/\tau_o) \lim_{\substack{N\to\infty \\ V\to\infty}} \left\{ \frac{4\pi}{V} \int_0^{R_V} \exp(-w(R)t)R^2 dR \right\}^N \qquad (2.37)$$

R_V is the radius of the sphere around a donor whose volume is V.

The function $\Phi(t)$ is proportional to the intensity of the donor luminescence. It is not, in general, an exponential function. At the start of the decay, the excited donors near the acceptors are quenched rapidly. With time the number of unexcited acceptors near the donors decreases. The quenching of donors continues with the energy transfer taking place between the donors and acceptors which are far apart. The rate of energy transfer decreases as $w(R)$ decreases with increasing distance R and approaches the intrinsic decay rate for large R.

The decay function can be calculated from equation (2.37) if the dependence of w on R is known. Various models that have been proposed are given below.

1. Perrin Model: In this model the rate constant $\omega(R)$ is given by

$$w(R) = \begin{cases} \infty & \text{for } R < R_o \\ 0 & \text{for } R > R_o \end{cases} \qquad (2.38)$$

where R_o is the critical radius for interaction.

The decay function for (2.38) is

$$\Phi(t) = \begin{cases} 1 \quad t=0 & \text{for } t = 0 \\ \exp(-t/c_o - c/c_o) & \text{for } t > 0 \end{cases} \qquad (2.39)$$

Here C is the acceptor concentration given by $C = 3N/4\pi R_v^3$ and C_o is the critical transfer concentration $C_o = 3/4\pi R_c^3$.

The expression for the decay function $\Phi(t)$ shows that the decay falls suddenly at t=0 followed by exponential decay.

2. Stern-Volmer Model: The interaction is assumed to be a constant ω in this model. The decay function $\Phi(t)$ is given by

$$\Phi(t) = \exp(-t/\tau_o) \lim_{N\to\infty} \exp(-Nwt) \qquad (2.40)$$

The factor Nw is proportional to the acceptor concentration and is finite in the limit $N \to \infty$ and $w \to 0$. Thus from (2.37)

$$\Phi(t) = \exp\left(-\frac{t}{\tau_o} - C/C_o \times t/\tau_o\right) \qquad (2.41)$$

C_o is the reference concentration which specifies the interaction strength. The decay is simple exponential.

3. Inverse Power Rate Model: Consider the case when the rate constant is proportional to the inverse power of the distance i.e.

$$w(R) = \frac{(R_o/R)^s}{\tau_o} \qquad (2.42)$$

where R_o is the critical transfer distance.

All the multipolar interactions are special cases of the above. The model corresponds to dipole-dipole interactions for s=6, dipole-quadrupole interactions for s=8 and quadrupole-quadrupole interactions for s=10.

The decay functions $\Phi(t)$ is given by

$$\Phi(t) = \exp\left(-\frac{t}{\tau_o} - \Gamma(1 - 3/s) \frac{\rho}{c_o} \left(\frac{t}{\tau_o}\right)^{3/s}\right) \qquad (2.43)$$

c, c_o have the same significance as in other models. $\Gamma(x)$ is the gamma function.

The decay function is nonexponential with a rapid fall in the beginning followed by a slow decay.

4. Exchange Interaction: The expression for the rate constant $w(R)$ has been derived by Dexter.

$$w(R) = \frac{2\pi}{\hbar^2} Z^2 \int f_D(E)\, F_A(E)\, dE \qquad (2.44)$$

with $Z^2 = K^2 \exp(-2R/L)$.

K is the constant with dimensions of energy. L is called the effective average Bohr radius $f_D(E)$ and $F_A(E)$ are the donor emission and acceptor

absorption spectra which are normalized on the photon energy scale so that

$$\int f_D(E)\, dE = \int F_A(E)\, dE = 1.$$

With this radial dependence, equation (2.37) becomes

$$\Phi(t) = \exp\left(- \frac{t}{\tau_o} - \gamma^{-3} \frac{C}{C_o}\, g\left(e^{\gamma} t/\tau_o\right)\right) \qquad (2.45)$$

where g(z) is difined by

$$g(z) = - z \int_0^1 \exp(- zy)\, (\ln y)^3 dy \qquad (2.46)$$

and $\gamma = 2R_o/L$

L is the distance characterizing the spatial extent of the ionic wave function and R_o is the critical transfer distance.

The plots of log $\Phi(t)$ against τ / τ_o for various γ's and C/C_o have been calculated by Inokuti and Hirayana. The results show that the nonexponentiality is more pronounced for larger C/C_o. As γ increases the rapid initial drop decreases followed by a nearly exponential decay.

When the migration of the excitation energy is possible the rate of energy transfer between the donor and acceptor ions is influenced by the rate of excitation diffusion. In the case of fast diffusion the variations in the transfer rate of various donor-acceptor pairs are averaged out and the donor decay is exponential[14].

The energy transfer between a donor ion and an acceptor ion in the presence of diffusion is described by the equation,

$$\partial \Phi / \partial t = D\nabla^2 \Phi(\underline{r}, t) - \frac{1}{\tau_o}(\underline{r}, t) - \sum_i V(|\underline{r} - \underline{R}_i(t)|) \times \Phi(\underline{r}, t) \qquad (2.47)$$

Here D is the donor diffusion constant and $V(|\underline{r} - \underline{R}_i(t)|)$ is the interaction of a donor ion with the i^{th} acceptor ion.

This equation has been solved by Yokota and Tanimoto[16] for dipole-dipole interaction between the donor and acceptor ions. The resulting decay function is

$$\Phi(t) = \Phi(o) \exp(-t/\tau_o) \exp\left(-\frac{4}{3}\pi^{3/2} N_a (Ct)^{\frac{1}{2}} \left(\frac{1+10.87x+15.5x^2}{1+8.743x}\right)^{3/4}\right) \qquad (2.48)$$

Diffusion is unimportant for times $t << C^{1/2} D^{-3/2}$ and the equation reduces to (2.43). In the other limit $t \rightarrow \infty$, the decay function reduces to an exponential function of time with a rate given by

$$\Phi(t) = \Phi(o) \exp\left(-\frac{t}{\tau_o} - 11.404\, N_a\, D^{3/4}\, C^{1/4} t\right) \qquad (2.49)$$

In this region, the relaxation depends on the energy migration to spatial regions where the energy transfer takes place. This expression is different from that predicted directly from equation (2.47) under the same conditions. The expression for these conditions is[17]

$$\Phi(t) = \Phi(o) \exp\left(-\frac{t}{\tau_o} - 8.54\, N_a D^{3/4} C^{1/4} t\right) \qquad (2.50)$$

The difference between the two arise from the approximations needed in deriving the equation (2.49).

REFERENCES

1. Hellwege, K.H. - Ann. Phys. (Leipz) 40, 529 (1942).

2. Botden, Th.P.S. - Phillips Research Reports 6, 425 (1951).

3. Perrin, F. - Ann. Chim. Phys. 17, 283 (1932).

4. Forster, Th. - (a) Ann. Physik 2, 55 (1948) and (b) Discussions Faraday Soc. 27, 7 (1959).

5. Dexter, D.L. - J. Chem. Phys. 21, 836 (1953).

6. Inokuti, M., and Hirayana, F. - J. Chem. Phys. 43, 1978 (1965).

7. Kiel, A. - In Quantum Electronics, edited by P. Grivet and N. Bloembergen (Columbia Univ. Press, New York 1964).

8.(a) Miller, M.M., and Fong, F.K. - Chem. Phys. Lett. 10, 408 (1971).

(b) Fong, F.K., Naberhius, S.L., and Miller, M.M. - J. Chem. Phys. 56, 4020 (1972).

(c) Wassam, W.A., and Fong, F.K. - J. Chem. Phys. 58, 956 (1973).

9. Fischer, S.F. - J. Chem. Phys. 53, 3195 (1970).

10. Judd, B.R. - Phys. Rev. 127, 150 (1962).

11. Ofelt, G.S. - J. Chem. Phys. 37, 511 (1962).

12. Krupke, W.F. - Phys. Rev. 145, 325 (1966).

13.(a) Weber, M.J. - Phys. Rev. 157, 262 (1967).

(b) Weber, M.J. - Phys. Rev. 171, 283 (1968).

14. Weber, M.J. - Phys. Rev. B4, 2932 (1971).

15. Grant, W.J.C. - Phys. Rev. B4, 648 (1971).

16. Yokoto, M., and Tanimoto, O. - J. Phys. Soc. Jap. 22, 779 (1967).

17. Van der Ziel, J.P., Kopf, L., and Van Uitert, L.G. - Phys. Rev. B6, 615 (1972).

18. Wright, J.C. - Private Communication.

CHAPTER III

EXPERIMENTAL DETAILS

3.1 Introduction

The decay times of fluorescence excited by a pulsed nitrogen laser (3371Å) have been measured in the systems $LaF_3:Nd^{3+}$ and $LaF_3:Dy^{3+}$. The nitrogen laser has been fabricated in the laboratory. The output power of the laser has not been measured. The pulsewidth of the laser is 7.5 nsec. The fluorescence output is collected in a direction perpendicular to the direction of the incident laser beam and is passed through a monochromator before detection with a photomultiplier tube. The detected output is displayed directly on an oscilloscope for measurement. The details of the experimental setup and the fabrication of the laser are discussed in the present chapter which is divided into three sections for convenience. The general theory and design consideration of the nitrogen laser are discussed in section 3.1.1. The actual fabrication details are given in section 3.2. Section 3.3 deals with the experimental setup used for the measurement of the decay times. Some of the

details of the nitrogen laser, discussed in this chapter have been published in our recent paper[24].

3.1.1. Nitrogen Laser - Theory and Design

Pulsed molecular nitrogen laser operating at 3371Å has attained considerable importance ever since it was first reported by Heard[1] in 1965. It is widely used as a pumping source for several organic dyes to obtain lasing action in the entire visible spectrum. The pulsewidth of the laser is not more than 10 nsec. This short pulsewidth is very helpful in the study of energy transfer processes in physical systems and their transient behaviour when excited.

A good number of papers have appeared in literature since 1965 on the improvement of the design for higher peak powers and better coherence. Most of the earlier workers have used pulsed electrical excitation methods[1-8] to obtain population inversion. Electron-beam pumping[14,15] has also been used recently with considerable success. The pulsewidth of the laser output is around 5-10 nsec in most of the cases. Decrease in pulsewidth to < 1 nsec has been obtained using high pressures[15,16,17]. The short pulses as indicated earlier, are extremely useful in the study of fast processes in physical systems for which, normally, mode locked lasers are used. The small pulsewidths of 5-10 nsec restrict the cavity length to 25-50 cms. The maximum number of possible 'round trips' (passes) for the photon inside the cavity is $\sim$ 5-10. High coherence of the beam is, thus not possible. Attempts have been made, successfully, to increase the pulsewidth of the N_2 laser to $\sim$ 100 nsec for use in tunable dye lasers.

Leonard[2] was the first worker to use the transverse excitation mechanism to obtain high power pulses (200 KW, 20 nsec). With a power density of 2.1 J/cm^3. In his design, a segmented aluminium plate is used as the anode. The cathode is a single solid aluminium block. The current pulses are obtained by discharging a capacitor through a spark switch. Coaxial cables are used to carry the pulses to the different segments of the anode. Based on the observations of Leonard, Gerry[3] developed the first theoretical model of the laser. He explained the excitation mechanism as due to the direct electron impact excitation of the triplet states $C^3\pi_u$ and $B^3\pi_g$. Frank-Condon factors favour excitation of $C^3\pi_u$ in comparison to $B^3\pi_g$. Steady state inversion is not possible by radiative deactivation alone as the lower level $B^3\pi_g$ has a longer radiative lifetime (10 μ secs) compared to the 40 nsec radiative lifetime of $C^3\pi_u$. He calculated the power output and power density in the medium assuming the laser medium to be coupled to a simple model of the electrical circuit - a capacitor C charged to a voltage V_o and coupled to the medium through a switch which is closed at t=0 to start the discharge. His calculations of power output and energy density were in good agreement with Leonard's results.

Calculations, based on the observations of Leonard[2] and Gerry[3], show that for efficient operation of the laser, a current density of 10^4 Amp/cm^2 and a current pulse risetime of 10^{12} Amp/sec are essential. Power output is more for higher current densities and faster rising current pulses. These requirements impose severe restrictions on the pulse generator. A low impedance, low inductance pulse generator capable of delivering high power is required. Geller[4] has made use of a coaxial pulse generator to meet these

requirements. The coaxial cables of low characteristic impedance are used as storage elements and as elements in the pulse forming network+. The stored energy is switched through a coaxial spark switch. This reduces the inductance of the circuit. Following the observation that the delay between the onset of the discharge and the start of the pulse is about a nsec, travelling wave excitation of the plasma was tried successfully. The basic idea is to start the excitation at one end of the plasma tube and then synchronize the excitation of each succeeding segment of the plasma with the arrival of the stimulated photons from the preceding segment, thereby obtaining laser radiation predominantly in the forward direction.

In the later modifications[7,9,10], flat plate transmission lines have been used as storage and PFN elements. Travelling wave excitation has been obtained by placing the spark gap judiciously at one corner of the transmission line as in the case of the designs of Basting et.al[7], Small and Ashari[8] or by placing the spark gap at the focus of the parabola etched out of the flat transmission line, as in the case of the design of Goddard[10]. Peak powers in the range of 1-5 MW have been obtained by many workers[9,10,11] with moderately high voltages of 10-15 KV. The pulsewidth is less than 8-10 nsec. The small signal gain of the laser is 100 dB/m. The gain saturates when the peak power exceeds 80 KW.

+ A pulse forming network (line) or a delay line is a pulse generator in which short pulses are produced by discharging the energy stored in a transmission line through the load resistance.

It has been observed that the residual ions and vibrationally excited metastable molecules degrade the performance of the laser if the discharge region is not cleared and replaced with a fresh volume of the gas immediately. The pulse repetition frequency is limited by the speed with which the gas is replaced. A repetition rate of 13 Kcps has been reported by Wilson[12] in a system in which the gas flows transversely between the electrodes with a speed of 2 Mach (twice the speed of sound in air). A similar work was reported by Targ[13].

Excitation methods, other than the electrical excitation, have been tried[14,15]. Dreyfus and Hodgson[14,15] have used electron-beam-pump excitation to excite the gas. The output pulse had a peak power of 2 MW with a width of 5 nsec. The efficiency of this method, as reported by them, is 0.15% which is small in comparison to the 0.6%-1% obtained with electrical excitation.

Increase of output power is possible if the density of the medium is very high. More number of molecules can be excited to the upper levels and a higher population inversion can be obtained. Higher voltages are required to keep the ratio of electric field per unit gas pressure the same. It has been observed that increase of excitation voltage and the gas pressure do not result in more power. Arching sets in with increased gas pressure and the output deteriorates. This problem has been overcome by establishing a preionization background plasma prior to the ionization of the main discharge. Lasing has been obtained using preionization for pressures upto 3 bar[15,16,17]. The pulsewidth of the power output is found to be narrower at high pressures. This is the result of the decreased lifetime of the upper laser level at high

pressures. Pulsewidth of 50 psec was reported for an operating pressure of 6 bar[19]. The shorter pulsewidth of the output makes it necessary to use the travelling wave mode of excitation, for, the plasma may not last longer than the single transit time of the photon in the plasma tube, if the plasma column is sufficiently long. Tapered electrode gaps have been used to axhieve this[17].

The high resolution study of $C^3\pi_u - B^3\pi_g(0,0)$ stimulated transition has been done by Parks et.al[18] and all the wavelengths in the 3371Å band have been recorded with the help of a crossed Echelle concave grating spectrograph. Their studies also led to the understanding of high gain profiles of travelling wave in a Doppler broadened transition.

Ali et.al[19] have improved the original theory of Gerry[3] by including collisional mixing of laser levels, the loss of energy to the vibrational levels of the ground state and the collisional ionization from the upper laser level. Assuming the laser medium to be coupled to a simple model of electrical circuit, Ali et.al have obtained, the dependence of power output on all the circuit parameters-voltage, capacitance, inductance and also on the fill pressure. The results show that the power density depends on the electron temperature and electron density. The loss of the energy to excited vibrational levels of ground state is less, the higher the electron temperature. The circuit parameter which affects the power output to a large extent is the circuit inductance. Based on their calculations, Ali et.al have discussed some of the design parameters.

The electrical equivalent circuit for the laser is due to Geller et.al[6]. They have treated it in terms of lumped circuit elements. Anderson[20] has

reported a much improved model which takes into account the inductance and impedance of spark gap, the transmission lines as distributed elements and the plasma tube. A complete mathematical analysis has been given. His calculations show that the performance of the pulse generator can be improved if rise-time of the voltage pulse generated by the spark gap does not exceed the formative time for the breakdown of the gas in the plasma tube. Similar conclusions were reported by Schwab et.al[21] from their measurements of voltage and current waveforms across the plasma tube before and after the breakdown of the plasma. The observations were explained by a circuit model in which all the elements are treated as lumped circuit elements.

3.1.2 Basic Theory of Nitrogen Laser

In this section the basic theory of the nitrogen laser is discussed. The treatments of Gerry[3], Ali et.al[19] and Goddard[10] have been followed to a large extent.

a. Rate equations and condition for inversion: The nitrogen laser can be treated as a three level system - the upper laser level $C^3\pi_u$, the lower laser level $B^3\pi_g$ and the ground level.

Let N_1, N_2, N_3 be the populations of the upper, lower and ground level respectively. Let X_{ij} represent the rate of excitation of the molecules from level i to level j by electron collisions, Y_{ji} the collisional deexcitation rate of molecules from level j to level i, R_{ji} the rate of induced emission including the Einstein coefficient A, energy density and line width and τ_{ij} the rate of radiative decay of the molecules from the level i to level j.

The rate equation can be written as

$$dN_3/dt = X_{13} N_1 + X_{13} N_2 - (Y_{31} + Y_{32} + \tau_{31}^{-1} + \tau_{32}^{-1}) N_3$$

$$- R_{32}^{i} (N_3 - (g_3/g_2)N_2) \qquad (3.1)$$

$$dN_2/dt = X_{12} N_1 + (\tau_{32}^{-1} + Y_{32})N_3 - (\tau_{21}^{-1} + Y_{21} + Y_{23}) N_2$$

$$+ R_{32}^{i} (N_3 - (g_3/g_2)N_2) \qquad (3.2)$$

$$dN_1/dt = -(X_{12}+X_{13})N_1 + (\tau_{31}^{-1} + Y_{31})N_3 + (\tau_{21}^{-1} + Y_{21})N_2 \qquad (3.3)$$

where g_2 and g_3 are the statistical weights of the lower and upper laser levels respectively.

These equations have been solved analytically under certain assumptions and general criteria have been obtained for the steady state and pulsed excitation.

Applying these equations to the case of nitrogen molecule-specifically to the electronic transition $C^3\pi_u(v=0) \longrightarrow B^3\pi_g(v=0)$ with the following approximations:

i. the induced emission and absorption rates (R_{ji}) as well as the collisional deexcitation rates of the upper (Y_{31}) and lower levels (Y_{21}) to the ground level are neglected,

ii. $\tau_{31} > \tau_{32}$ (since level C is metastable), $X_{13} > X_{12}$ according to Frank-Condon principle and $\tau_{21} >> \tau_{32}$, we have

$$N_3 + N_2 = X_{13} N_1 t \qquad (3.4)$$

Equation (3.4) and (3.1) lead to

$$dN_3/dt = X_{13} N_1 + (X_{13} N_1 t - N_3)X_{23} - (\tau_{32}^{-1} + Y_{32})N_3 \qquad (3.5)$$

Equation (3.5) on solving gives

$$N_3 = (N_1 X_{13}/\alpha^2)(Y_{32} + \tau_{32}^{-1}) - (N_1 X_{13}/\alpha^2)(Y_{32} + \tau_{32}^{-1}) + (N_1 X_{13} X_{23} t/\alpha) \qquad (3.6)$$

where $\alpha = \tau_{32}^{-1} + Y_{32} + Y_{23}$

For small times

$$N_3 = N_1 X_{13} t - N_1 X_{13} (Y_{32} + \tau_{32}^{-1})t^2/2 \qquad (3.7)$$

Equation (3.7) and (3.2) yield

$$N_2 = \tfrac{1}{2} N_1 X_{13} (Y_{32} + \tau_{32}^{-1})t^2 \qquad (3.8)$$

from which we get the expression for population inversion as

$$N_3 - N_2 = N_1 X_{13} t (1-(Y_{32} + \tau_{32}^{-1})t) \qquad (3.9)$$

Thus, population inversion occurs for times of the order of

$$t < 1/(\tau_{32}^{-1} + Y_{32}) \qquad (3.10)$$

If we neglect the effect of collisional mixing i.e. $\tau_{32}^{-1} \gg Y_{32}$ the above inequality reduces to Bennet's criterion for inversion in a pulsed laser with a bottle neck lower level. However, for

electron densities of $N_e > 6 \times 10^{14}$ cm^{-3}, Y_{32} will exceed the radiative decay rate τ_{32}^{-1} and the time of inversion is reduced further[19].

b. Rate equations coupled to the circuit: Consider now the case of the nitrogen molecule as a lasing medium coupled to the electrical circuit consisting of a capacitor C charged to a voltage V_o with a fixed external resistance R_e and inductance L. The lasing medium acts as a time varying resistance R(t) which is the sum of the resistance due to ion-electron collisions and the electron-neutral molecule collisions.

The rate equations are

$$dN_3/dt = X_{13} N_1 + X_{23} N_2 - (\tau_{32}^{-1} + Y_{32}) N_3 - R_{32}^{i} (N_3 - N_2) \qquad (3.11)$$

$$dN_2/dt = X_{13} N_1 + N_3 (\tau_{32}^{-1} + Y_{32}) - (\tau_{21}^{-1} + Y_{23}) N_2 + R_{32}^{i} \times (N_3 - N_2) \qquad (3.12)$$

The energy density ρ at the laser frequency is given by

$$(1/E_1)(d\rho/dt) = N_3 \tau_{32}^{-1} + R_{32}^{i} (N_3 - N_2) \qquad (3.13)$$

where E_1 is the energy of the laser photon.

The rate of ionization is

$$dN_e/dt = N_e N_1 S \qquad (3.14)$$

where S is the ionization rate coefficient.

The electron energy equation is given by

$$d/dt\ (3/2\ N_e T_e) = \gamma\ I^2 R(t) - N_1(X_{13}\ E_{31} + X_{12}\ E_{21}) - N_e\ N_1\ SE_{\infty}$$

$$- N_e\ N_1\ \overline{X_V E_V} - E_{32}(N_2\ X_{23} - N_3\ Y_{32}) \qquad (3.15)$$

where E_{ji} is the energy of transition from $j \rightarrow i$. E_{∞} is the ionization energy of the nitrogen molecule, T_e is the electron temperature, I is the total current and γ conversion factor. Here the first term on the right represents the Joule component of electron energy input into the medium while the second and third terms represent energy loss by collisional excitation to the laser levels and to ionization. The fourth term is the loss of energy to excited vibrational states of the ground level. The last term gives difference between the energy loss due to the collisional excitation of lower laser level to the upper laser level and the gain due to the collisional de-excitation of the upper laser level to the lower laser level.

The circuit equation is

$$LdI/dt + R(t)\ I = V_o - \int_o^t (Idt'/C) \qquad (3.16)$$

Power density can be calculated by solving the above equation numerically. Since it has been observed that saturation occurs with moderate pressures, it would be worthwhile to examine the above equation under saturation assumption.

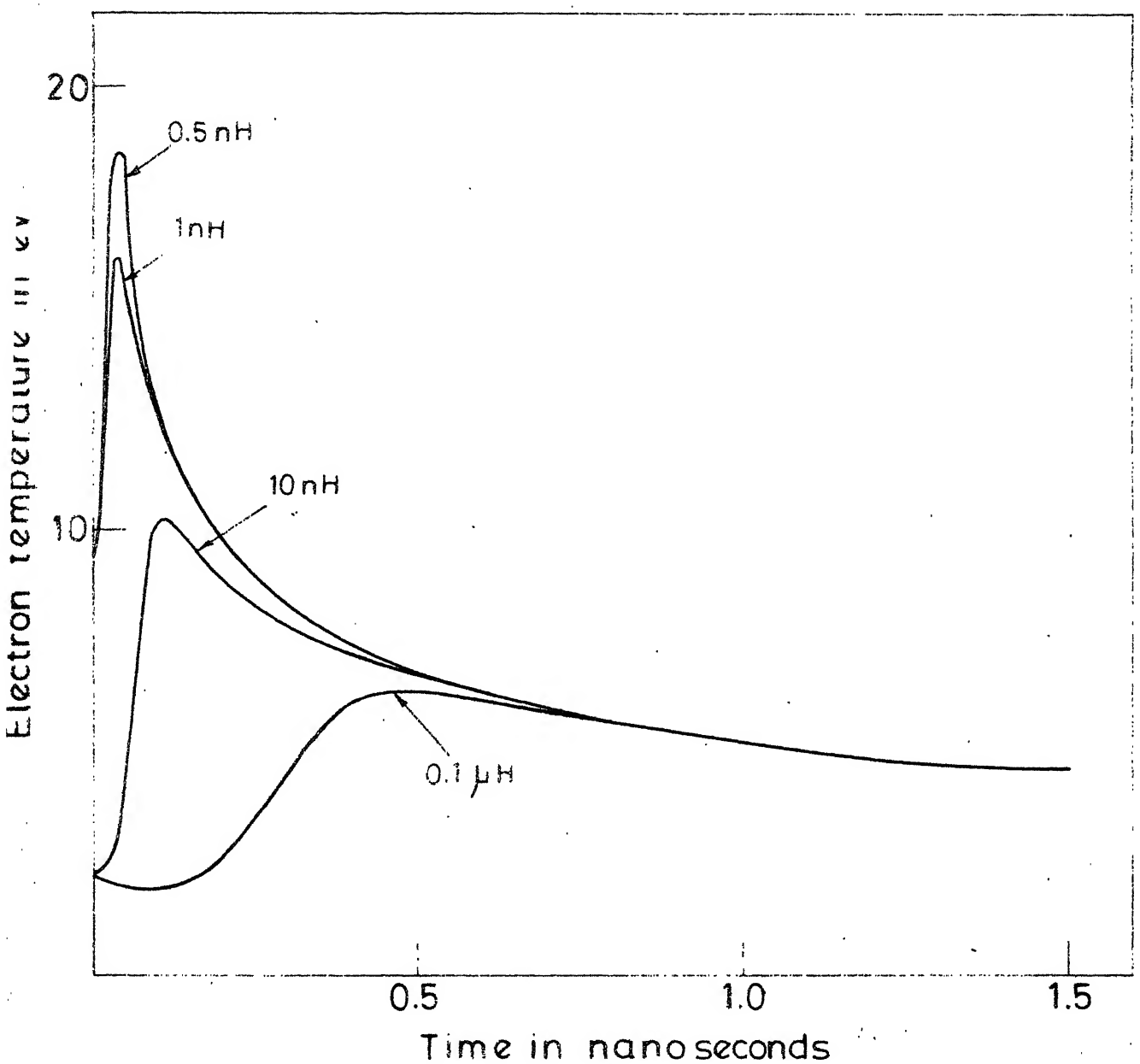

Fig. 3.1 Time history of the electron temperature for different inductances (ref.19b).

Thus, with $N_3 - N_2 \ll N_3$ and $N_3 \approx N_2 = N$, the equations (3.11) and (3.12) lead to

$$dN/dt = - N/2\,\tau_{21} + (N_1/2)(X_{13} + X_{12}) \qquad (3.17)$$

and $$P = R^{i}_{32}(N_3 - N_2) = (N_1/2)(X_{13} - X_{12}) - N/\tau_{32} + N/\tau_{21}$$

$$- N\,(Y_{32} - Y_{23}) \qquad (3.18)$$

Equations (3.13-3.18) have been numerically solved by Ali[19] for two different methods of excitation, one, a fast rising current pulse (rise time $\sim$ 0.3 nsec) and decaying slowly, and the other, a sine wave current discharge with a time period larger than that of the laser pulse. The power output in the first case is very much larger than in the second case. This is easy to understand, since, with a faster current pulse, higher electron densities and electron temperature can be obtained and the loss of energy to the excited vibrational states of the ground level is small.

The results also show that after the onset of discharge, the electron temperature reaches a maximum within the first nanosecond and falls off rapidly (fig. 3.1). The electrons are rapidly cooled down to temperatures below 6 eV in the first 2 nsec. The rate of energy loss to the excited vibrational states predominates all other loss mechanisms at these temperatures curtailing the excitation of molecules to the upper laser level (fig. 3.2). Thus the power pulse is narrower than what it would have been had there been no excitation of vibrational states of

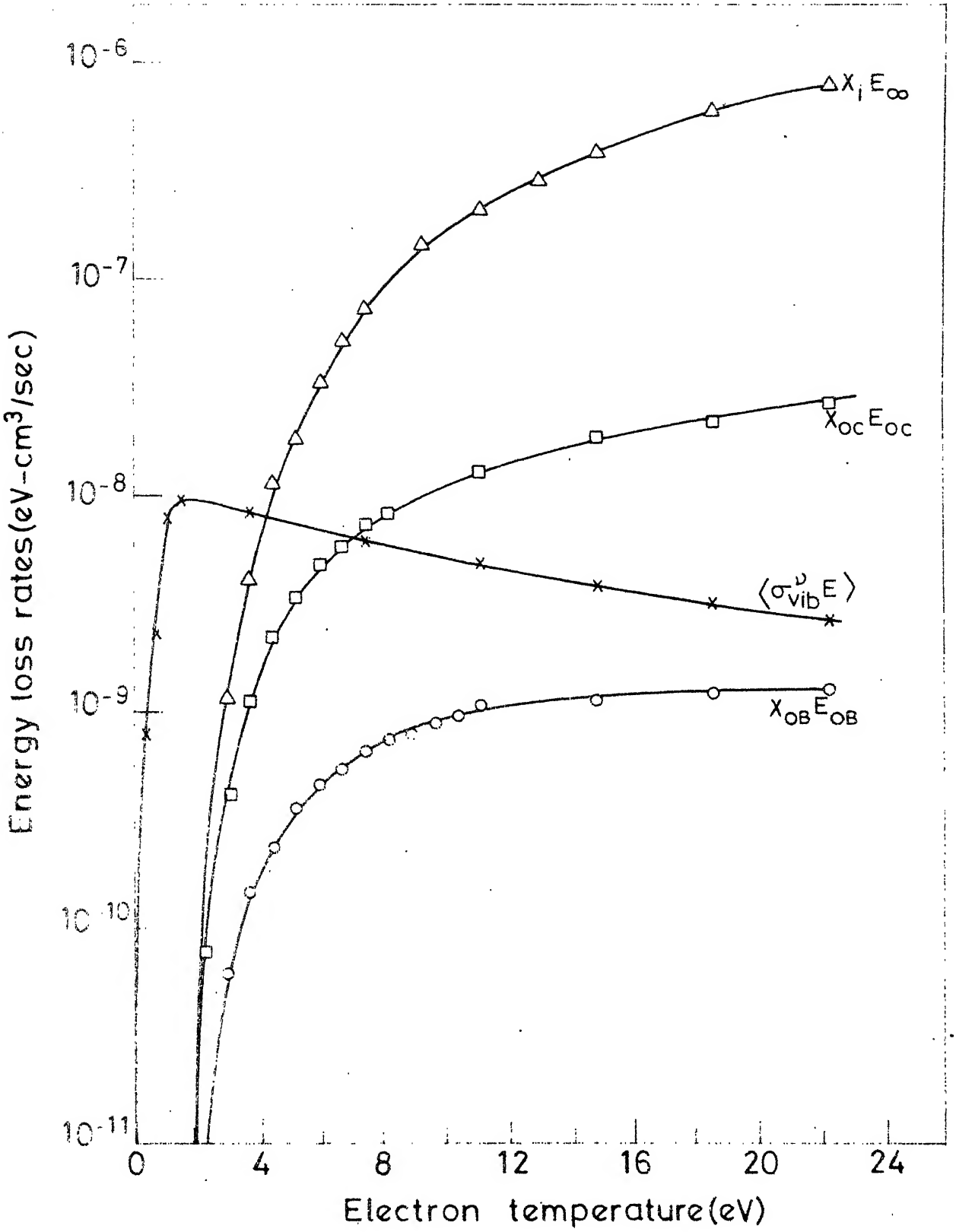

Fig. 3.2 Electron energy loss rates as a function of electron temperature. Here $X_{OC}E_{OC}$ and $X_{OB}E_{OB}$ are the rates of energy loss in the excitation of levels C and B respectively. X_iE_∞ is the rate of energy loss in the ionization of the nitrogen molecules. The energy loss by the excitation of the vibrational states is shown by $\langle \sigma^{\nu}_{vib} E \rangle$ (From ref. 19b)

ground level. The effect of collisional mixing of laser levels is to reduce the width and the peak of the pulse furthermore.

Good agreement with experimental results has been obtained by Ali[19] using the equations under saturation approximation.

The exact solution of the equations is in agreement with what is obtained under saturation approximation except for one difference. The exact solution predicts a very intense short duration oscillation (psec) within the first 0.3 nsec after the buildup from noise. This is not difficult to see. A fast rising current pulse will populate the upper level at a very fast rate resulting in $N_3 >> N_2$ which gives rise to the early oscillation. Saturation approximation ($N_3 \simeq N_2$), however cannot predict this behaviour.

The dependence of peak power and pulsewidth of the power output on the circuit parameters like inductance, charging voltage and storage capacitance have been obtained by Ali[19] from the above equations. The following are the conclusions.

1. The power density, the electron density and electron temperature increase with decreasing circuit inductance whereas the pulse width decreases. However, the total energy density i.e. peak power density times the half width of the laser pulse is larger for smaller circuit inductance (fig. 3.3).
2. The electron density and electron temperature and hence the power density increase with increasing charging voltage. The pulse becomes narrower.
3. The peak power density is higher and the pulse is narrower as the pressure is increased. However, there is an optimum value for the pressure. Increasing pressure beyond this would cool the electrons and the output power is reduced.

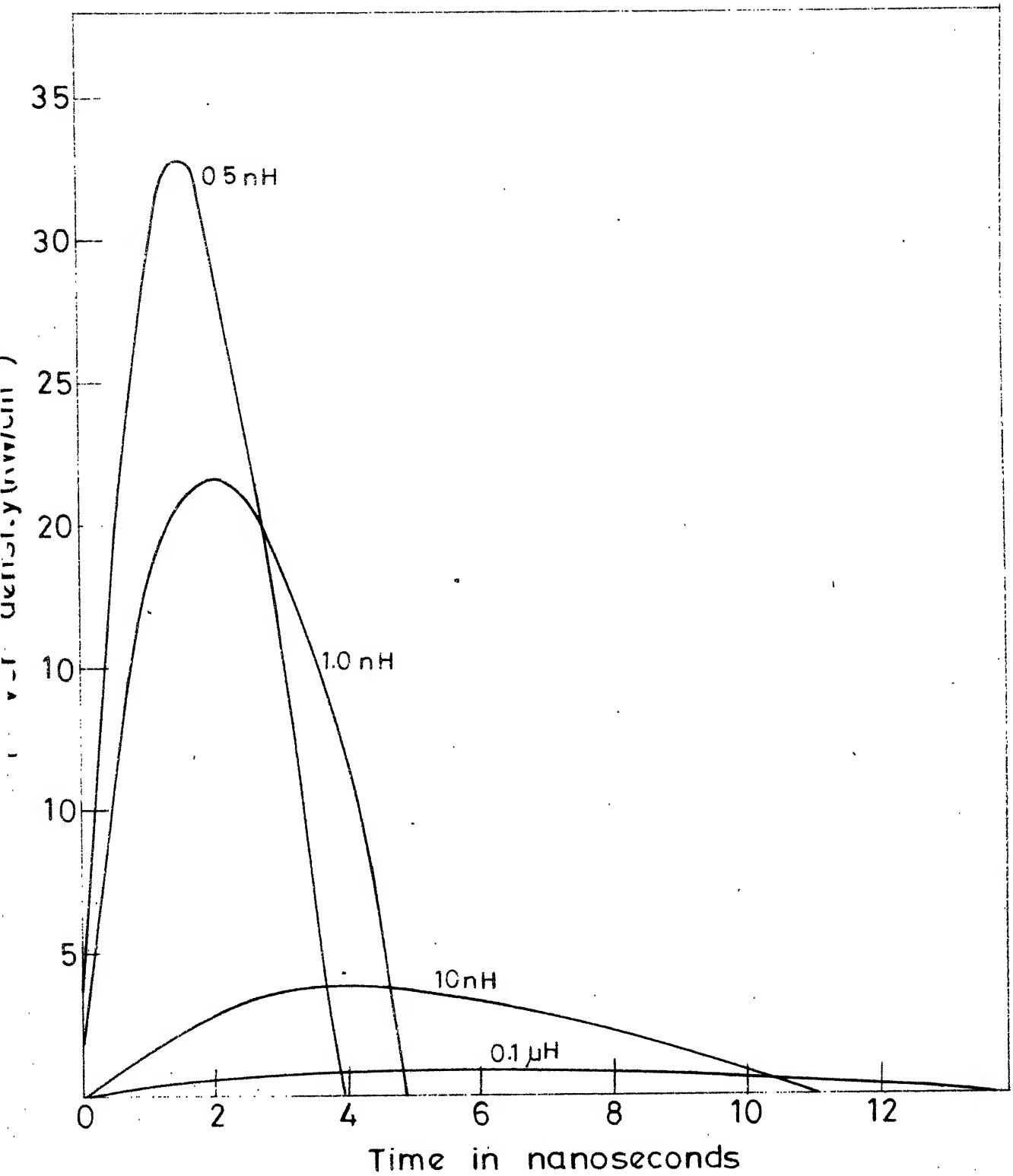

Fig.3.3 Power density as a function of time for several different values of circuit inductances. (From ref.19b)

The efficiency of the laser can be calculated from the calculated power output. The energy input to the system is $\iint j^2 dVdt$ and the energy output is $\iint P\, dVdt$ where the volume integration is over the total volume of the active medium and the time integration is over the current pulsewidth. Gerry's calculations predicted an efficiency of 2.1% while the observed value is 0.6%-1%.

c. Calculation of best value for E/p(electric field per unit pressure): Cartwright[21] has worked out the total cross section for the excitation of the triplet electronic states of nitrogen molecules as a function of electron energy for v"=0 of the ground state. From his results it is found that an energy of 16 eV is required to produce the highest possible population inversion between $C^3\pi_u$ and $B^3\pi_g$ levels. Goddard[10] has calculated the mean free path of the electrons of 16 eV in nitrogen from the relation

$$\lambda = (\sigma N)^{-1} \qquad (3.19)$$

where σ is the total cross section for excitation of nitrogen molecules to higher electronic states by collisions and N is the density of the molecules of the gas. He has shown that λ comes out to be 0.064 cm/torr. Hence the maximum field required for an electron to acquire an energy of 16 eV in one mean free path at a pressure of one torr is $E=16/\lambda$. This gives a value of 250 V/torr approximately. The experimentally observed value for best E/p is 200V/cm torr.

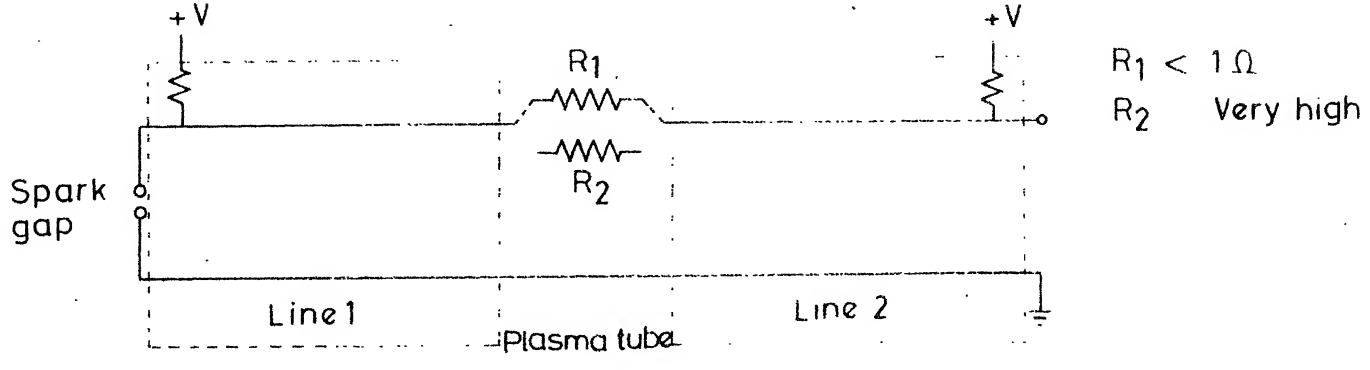

Fig. 3.4 Blumlein circuit.

3.1.3 Principle of Operation

In this section the principle of operation of an actual circuit is described. The various designs that have been reported assume ideal circuit elements. This has been contested by some of the authors specifically, in the case of the travelling wave excitation mechanism. The idea was first proposed and tried successfully, by Shipman[5]. He obtained a ratio of 10:1 between the forward and backward laser power outputs in a plasma column of 1.83 m. This has been confirmed later, by Basting et.al[7], and Goddard[10]. A number of papers have appeared since then, which provide evidence to the contrary. A more detailed discussion of this point is presented at the end of the section.

It has been observed that the efficiency and the output of the laser depend on the spark gap parameters to a great extent. The behaviour of the electrical circuit is very close to the ideal circuit if the spark gap rise-time is smaller than the formative time of the plasma. The operation of the ideal circuit can be explained in terms of the transmission line theory. On the other hand, if the spark gap risetime is much larger than the formative time, the behaviour of the circuit is far from ideal. The circuit can only be explained in terms of lumped circuit elements[6,21,23].

a. Case of ideal circuit: The flat plate transmission line circuit is shown in Figure 3.4. The lines are of equal length and impedance. They are connected such that the load (the plasma) comes in series with them. The lines are charged in parallel to a voltage V and discharged in series through a switch S. This configuration is called the Blumlein circuit. Unlike the original Blumlien circuit, this circuit has, for

load, a rapidly time varying resistance which varies from a very high value to a fraction of an ohm in a nanosecond.

Let the lines be initially charged to a voltage V. At t=0 one of the lines - line 1 is shorted through the switch S. This sets up a voltage pulse of -V which travels towards the load-end. There is an impedance mismatch at the beginning of line resulting in a transmitted pulse whose amplitude is less than -V.

Assume that the impedance of the line and of the switch are equal. The transmitted pulse, in this case, has an amplitude of -V. At the load-end there is another impedance mismatch. The load behaves as an open circuit to begin with, resulting in a total reflection of the pulse with a reflection coefficient of +1. This leaves the terminal of the load at the end of line 1 (cathode) at -V. The anode is at +V thereby creating a potential difference of 2V. The plasma discharge does not start immediately as it has a finite formative time. The reflected pulse travelling towards the shorted end of line 1 takes a finite time 2τ to return to the load with an amplitude of +V. In most of the cases the transit time τ is larger than the formative time T with the result that the discharge starts before the pulse reaches the load. The breakdown pulse travels from the anode to cathode and also towards the shorted end of line 1. On reaching the cathode a current pulse is reflected back and forth in the discharge tube, gradually attenuating in each passage. All the subsequent reflections from the end of the lines elongate the current pulse. The total power output

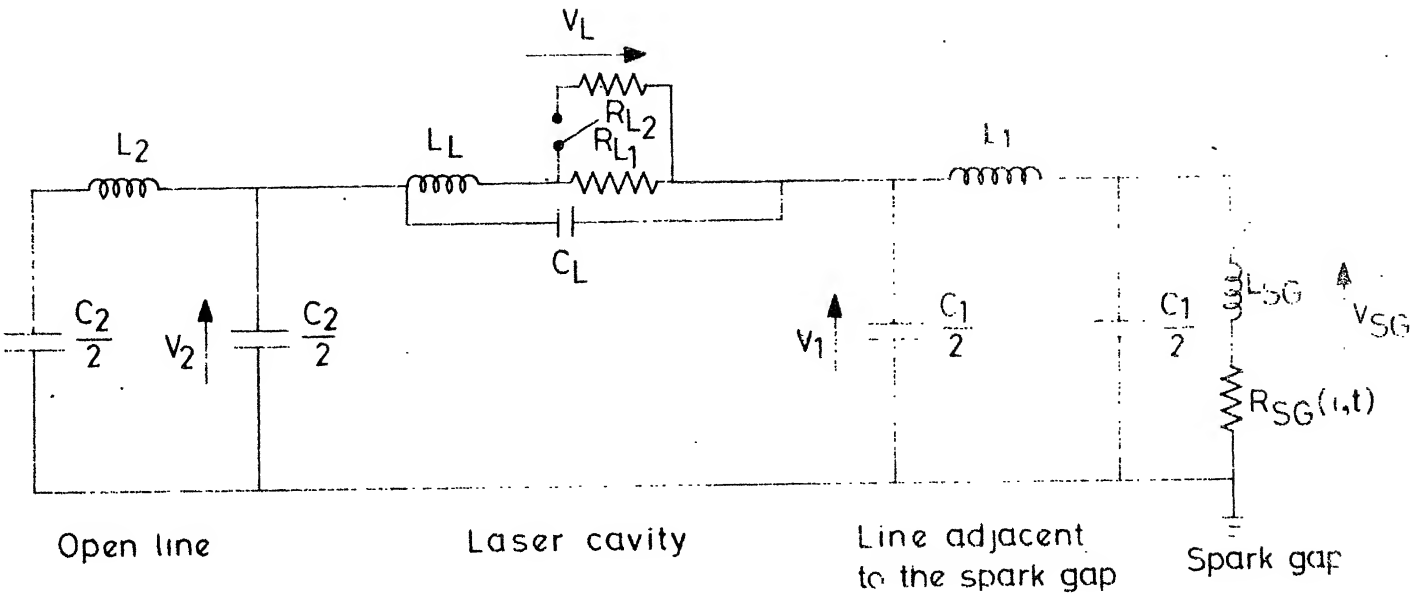

Fig. 3.5 Equivalent circuit of nitrogen laser-Schwab's model.

depends on the energy transferred from the lines to the plasma in the first transit of the pulse, since the electron density and electron temperature reach to a maximum in the first 2-4 nsec.

b. Case of nonideal circuit: The circuit is the same as shown in Figure 3.4. The spark gap which has been assumed to be ideal in the first case, has a risetime which is longer than the transit time of the electromagnetic wave in the line.

In this case, it is not possible to treat the flat plates as transmission lines. They act as simple storage capacitors with small inductance. The plates are initially charged to a voltage V. At a set time t=0, the capacitor C_1 is shorted through a switch S. The voltage across the capacitor C_1 falls to zero with the time constant of the switch S. This creates a potential difference between the two electrodes of the plasma tube. After a finite formative time the discharge starts in the tube.

The equivalent circuit for this case has been given by Schwab et.al[4] (fig. 3.5). They have calculated the voltage pulses on the switch and the electrodes. Their experimental measurements were in agreement with the calculated values.

The power output in this case depends on the impedance matching that can be obtained between the capacitor 2 and the plasma resistance.

Travelling wave excitation of the plasma is possible only in (a). This is not difficult to understand. The spark gap has a small inductance. This results in high electron temperature and electron densities

(see 3.1.2). The electron temperature falls to $\lesssim 6$ eV within 2 nsec after the onset of discharge, thereby increasing the energy losses. The rate of stimulated emission depends on the population inversion encountered by the stimulated photons at the time of interaction. Hence, if the population inversion is maintained at near maximum at the time of interaction, the output will be maximum. This is achieved by travelling wave excitation.

3.1.4 Design Considerations

It was seen in the earlier sections that flat plate transmission lines are ideally suited for energy storage and pulse forming network. The low impedance and low inductance offered by these, make it possible to achieve high current densities and small current risetimes. The only critical circuit element is the spark gap. Efficiency of the laser can be improved by improving the performance of spark gap. The following equivalent circuit for the spark-gap[20] makes this point clear.

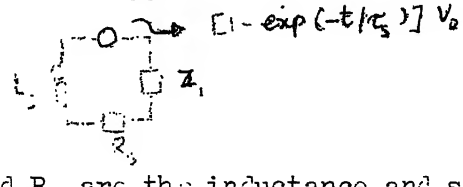

Here L_s and R_s are the inductance and spark resistance of the gap. Z_1 is the impedance of the line connected to the gap. τ_s is the time constant of the spark gap. This includes the finite breakdown time of the spark. V_o is the voltage applied to the spark gap before the breakdown. The voltage appearing across Z_1 is given by

$$V_1(t) = V_o \frac{1}{R_s+Z_1} \left(1 - \frac{b}{b-a} e^{-at} - \frac{a}{a-b} e^{-bt}\right) \qquad (3.20)$$

where $a = (R_s + Z_1)/L_s$ $\qquad b = 1/\tau_s$

This equation shows that the voltage pulse in Z_1 depends on the time constants a and b. For sharp pulses both a^{-1} and b^{-1} have to be small. τ_s can be decreased by pressurizing and reducing the gap length of the spark gap. L_s can be decreased by decreasing the overall size of the gap and careful design.

3.2 Fabrication Details - Nitrogen Laser

In this section construction details of the nitrogen laser are presented. The first half of the section describes the Blumlein circuit and the plasma tube. Power supply and triggering circuit are given in the second half.

3.2.1 Blumlein Circuit

The Blumlein circuit is shown in Figure 3.6. Two double copper clad glass epoxy sheets (M/s. Formica India Ltd.) of sizes 90 x 60 cm^2 x 1.5 mm thickness are used as the transmission lines. The outer conductors are at ground potential while the inner conductors are charged to high DC voltage of 10-12 kV. Part of the copper is etched out from the edges on all sides of the sheets to avoid surface breakdown. Parabolic etching is done at one end of the top conductor of the bottom sheet for obtaining travelling wave excitation (fig. 3.7). The spark gap is placed at the focus of the prabola. The diverging wavefront produced by the spark gap is reflected from the parabola and

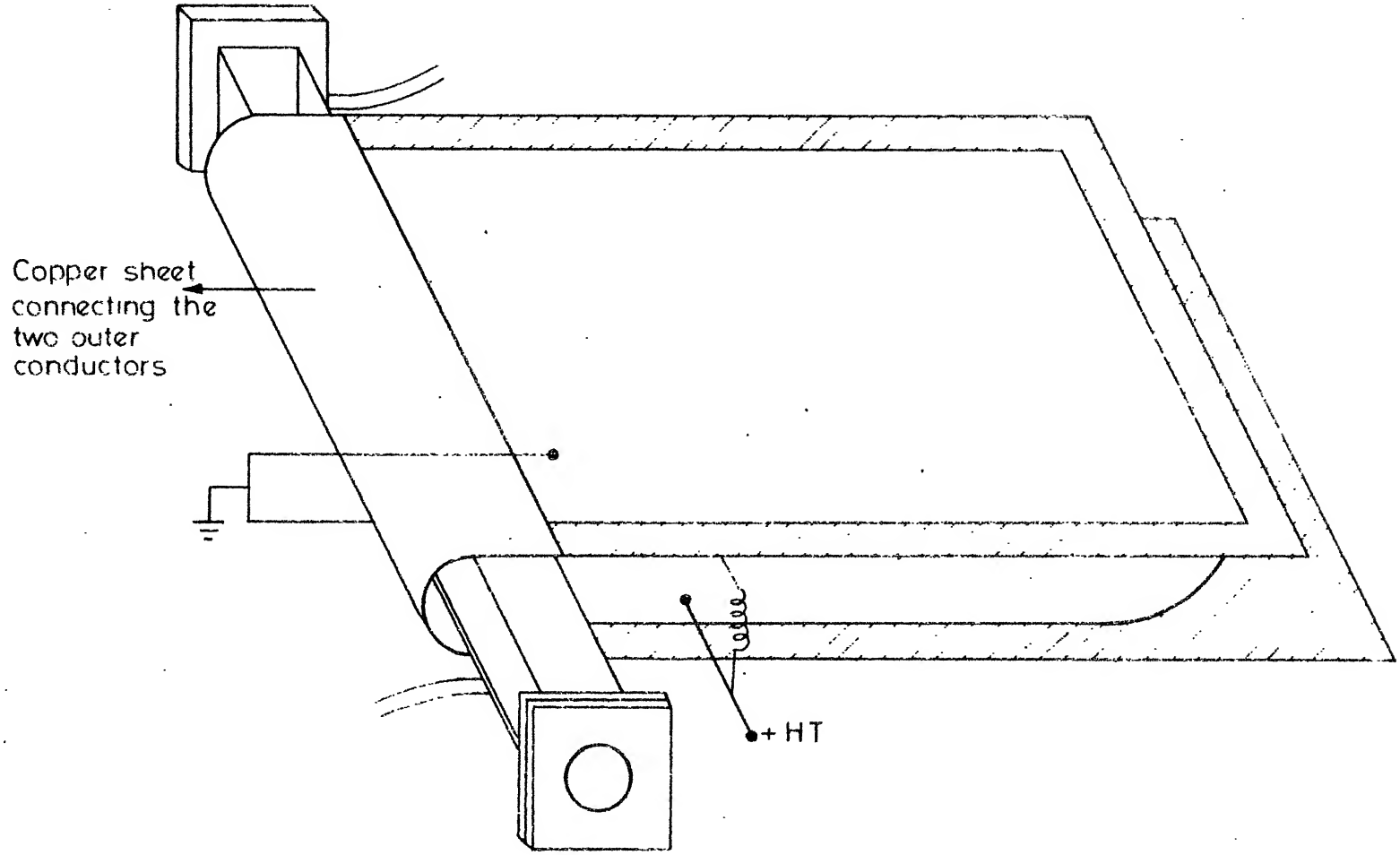

Fig. 3.6 Blumlein circuit - actual.

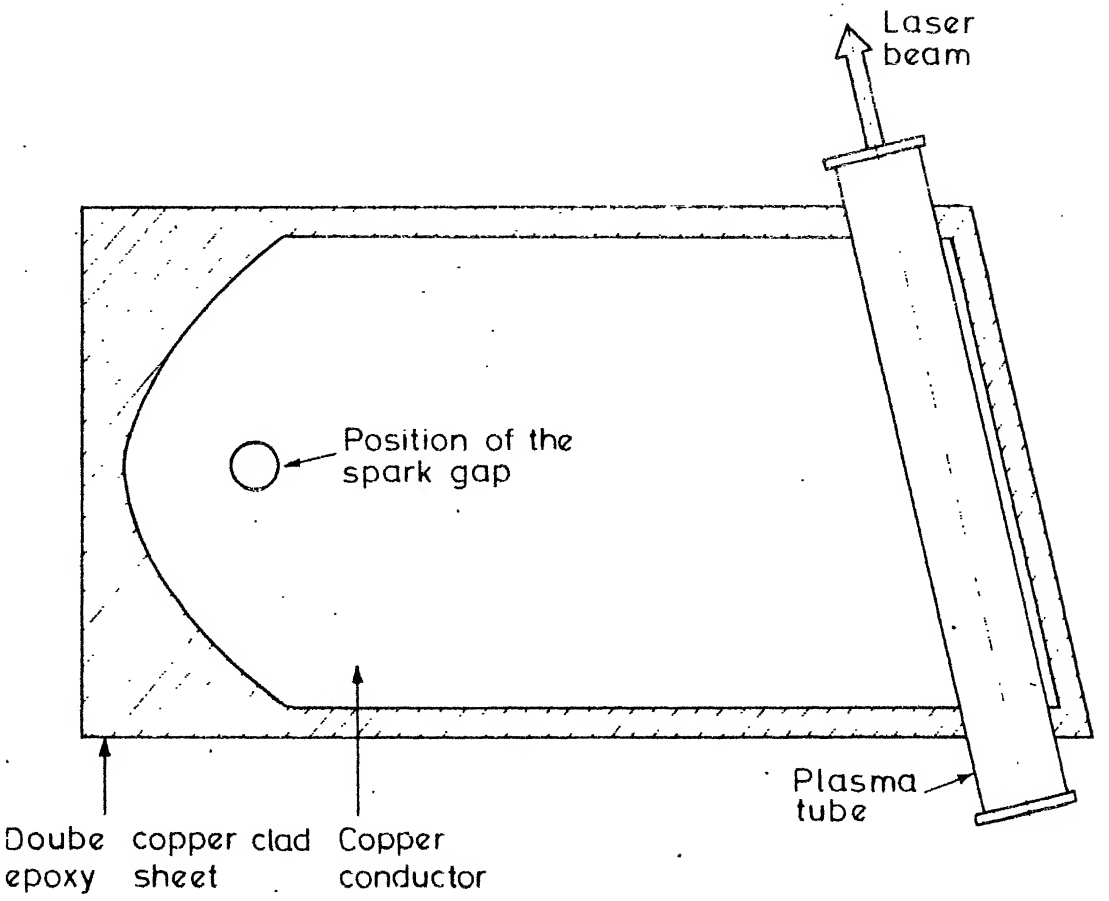

Fig. 3.7 Parabolic etching of the double copper clad sheet.

is converted to a plane wave while the direct forward wavefront is blocked by insulating the spark gap from the conducting sheet. The plasma tube is placed on the conductor with its axis at an angle θ to the axis of the parabola. This introduces a time delay between the excitation of the different segments of the plasma. The angle is so chosen that the time taken by the photon to travel the distance between any two points in the plasma tube is equal to the difference in the time taken by the travelling wave to reach these points. A simple calculation shows that θ is given by the relation $\sin\theta = \sqrt{1/\varepsilon}$ where ε is the permittivity of the dielectric of the line. At the focus of the parabola where the spark gap is placed, a hole is punched in the sheet for the spark to pass. Enough insulation is provided around the hole by etching the copper. The characteristic impedance Z of the parallel plate transmission line is given by

$$Z = Z_0 s/L\sqrt{\varepsilon}$$ and the capacitance by

$$C = \frac{\varepsilon L l}{s}$$

where $Z_0 = 377\ \Omega$ is the characteristic impedance of free space, s is the thickness of the dielectric, L is the width of the sheet, l is the length of the sheet and ε is the permittivity of the dielectric.

In the present case $\varepsilon = 4.8$, s=1.5 mm, L=55 cm and l=85 cm.

This gives a sheet capacitance of 30 nF per sheet and less for the other, and a total impedance of 0.43 Ω per sheet. The total stored energy is about 2 J/sheet at an operating voltage of 12 KV. The one-way transit time $\tau = l\sqrt{\varepsilon}/C$ is 6.2 nsec. The angle of tilt θ is 27°6'.

3.2.2 The Plasma Tube

The plasma tube is a perspex box with rectangular cross-section - 5.5 cm x 5.0 cm (fig. 3.8). The length of the box is 80 cm. Two sides of the box are made of perspex. The T shaped brass electrodes themselves form part of the other two sides, the rest being made of perspex. The electrodes are rounded off to avoid sharp edges. A gap of 12 mm is maintained between the electrodes. All the sides of the plasma box are sealed tightly with araldite to avoid gas leaks. The box is so placed on the sheets that the two electrodes touch the two inner surfaces. The box and sheets are held in position by clamping them together. A silver coated plane mirror is placed at one end of the box. The other end is closed with a plane quartz window.

Two ports are provided at the two ends of the tube for gas flow. One port is connected to a rotary vacuum pump. The other port is connected to a gas cylinder through a needle valve and a manometer to regulate the pressure. Commercial nitrogen gas is used. The optimum pressure for an excitation voltage of 12 KV DC is found to be 40 mm of Hg.

3.2.3 Spark Gap

The spark gap consists of two metal (brass) cups, each of diameter 7 cm OD to which the electrodes (cylindrical rods) are attached as shown in Figure 3.9. Two bakelite discs, together with the central teflon tube lock the brass cups on to the two conducting sides of the bottom plate. The trigger pin passes through the grounded electrode. Air inlet and outlets are provided for circulating gas under pressure. Normally, the gap is operated with air flowing

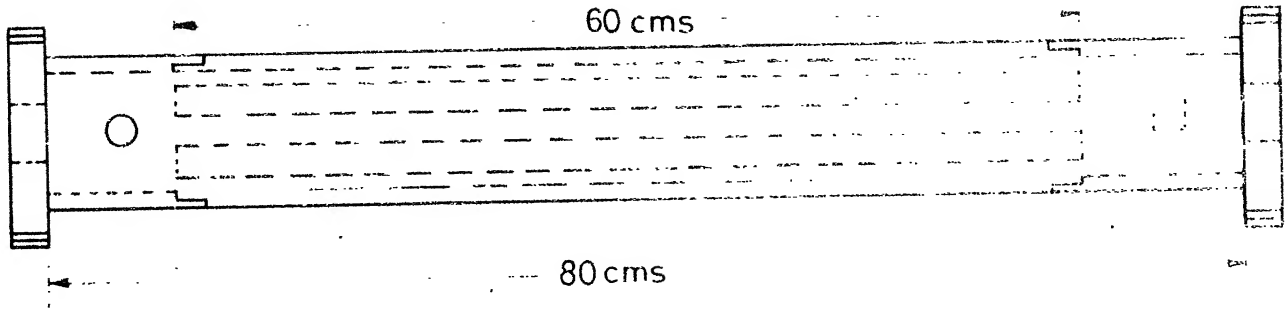

(a)

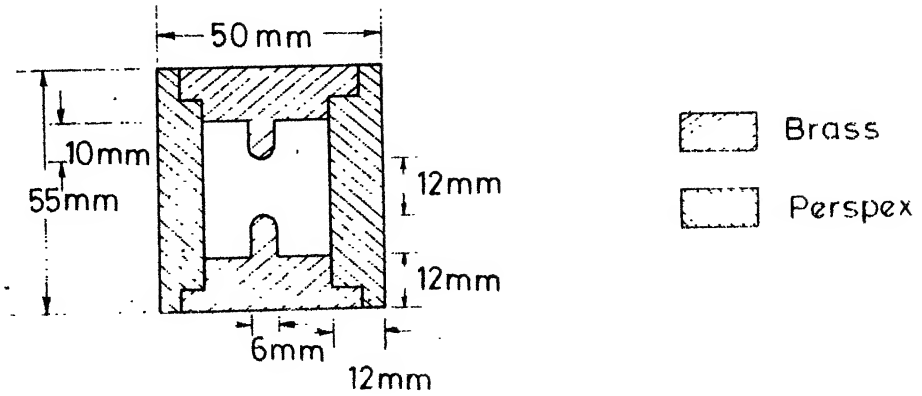

(b)

Fig. 3.8 Plasma tube.

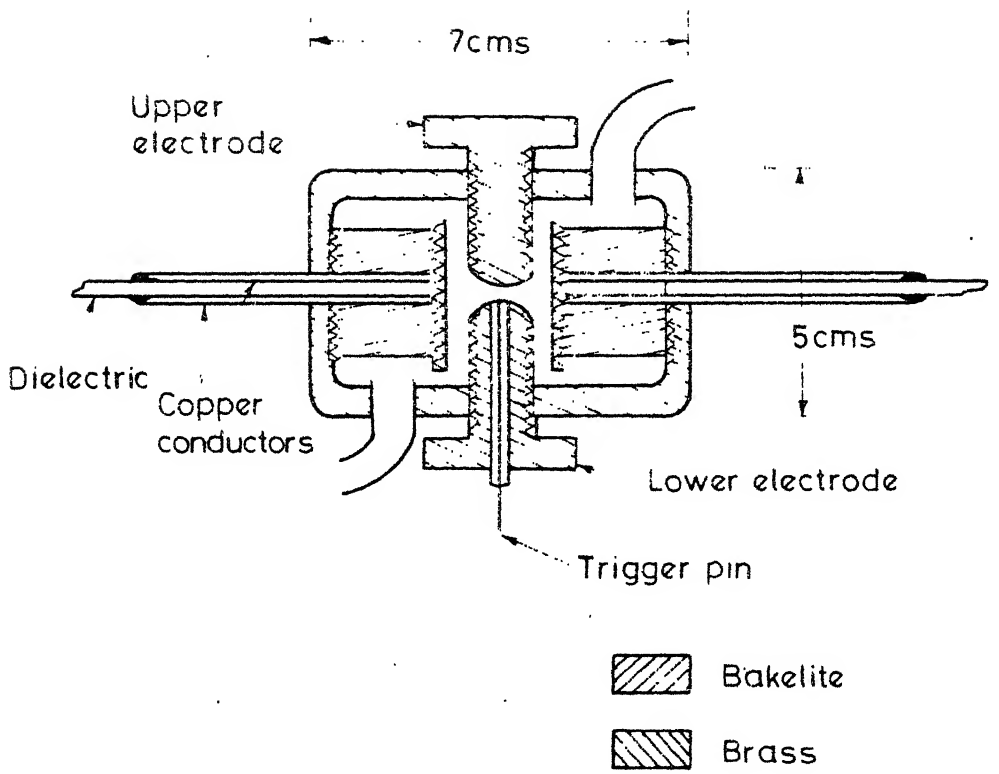

Fig. 3.9 Spark gap.

through it at a pressure of about 2 bar. The entire spark gap structure is more or less symmetrical. Enough insulation space is provided around the hole in the sheet through which the central teflon tube enclosing the electrodes is inserted. It is found that the electrode surface has to be cleaned periodically for good performance.

3.2.4 High Voltage Power Supply

The high voltage required for the excitation is obtained from a 40 KV power supply built for general purpose. The circuit diagram is shown in Figure 3.10.

The power supply has two charging resistors. One is of 500 KΩ, 1200 W and the other of 50 MΩ, 50 watts, both connected in series. Both are used for low repetition rate. The high resistance is shorted at high repetition rate with the short that is provided.

3.2.5 Trigger Pulse Generator

The pulse repetition frequency of the laser is controlled by the triggering rate of the spark gap. The trigger pulses are produced by a trigger generator, the circuit diagram of which is given in Figure 3.11a. The trigger generator consists of a hydrogen thyratron acting as a switch, a coaxial pulse forming network and the auxillary mercury thyratron to fire the hydrogen thyratron. The auxillary mercury thyratron is triggered by the gate pulses of a scope (Tetronix 545 A or B) or by a standard pulse generator. The pulse forming network, the hydrogen thyratron and the spark gap together, act as a Blumlein

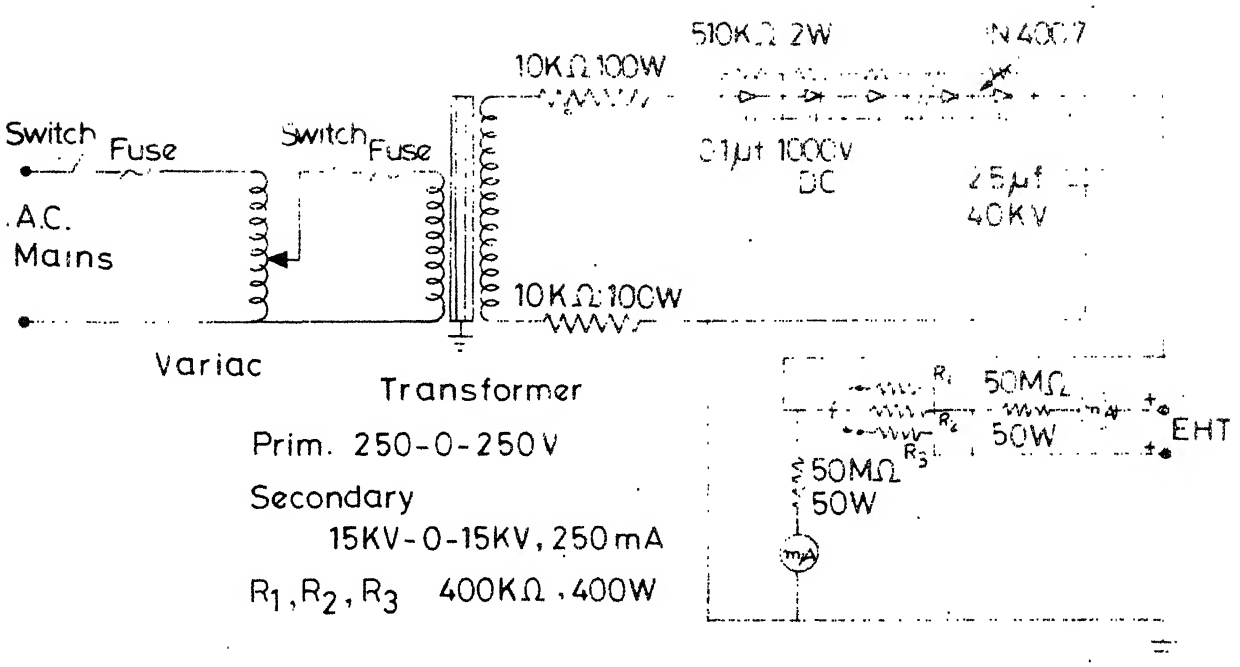

Fig. 3.10 EHT power supply.

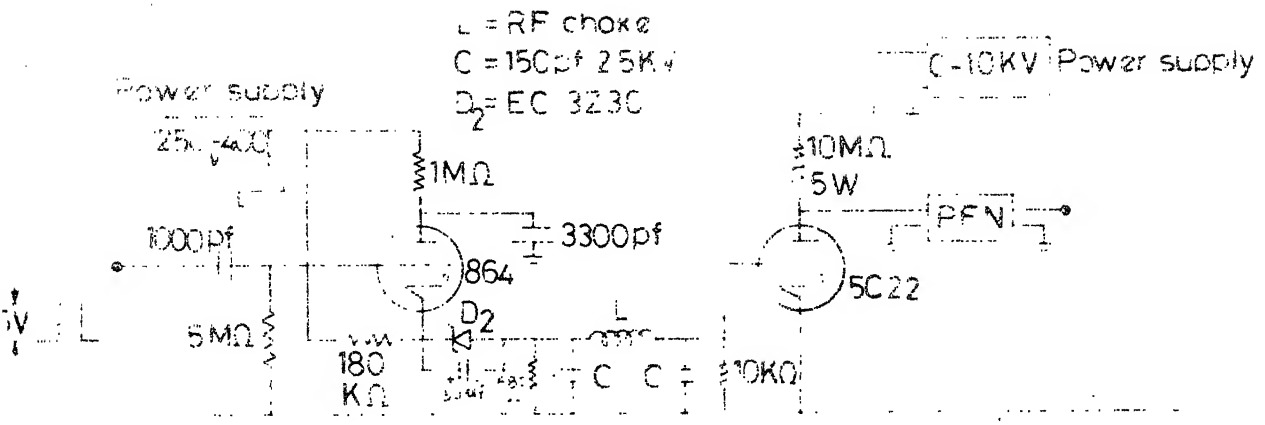

ig.3.11 a. Trigger pulse generator-circuit diagram.

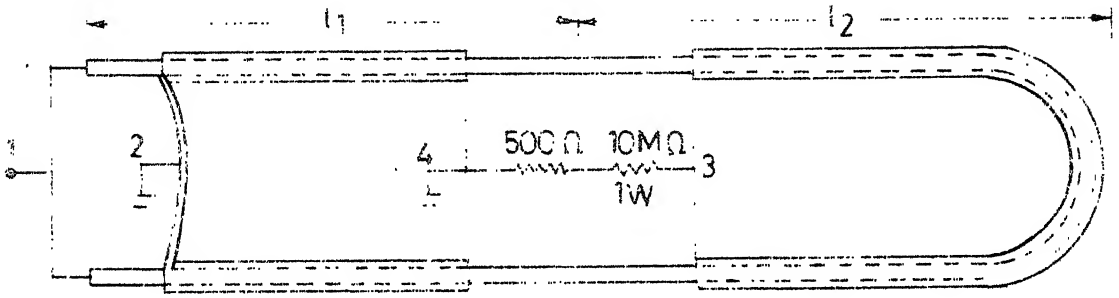

Fig. 3.11 b. Trigger pulse generator - pulse forming network.

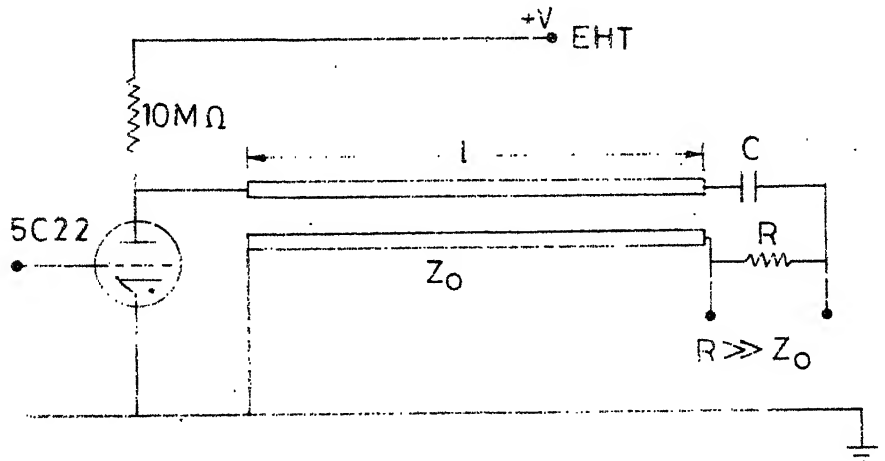

Fig. 3.11 c. Trigger pulse generator - equivalent circuit.

circuit, the spark gap being the load. The equivalent circuit of the generator is shown in Figure 3.11c. A brief discription of the operation is as follows.

The anode of the thyratron 5C22 and the capacitance C are initially charged to a voltage V through a resistance R_e (10 MΩ). A trigger pulse of at least 150 volts pulse height and a width of 1-5 μ sec, generated from a mercury thyratron is used to trigger the hydrogen thyratron. The output pulse from the thyratron (now a peak voltage of -V) travels from the shorted end of the transmission line and reaches the open end. This gets reflected without phase change, thus, changing the voltage from V to -V, hence, by an amount 2V volts. This change is transmitted to the resistance R as the voltage on the capacitor does not change suddenly. The spark gap connected across the resistance R breaks down at the sudden application of the voltage. The capacitor C is then discharged through the gap and a new pulse is launched down the cable. A series of pulses and reflections occur on the transmission line, but are of little importance, as the main gap breaks down before the first of the reflected pulses reaches R_1. It is possible to ground either side of R and obtain either +ve or -ve pulses.

In the actual circuit, the capacitor C is a cable of length l. The resistance R is connected between the points 3 and 4 (fig. 3.11b). The coaxial cable RG 8/U is used for the pulse forming network. It is wound in a coil and housed in a perspex box.

The laser has been operated successfully for a maximum of 70 pps with some decrease in the peak output power per pulse. The pulse width was measured with a photodiode HP 4207 (Hewlett-Packard) and found to be 7.5 nsec.

Absolute power measurements could not be made for lack of measuring system. The forward and backward power outputs were measured without the back mirror. No difference was found indicating that a plane wave excitation was not achieved. The reason could be the high inductance of the spark gap.

The output power of the laser was sufficient to pump Rhodamine 6G to superradiance. Lasing was also obtained in this dye.

The laser has been used for the study of fluorescence of rare earth doped single crystals. Some of the results obtained are presented in the next chapter.

3.2.6 Further Remarks

The nitrogen laser has been fabricated using available materials. The power of the laser is found to be sufficient to pump Rhodamine 6G to lasing.

It is possible to obtain considerable improvement in the output power by proper design and selecting suitable materials. Double copper clad glass epoxy sheets are now available with smaller thickness (0.8 mm). Use of these will reduce the impedance of the lines and provide better matching with the plasma. A lot of improvement is possible in the design and fabrication of the spark gap. It has been shown in the section 3.1.4, that the major limitation in achieving higher power and better efficiency is the spark gap.

3.3 Experimental Setup

The experimental setup assembled for observation of lifetimes of impurity ions in solids is shown in Figure 3.12. A nitrogen laser is used as a source of

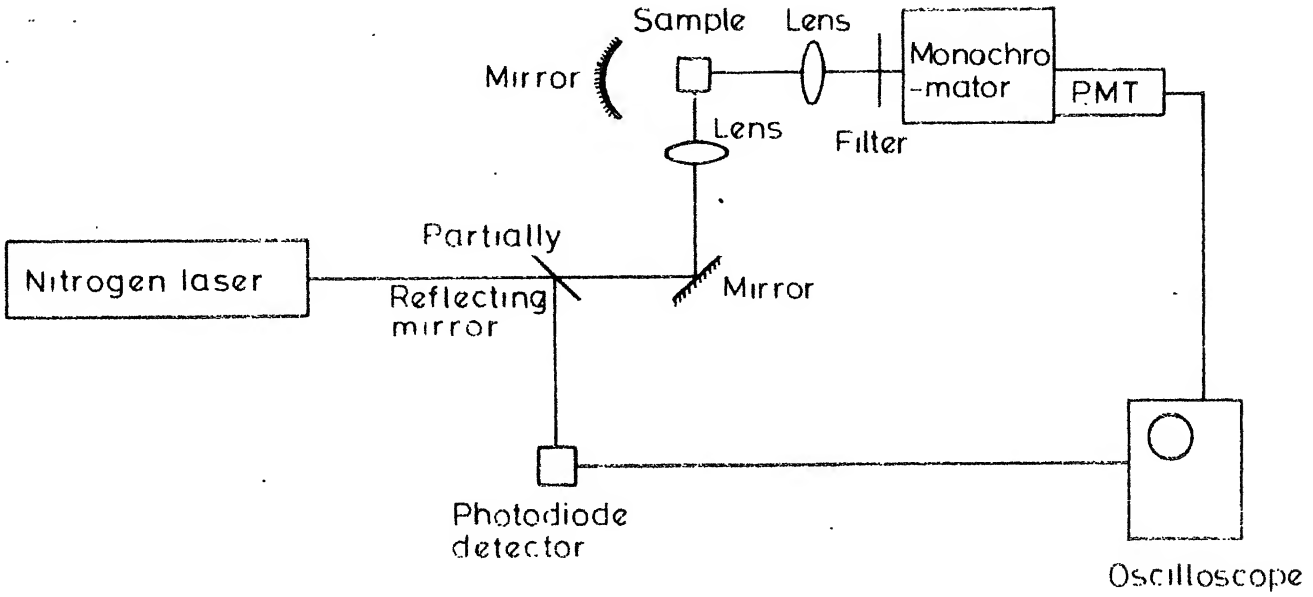

Fig. 3.12 Experimental setup for measurement of decay times.

pumping, the details of which are presented in Section 3.2. The laser beam is reflected upwards by a front coated (aluminium) mirror inclined at 45° to horizontal. The reflected beam is condensed by a quartz lens into the crystal held in a holder. The aperture and the focal length of the lens are 2"diameter and 1" respectively. Fluorescence output from the crystal is collected in a direction perpendicular to the direction of the laser beam and is condensed onto the entrance slit of the monochromator by another lens (2" diameter aperture and 1" focal length). Back reflectors are used, whenever it is necessary, to increase the intensity of the collected light.

3.3.1 The Monochromator

Jarrell Ash 0.25 m monochromator model 82-462 is used in the lifetime measurements. This instrument has two gratings - one of them blazed for low wavelength (3000Å, 2360 grooves/mm) and the other for longer wavelength (6000Å, 1180 grooves/mm). The dispersion is 33Å/mm for high blaze grating and 16Å/mm for low blaze grating while the resolution is 3Å with 150 μ slits measured at 3131Å in second order with high blaze grating. This resolution is sufficient for measuring the lifetimes of the J multiplets in rare earth ions which are well separated.

The slit width is increased to get detectable signals when the fluorescence is weak. The mixing of fluorescence from different J levels is avoided by choosing fluorescing groups which are well separated from others. In $LaF_3:Nd^{3+}$ system, the decay times of K and L levels[25] have been measured with 150 μ slit width while for R level[25] the slits are wide open (~10 mm). The R level

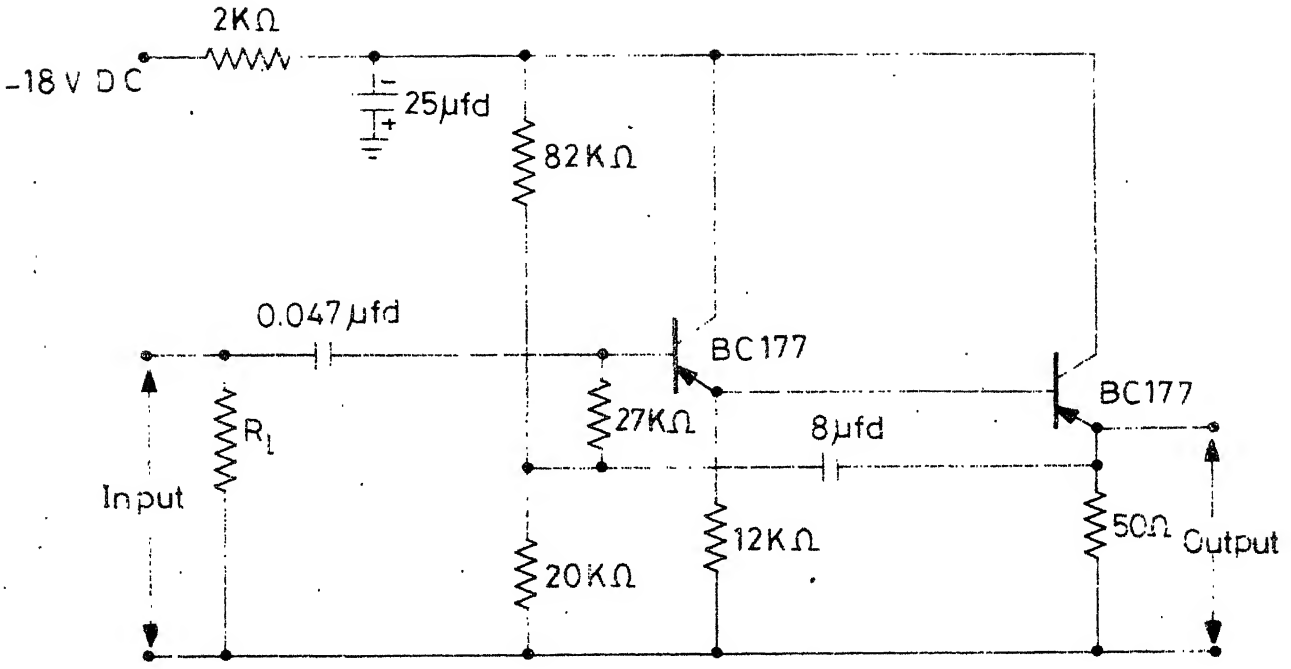

Fig. 3.13 Emitter follower.

fluorescence (R-Z group at ~8500Å) is spread over 500Å with no overlapping groups and is separated from other fluorescing groups by 400Å. The increase in slit width, thus, does not affect the measurement. In $LaF_3:Ly^{3+}$ system, decay time of $Dy^{3+}:{}^4F_{9/2}$ level has been measured with 150 μ slit width while for the Nd^{3+}:L level decay time, the output slit is kept wide open. The fluorescing group at 3850Å (L → Y) has been chosen for measurement of decay times of L. Fluorescence from K and R levels of Nd^{3+} in $LaF_3:Dy^{3+}$ system is very weak and could not be detected.

3.3.2 Detection

The light output from the monochromator is detected with a photomultiplier tube. RCA 6199 is used for the region 3500-6500Å and RCA 7102 for region beyond 6500Å. Corning glass filters are used to cut off the light from all the wavelengths lower than the region of interest. The DC voltage for the photomultiplier tube is obtained from a regulated power supply which is continuously variable from - 600 VDC to -1200 VDC. No attempt is made to cool the photomultiplier tube below room temperature.

The output of the photomultiplier tube is directly connected to the input of the emitter-follower (fig. 3.13). The emitter-follower is necessary for the time measurements as the output impedance of the photomultiplier tube and the characteristic impedance of the cable used to feed the signal to the oscilloscope, are not matched, resulting in the distortion of the pulse. A similar distortion occurs at the scope-end also. To avoid these distortions, an emitter-follower, with a large input impedance and an output impedance to

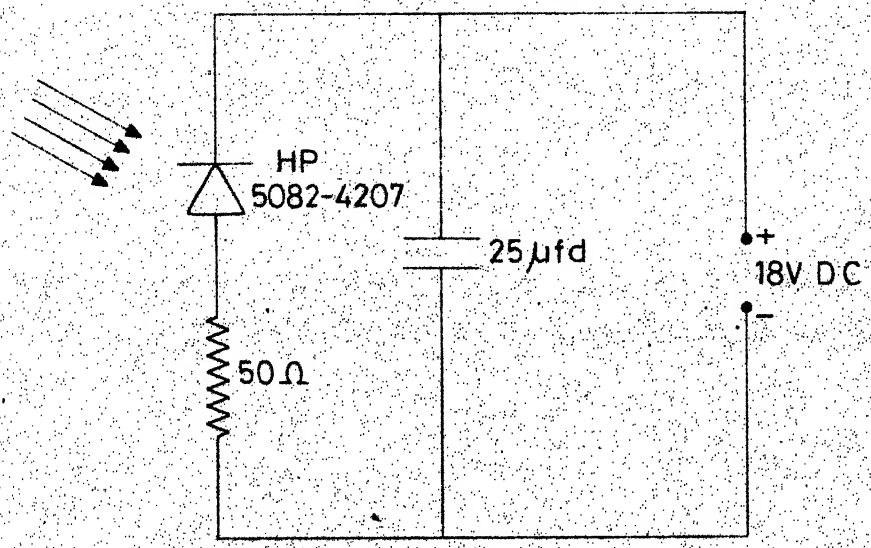

Fig. 3.14 Photodiode detector.

match the impedance of the cable, is used. The cable is terminated at the scope-end with its characteristic impedance. The total time constant of the system is measured with the nitrogen laser pulse (3371Å, 7.5 nsec width) as the input light pulse. The following are the rise times (10%-90%) of the output pulse for different photomultiplier tube load distances.

load resistance	rise time
20 K	0.1 μ sec
100 K	0.5 μ sec
180 K	1.0 μ sec

A storage oscilloscope OS 768S (ECIL India) is used to store and display the signal. It has a minimum deflection factor of 10 mV/cm and a writing speed of 0.1 cm/μ sec. Single pulses can be stored if the pulsewidth is not less than ~ 100 μ sec. The oscilloscope is triggered externally with the output of a photodiode HP 4207 which senses a part of the laser beam reflected from the main beam by a thin glass plate (fig. 3.14). For signals faster than ~100μ sec, multiple pulses have been used for storing the signal. The stored signal is traced on a transparent paper for analysis. A few typical signals which have been photographed using the polaroid camera C-12 are shown in Figure 4.2.

3.3.3 Dewar for Low Temperature Work

A demountable cold finger glass dewar (fig. 3.15) has been fabricated for the low temperature work. The upper half of the dewar is double-walled with inner-wall terminating in a glass-to-metal seal (Kovar seal). A copper block is soldered to the tip of the seal. The crystal is mounted on the

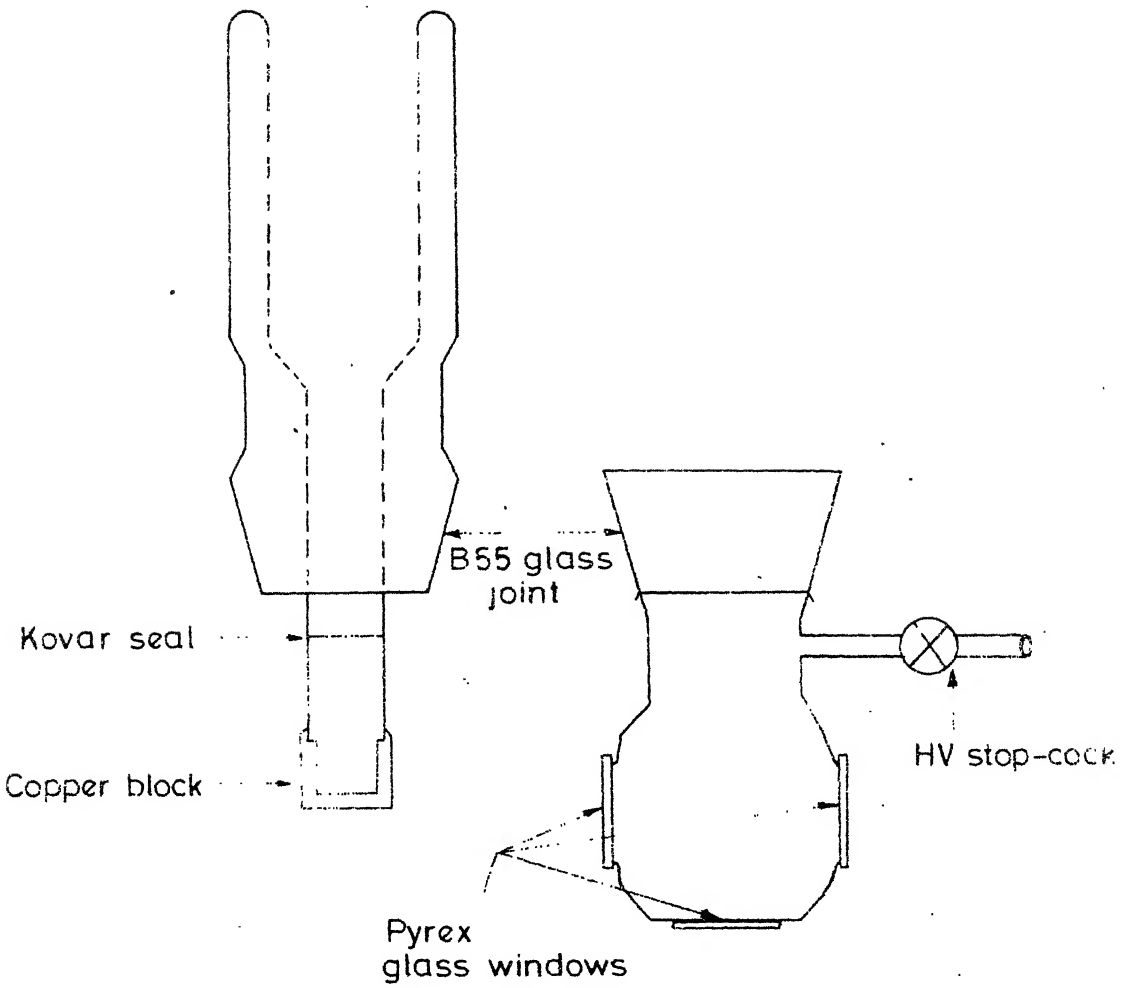

Fig. 3.15 Cold finger dewar used for work at 77°K.

copper block. The lower half of the dewar has three windows - two of them on the jacket opposite to each other and one on the bottom for the laser beam to enter the dewar. An outlet is also provided in the lower half of the dewar for evacuation. The dewar is normally evaluated to 0.1 micron of mercury.

The same dewar is used for temperature variation with the following modifications. A thin strip of bakelite isolates the copper block from the cold finger. The block is covered with mica sheet and a nichrome heater is wound on it. Copper-constantan thermocouple is used for measuring the temperature. The cold junction is fixed to the copper block. The leads of the thermocouple wire and the heaters are taken out through the jacket of the upper half of the dewar. Heating is done by passing a.c. current through the heater. The thermo e.m.f is measured with a Honeywell potentiometer Model 2705B which has an accuracy of $\pm$ 25 μV. Variation in the temperature of the copper block during the experiment is found to be negligible.

3.3.4 The Crystals

The single crystals LaF_3:Nd 2% and LaF_3:Dy 0.5% from Optovac Co., have been loaned to us by Professor H.P. Broida, Department of Physics, University of California, Santa Barbara. Excitation of the crystals with Ar^+ laser has shown the presence of Pr^{3+} as an additional impurity. Similarly, excitation of LaF_3:Dy^{3+} crystal with N_2 laser has indicated the presence of Nd^{3+} as a third impurity. This is confirmed from the comparison of the spectra photographed in the region 3500Å-4250Å with Carl Zeiss Q-24 UV spectrograph for both the systems. The Pr^{3+} ion is not excited with nitrogen laser radiation. Fluorescence spectra of LaF_3:Dy^{3+} and LaF_3:Nd^{3+} do not therefore show any lines attributable to Pr^{3+} under N_2 laser excitation.

REFERENCES

1. Heard, H.G. - Nature 200, 667 (1963).

2. Leonard, D.A. - App. Phys. Lett. 7, 4 (1965).

3. Gerry, E.T. - App. Phys. Lett. 7, 6 (1965).

4. Geller, M., Altman, D.E., and De Temple, F.A. - J. App. Phys. 39, 3639 (1966).

5. Geller, M., Altman, D.E., and De Temple, F.A. - App. Optics 7, 223 (1968).

6. Shipman, J.D. - App. Phys. Lett. 10, 3 (1967).

7. Basting, D., Schafer, F.P., and Steyer, R. - Opto Electronics 4, 43 (1972).

8. Small, J.G. and Ashari, R. - Rev. Sci. Inst. 43, 1205 (1972).

9. Nagata, I., and Kimura, Y. - J. of Phys. E6, 1193 (1973).

10. Goddard, B. - IEEE J. Quantum Electronics QE 10, 147 (1974)

11. Wang, C.P. - Rev. Sci. Inst. 47, 92 (1976).

12. Wilson, J. - App. Phys. Lett. 13, 142 (1968).

13. Targ, R. - IEEE J. Quantum Electronics QE 8, 734 (1972)

14. Dreyfus, R.W., and Hodgson, R.T. - App. Phys. Lett. 20, 195 (1972).

15. Dreyfus, R.W. and Hodgson, R.T. - J. of Vac. Science and Tech. 10, 1033 (1973).

16. (a) Von Bergmann, H.M., Hasson, V., and Preussler, D. - App. Phys. Lett. 27, 553 (1975).

    (b) Hasson, V., Preussler, D., Klimek, J., and Von Bergmann, H.M. - App. Phys. Lett. 25, 654 (1974).

    (c) Hasson, V., Von Bergmann, H.M., and Preussler, D. - App. Phys. Lett. 28, 17 (1976).

    (d) Hasson, V., and Von Bergmann, H.M. - J. of Phys. E9, 73 (1976).

    (e) Bergmann, E.E. - App. Phys. Lett. 28, 84 (1976).

17. Strohwald, H., and Salzmann, H. - App. Phys. Lett. 28, 272 (1976).

18. Parks, J., Ramachandra Rao, D., and Javan, A. - App. Phys. Lett. 13, 142 (1968).

19. (a) Ali, A.W., Kolb, A.C., and Anderson, A.D. - App. Optics 6, 215 (1967).

(b) Ali, A.W. - App. Optics 8, 993 (1969).

20. Anderson, H.E.B - Physica Scripta 4, 215 (1971).

21. Schwab, A.J. and Hollinger, F.W. - IEEE J. Quantum Electronics QE 12, 183 (1976).

22. Cartwright, D.C. - Phys. Rev. A2, 1331 (1970).

23. Levatter, J.I., and Lin, S.C. - App. Phys. Lett. 25, 703 (1974).

24. Ramachandra Rao, D., Jagannath, H., Chakrapani, G., and Venkateswarlu, P. - Ind. J. of Phys. 50, 267 (1976).

25. Kumar, U.V., Jagannath, H., Ramachandra Rao, D., and Venkateswarlu, P. - Ind. J. of Phys. 50, 90 (1976).

CHAPTER IV

EXPERIMENTAL RESULTS

4.1 $LaF_3:Nd^{3+}$ System

The nitrogen laser described in Chapter III has been initially used for excitation of fluorescence in $LaF_3:Nd^{3+}$ and the spectrum has been photographed in the region 3500Å-10,000Å. The results suggest that three levels L, K and R fluoresce and these are reported by Kumar et.al[1]. The level K has been established from the same fluorescence data. A total of 11 groups of transitions from these levels to various lower levels have been analysed, a majority of them being from the level L (fig. 4.1).

A major portion of the experimental results reported in this thesis is on the decay times of the levels L, K and R. The decay times of the following groups of transitions at different temperatures have been measured.

L level	L → Z (3500Å-3600Å)	L → Y (3730Å-3950Å)
K level	K → W (4850Å-5050Å)	
R level	R → Z (8600Å-9000Å)	

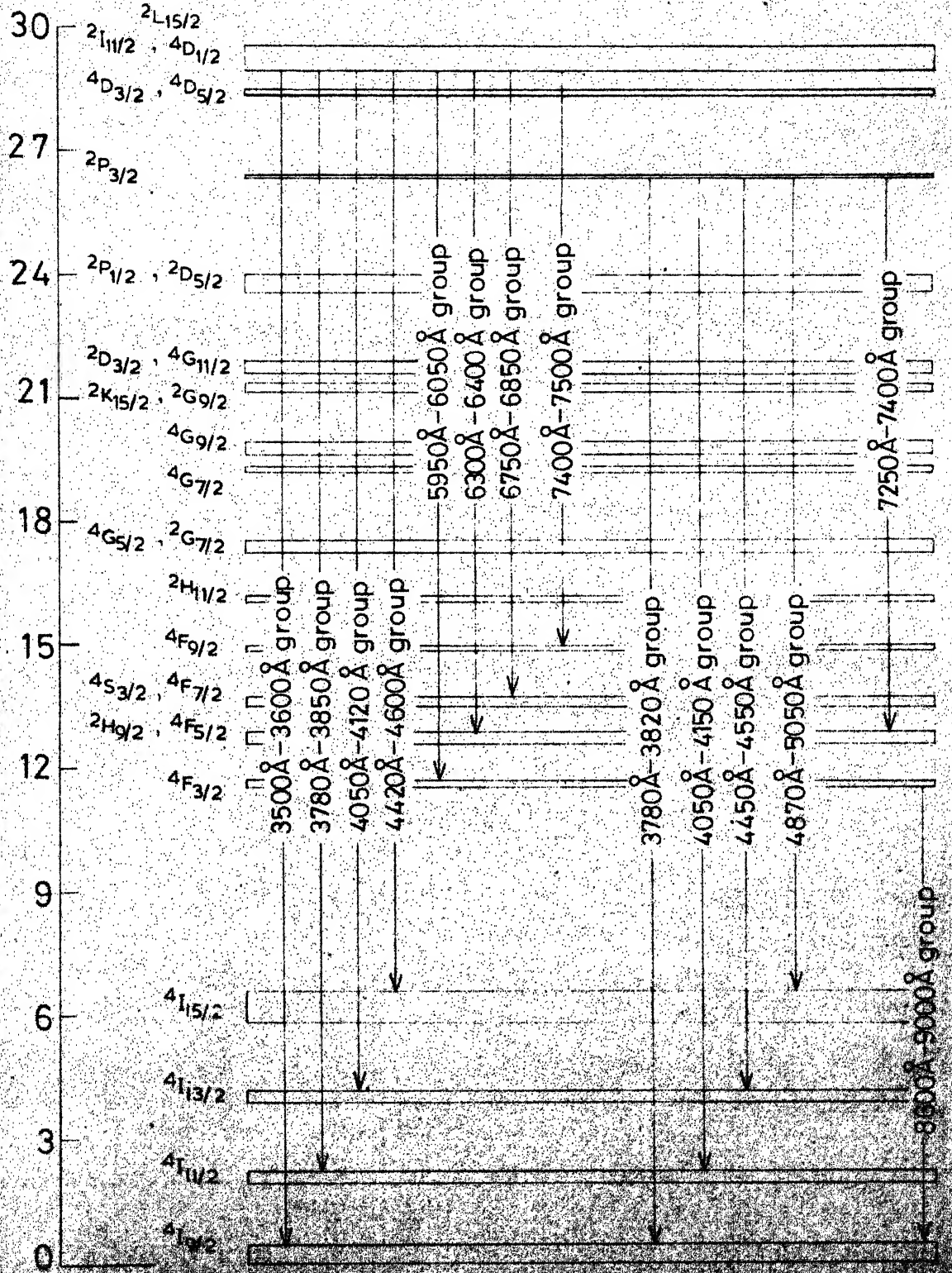

Fig. 4.1 Energy level diagram showing the observed fluorescence transitions of Nd^{3+} in LaF$_3$ crystal.

In each case, decay times of various transitions from Stark levels of the upper state to different Stark levels of the lower state have been measured. The reported values are the average of these measurements.

4.1.1 Level L

Fluorescence from the level L decays nonexponentially - a rapid fall in the beginning followed by a slow decay. The 'tail' of the decay shows a near exponential decay with a decay time of 18 μ sec. at liquid nitrogen temperature and varies with temperature. The time delay between the peak of the laser pulse and the peak of the fluorescence (t_{max}) is found to be negligible indicating that the level is pumped faster than the risetime (0.1 μ sec.) of the photo multiplier tube and emitter follower.

4.1.2 Level K

The level K decays as a difference of exponentials. The intensity of fluorescence increases in the beginning, reaches a maximum at t_{max} and decays again. The decay 'tail' has a decay time of 120 μ sec. at room temperature and is about the same at liquid nitrogen temperature. The t_{max} is about 27.5μ sec. at room temperature and 31μsec. at liquid nitrogen temperature. Temperature variation of t_{max} is not studied as the peak is not sharp.

4.1.3 Level R

The level R also decays as a difference of exponentials. The initial rise is fast. The decay is a single exponential and has a time constant of

ach case, (

Scale

10 μ Secs

(a)

Scale

20 μ Secs

(b)

Fig. 4.2 - Decay of fluorescence from level I of Nd^{3+} in $LaF_3:Nd^{3+}$ (a) room temperature and (b) liquid nitrogen temperature.

The scales arenot visible as the oscilloscope OS 768 S does not have the provision for scale illumination. The time scale is shown separately. The picture is slightly out of focus as the Camera (Tetronics C12) could not be fully adapted to the oscilloscope OS 768 S .

Table 4.1

Observed Relaxation Rates at Different Temperatures

Level L (Nd^{3+})					
$LaF_3:Nd^{3+}$			$LaF_3:Dy^{3+}$		
Temp.	Decay time in micro-seconds	Decay rate in sec^{-1}	Temp.	Decay time in micro seconds	Decay rate in sec^{-1}
°K	(19.7 ± 0.8)	$(5.066^{0.194}_{0.187}) \times 10^4$	77°K	(29.0 ± 0.9)	$(3.451^{0.110}_{0.101}) \times 10^4$
°K	(18.2 ± 0.6)	$(5.509^{0.177}_{0.166}) \times 10^4$	160°K	(27.3 ± 3.4)	$(3.662^{0.521}_{0.403}) \times 10^4$
°K	(16.6 ± 1.0)	$(6.039^{0.369}_{0.329}) \times 10^4$	196°K	(24.7 ± 1.0)	$(4.120^{0.168}_{0.157}) \times 10^4$
°K	(15.3 ± 1.0)	$(6.545^{0.479}_{0.419}) \times 10^4$	223°K	(21.2 ± 1.3)	$(4.726^{0.309}_{0.274}) \times 10^4$
°K	(13.2 ± 0.7)	$(7.577^{0.392}_{0.357}) \times 10^4$	273°K	(16.2 ± 1.4)	$(6.190^{0.558}_{0.504}) \times 10^4$
°K	(11.2 ± 0.3)	$(8.915^{0.286}_{0.267}) \times 10^4$	308°K	(14.7 ± 0.9)	$(6.826^{0.431}_{0.382}) \times 10^4$

Table 4.2

Observed Relaxation Rates at Different Temperatures

Level K (Nd^{3+})		
Temp.	Decay time in microseconds	Decay rate in sec^{-1}
77°K	118.5 ± 5.3	$(8.436 \pm \begin{smallmatrix}0.388\\0.355\end{smallmatrix}) \times 10^3$
181°K	114.8 ± 14.8	$(8.710 \pm \begin{smallmatrix}1.286\\1.003\end{smallmatrix}) \times 10^3$
208°K	114.6 ± 3.5	$(8.726 \pm \begin{smallmatrix}0.274\\0.259\end{smallmatrix}) \times 10^3$
248°K	121.2 ± 5.2	$(8.252 \pm \begin{smallmatrix}0.370\\0.341\end{smallmatrix}) \times 10^3$
273°K	114.9 ± 6.3	$(8.704 \pm \begin{smallmatrix}0.537\\0.508\end{smallmatrix}) \times 10^3$
308°K	107.3 ± 6.3	$(9.316 \pm \begin{smallmatrix}0.580\\0.526\end{smallmatrix}) \times 10^3$

Table 4.3

Observed Relaxation Rates at Different Temperatures

Level R (Nd^{3+})		
Temp.	Decay time in microseconds	Decay rate in sec^{-1}
77°K	455.5 ± 21.7	$(2.195 \pm {}^{0.110}_{0.100}) \times 10^3$
181°K	474.6 ± 8.7	$(2.107 \pm {}^{0.039}_{0.038}) \times 10^3$
248°K	560.1 ± 36.9	$(1.785 \pm {}^{0.126}_{0.110}) \times 10^3$
208°K	521.1 ± 28.3	$(1.919 \pm {}^{0.110}_{0.098}) \times 10^3$
273°K	531 ± 34.7	$(1.883 \pm {}^{0.131}_{0.115}) \times 10^3$
308°K	518 ± 13.0	$(1.930 \pm {}^{0.05}_{0.05}) \times 10^3$

518 μ sec. at room temperature and 455 μ sec. at liquid nitrogen temperature. No systematic variation in the decay time of the 'tail' is found with temperature. The t_{max} is 20.5 μ sec. at room temperature and 30μ sec. at liquid nitrogen temperature. Temperature variation of t_{max} is not studied.

The measured decay times of the 'tail' of the level L, K and R at different temperatures are shown in Table 4.1, 4.2 and 4.3 respectively. Typical decay curves of some of the groups are shown in Figure 4.2.

4.2 $LaF_3:Dy^{3+}$ System

The fluorescence spectrum of $LaF_3:Dy^{3+}$ has been photographed on a Carl Zeiss 3 prism (glass) spectrograph and on a Q-24 uv spectrograph. The spectrum in the region 4500Å-9000Å is the same as has been obtained by Fry et.al[2] for $LaF_3:Dy^{3+}$. Below 4500Å, 4 groups of transitions have been observed. A weak group around 3400Å is easily identifiable as from Dy^{3+}[3] (fig. 4.4). The other three groups which are of medium intensity have been found to coincide with the spectrum of $LaF_3:Nd^{3+}$. The spectra of Nd^{3+} in $LaF_3:Dy^{3+}$ and $LaF_3:Nd^{3+}$ in these regions under nitrogen laser excitation are shown in Figure 4.3 for comparison. No spectrum of Nd^{3+} is observed in the other regions. This is possibly due to the very low concentration of Nd^{3+} in $LaF_3:Dy^{3+}$ crystal. The transitions of the Nd^{3+} lines and their wave lengths are shown in Figure 4.3. The wave lengths marked in the figure are slightly more accurate than those given in our earlier paper[1] as the present spectra are slightly better recorded than the earlier one[1].

Wavelength in Å	Transition	$LaF_3:Dy^{3+}$	$LaF_3:Nd^{3+}$	Transition	Wavelength in Å	Standard wavelength in Å
3371.0	N_2					3371.0 N_2
						3441.0 Fe
						3475.5, 76.7 Fe
3529.7	L_3-Z_2			L_3-Z_2	3529.7	
3533.7	I_2-Z_2			I_2-Z_2	3533.7	
3591.8	I_2-Z_5			L_3-Z_3	3541.3	
				I_2-Z_3	3545.4	
				I_2-Z_4	3564.3	
3801.2	L_2-Y_2			I_2-Z_5	3591.8	
3824.0	L_2-Y_5					3617.8, 18.8 Fe
						3631.5 Fe
						3734.9 Fe
						3748.5 Fe
				I_3-Y_1	3787.9	
				I_2-Y_2	3801.2	
				I_3-Y_5	3817.8	
				L_2-Y_5	3824.0	
						3886.3, 87.1 Fe
				I_2-Y_1	4094.2	4044.4, 45.8 Fe
4104.4	L_2-X_2			L_2-X_2	4104.4	
4110.2	K_1-Y_2			L_2-X_5	4127.6	
4155.2	L_2-X_7			L_2-X_7	4155.2	
						4271.8 Fe
						4325.8 Fe
						4404.8 Fe
4526.5	K_1-X_7			L_3-X_3	4463.1	
				Y_1-X_7	4526.5	

Fig. - 4.3 - Fluorescence spectrum of Nd^{3+} in $LaF_3:Nd^{3+}$ and $LaF_3:Dy^{3+}$ at 77°K in the region 3400Å-4600Å.

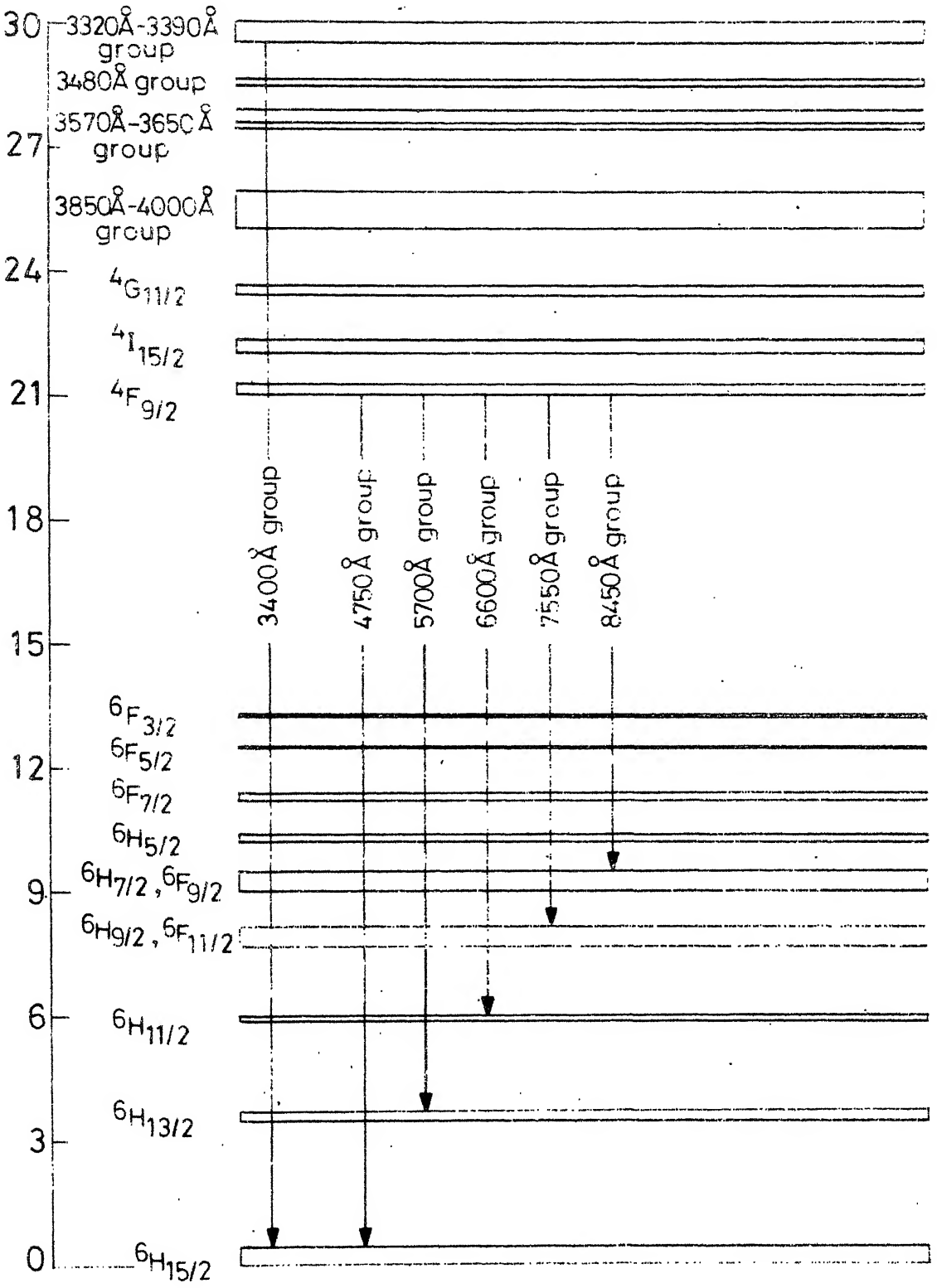

Fig.4.4 Energy level diagram showing the observed fluorescence transition groups of Dy^{3+} in LaF_3 at 77°K. Excitation source-nitrogen laser (3371 Å).

Table 4.4

Observed Relaxation Rates at Different Temperatures

Level $^4F_{9/2}$ (Dy^{3+})		
Temp.	Decay time in milli seconds	Decay rate in sec^{-1}
77°K	(1.581 ± 0.087)	$(6.325 \pm \substack{0.370 \\ 0.328}) \times 10^2$
160°K	(1.750 ± 0.078)	$(5.714 \pm \substack{0.268 \\ 0.244}) \times 10^2$
196°K	(1.754 ± 0.087)	$(5.701 \pm \substack{0.296 \\ 0.270}) \times 10^2$
227°K	(1.783 ± 0.087)	$(5.609 \pm \substack{0.287 \\ 0.260}) \times 10^2$
273°K	(1.798 ± 0.066)	$(5.562 \pm \substack{0.210 \\ 0.194}) \times 10^2$
308°K	(1.791 ± 0.083)	$(5.583 \pm \substack{0.285 \\ 0.258}) \times 10^2$

REFERENCES

1. Kumar, U.V., Jagannath, H., Ramachandra Rao, D., and Venkateswarlw, P. - Ind. J. of Phys. 50, 90 (1976).

2. Fry, J.L., Caspers, H.H., Rast, H.E., Miller, S.A., and Freasier, B. - J. Chem. Phys. 48, 2342 (1968).

3. Four weak transitions have been observed at 29592 cm^{-1}, 29526 cm^{-1}, 29464 cm^{-1} and 29348 cm^{-1}. Three of these - 29526 cm^{-1}, 29464 cm^{-1} and 29348 cm^{-1} can be assigned as the transitions from the level at 29526 cm^{-1} to the lowest level ($^6H_{15/2}$) Stark components 0 cm^{-1}, 69 cm^{-1} and 184 cm^{-1} respectively. The transition 29592 cm^{-1} is from the level at 29658 cm^{-1} to the Stark component at 69 cm^{-1} of $^6H_{15/2}$.

4. Here and in the next chapter, the alphabetical nomenclature (A-Z) has been used for the Stark multiplets of Nd^{3+} while the Stark multiplets of Dy^{3+} are referred to by the SLJ designations. The alphabetical nomenclature used is similar to the nomenclature used by Dieke (Spectra and energy levels of rare earth ions in crystals, Interscience Publishers) and Carlson and Dieke (J. Chem. Phys. 29, 229 (1958), and Ibid 39, 1602 (1961)). The multiplets L and K of Nd^{3+} are a mixture of different SLJ levels. These are conveniently referred to by the alphabetical nomenclature than by the SLJ designation and hence, the choice.

CHAPTER V

DISCUSSION

5.1.1 Fluorescence Lifetimes of Nd^{3+}

The observed transition rate of a Stark multiplet of an ion in a crystalline lattice is the sum of the rate of radiative and nonradiative transitions. The nonradiative relaxation includes the relaxation due to the multiphonon processes and the ion-ion interaction relaxation. The three contributions can be separated experimentally by studying the variation of the fluorescence decay time with temperature and concentration and by measuring the multiphonon quantum efficiency. The ion-ion interaction relaxation rate can be neglected in crystals with low concentration of impurity ion. The multiphonon quantum efficiency, thus, gives the ratio of the multiphonon transition rate and the radiative transition rate to the total decay rate. At any higher concentration of the impurity ion, the contribution due to the ion-ion interaction relaxation, $(1/\tau_c^{II})$ at temperature T can be calculated by substracting the total transition rate observed in a dilute crystal $(1/\tau_o(T))$ at the same temperature from the observed transition rate $1/\tau_c(T)$ i.e.

$$1/\tau_c^{II}(T) = 1/\tau_c(T) - 1/\tau_o(T) \qquad (5.1)$$

The temperature dependence of the decay rate is mainly due to the contribution from the nonradiative transitions. The multiphonon transition rate is temperature dependent. The ion-ion interaction transitions contribute to the temperature dependence of the non-radiative transition rate only in those cases in which the absorption or emission of phonons is necessary to conserve the energy. In all the resonant ion-ion interaction transitions, contribution to temperature dependence is negligible.

The decay of fluorescence of Nd^{3+} in LaF_3 (2% by wt) has been observed and the decay times have been measured for the levels L, K and R at six different temperatures between liquid nitrogen temperature and room temperatures. In addition, the decay times of level L of Nd^{3+} at different temperatures have been measured in $LaF_3:Dy^{3+}$ in which neodymium occurs as an additional impurity+. Comparison of the results of the two systems indicates that the level L exhibits relaxation due to radiative and multiphonon transitions in $LaF_3:Dy^{3+}$ and all the three processes in $LaF_3:Nd^{3+}$ while the levels K and R show predominant radiative and ion-ion interaction relaxation in $LaF_3:Nd^{3+}$.

The discussion of the results on Nd^{3+} has been divided into three parts. Each of them deals with one relaxation process. Quantitative explanation of the observed decay rates and decay functions is given wherever it is possible. Discussion is limited to qualitative explanation in the case of insufficient data.

+ While the concentration of Nd^{3+} in $LaF_3:Nd^{3+}$ is 2% by weight, the concentration of Nd^{3+} in $LaF_3:Dy^{3+}$ is not known. It is detected only through the presence of Nd^{3+} fluorescence along with Dy^{3+} fluorescence under nitrogen laser excitation. However, by comparing the intensities of Nd^{3+} fluorescence in the two crystals, we estimate the Nd^{3+} concentration in $LaF_3:Dy^{3+}$ to be about $1/100^{th}$ of what it is in the $LaF_3:Nd^{3+}$ crystal.

.1.2 Radiative Relaxation

The observed rate of decay of the level L of Nd^{3+} in $LaF_3:Dy^{3+}$ is the um of the radiative transition rate to all the levels below it and the multihonon transition rate to level K. The temperature dependence of the observed lecay is due to multiphonon transitions. Separation of the two contributions .s obtained by measuring the multiphonon quantum efficiency+. This is not possible in $LaF_3:Nd^{3+}$ system as the level K has a very small absorption coefficient[3]. The K level has, infact, been identified only in the fluorescence spectrum[1]. The alternate method is to calculate the radiative transition probabilities from the level L to obtain the radiative transition rate. The multiphonon transition rate is obtained by substracting the radiative transition rate from the observed decay rate. This method is followed here.

5.1.3a Calculation of the Radiative Transition Probabilities: Electric Dipole Transitions

The total radiative transition probability of an electronic level is the sum of the transition probabilities for electric dipole and magnetic dipole transitions. The electric quadrupole transitions which are parity allowed between the levels of the ground configuration $4f^n$ are very weak and hence, neglected.

+ The quantum efficiency of the process A $\longrightarrow$ B, where the level A lies above B by an amount of energy greater than kT, is experimentally determined from the excitation spectrum of an arbitrary transition originating from level B, and the absorption spectra of levels A and B which are obtained from the same monochromatic source[2].

The spontaneous emission probability for an electric dipole transition between the levels $|(\alpha SL)J\rangle$ and $|(\alpha'S'L')J'\rangle$ of the ion can be written as[4]

$$A_{ed}[(\alpha SL)J, (\alpha'S'L')J'] = 64\pi^4 e^2 \nu^3 \chi_{ed} (3h)^{-1}(2J+1)^{-1} \times \sum_{\lambda} \Omega_{\lambda} \langle f^n(\alpha SL)J \| U^{\lambda} \| f^n(\alpha'S'L')J' \rangle^2 \quad (5.2)$$

where χ is a correction factor for the dielectric constant of the medium, ν is the average frequency of transition, Ω_λ are the phenomenological factors which are experimentally obtained and $\langle f^n(\alpha SL)J \| U^{\lambda} \| f^n(\alpha'S'L')J' \rangle$ are the matrix elements of the unit matrix U^{λ}.

The spontaneous emission probability for a magnetic dipole transition between the levels $|(\alpha SL)J\rangle$ and $|(\alpha'S'L')J'\rangle$ can be written as

$$A_{md}[(\alpha SL)J, (\alpha'S'L')J'] = 64\pi^4 \nu^3 \chi_{md} (3h)^{-1}(2J+1)^{-1} \times |\langle f^n(\alpha SL)J \| M \| f^n(\alpha'S'L')J' \rangle|^2 \quad (5.3)$$

where M is the magnetic dipole operator given by $M = -\frac{e}{2mc}(L + 2S)$. The other symbols have the same significance as in (5.2).

The equation (5.2) and (5.3) are derived under the assumptions that (1) J-J mixing is negligible and (2) all the Stark components of the fluorescing multiplet have equal transition probability for transitions to any lower multiplet . Application of the equations (5.2) and (5.3) is not strictly

Table 5.1

The Eigen Values and Eigen Functions of $PbMoO_4:Nd^{3+}$

1) Energy in cm^{-1}	^2F	^2D
28559.5	-0.2608	0.9654
23039.8	0.9654	0.2608

Energy in cm^{-1}	^4S	^2P	$^2D(20)^a$	$^2D(21)^a$	^4D	^4F
33263.1	-0.0086	0.0773	0.1402	0.9087	-0.3852	0.0171
28001.7	0.0274	-0.1804	0.0451	0.3904	0.9012	0.0120
26116.7	-0.1213	0.6927	0.6768	-0.0976	0.1514	-0.1211
21138.0	0.1931	-0.6559	0.6865	-0.0983	-0.1264	-0.1885
13336.0	0.9721	0.2198	-0.0415	0.0018	0.0140	0.0687
11251.2	-0.0465	-0.0556	0.2174	-0.0521	-0.0110	0.9719

Energy in cm^{-1}	$^2D(20)^a$	$^2D(21)^a$	^4D	$^2F(10)^a$	$^2F(21)^a$	^4F	^4G
68013.4	0.0110	-0.0054	0.0180	-0.7942	-0.6071	0.0006	-0.0128
39300.7	-0.0079	0.3999	-0.0481	0.5537	0.7213	0.0426	-0.0948
34557.4	-0.0912	0.8204	-0.4153	-0.2192	-0.3091	0.0088	0.0498
28227.3	-0.0536	0.3950	0.9081	-0.0857	-0.0903	0.0107	0.0268
23524.3	0.9837	0.1028	0.0107	-0.0252	-0.0162	-0.1439	0.0115
17059.6	-0.0032	-0.0151	-0.0082	0.0762	0.0785	0.0240	0.9936
12283.4	0.1451	-0.0134	-0.0023	-0.0270	-0.0312	0.9883	-0.0191

Table 5.1 (continued)

Energy in cm^{-1}	^4D	$^2F(10)^a$	$^2F(21)^a$	^4F	$^2G(20)^a$	$^2G(21)^a$	^4G
66962.3	0.0417	0.8353	-0.5365	0.0033	0.0523	0.0687	-0.0123
47824.4	-0.0040	-0.0385	0.0999	0.0089	0.6365	0.7634	-0.0222
40633.9	0.0948	0.5340	0.8334	0.0405	-0.0703	-0.0252	-0.0637
30224.7	0.9946	-0.0857	-0.0560	-0.0064	0.0100	0.0004	0.0135
18838.3	-0.0074	0.0472	0.0534	0.1262	0.4346	-0.3446	0.8194
16979.1	0.0017	-0.0122	-0.0124	0.2346	0.5967	-0.5157	-0.5680
13254.2	0.0031	-0.0280	-0.0385	0.9630	-0.2054	0.1645	0.0340

Energy in cm^{-1}	^4F	$^2G(20)^a$	$^2G(21)^a$	^4G	$^2H(11)^a$	$^2H(21)^a$	^4I
46945.7	0.0157	0.6409	0.7617	-0.0224	0.0838	0.0358	0.8005
32281.9	0.0036	-0.0176	-0.1019	0.0672	0.9254	0.3582	0.0053
20776.0	0.2723	0.5969	-0.4822	0.5363	0.0039	-0.2209	-0.0242
19311.7	0.2007	0.3153	-0.2963	-0.8236	0.1331	-0.2589	-0.0351
14540.1	0.8667	-0.1278	0.0861	-0.0356	-0.1634	0.4373	0.0764
12398.5	-0.3662	0.3413	-0.2055	-0.1399	-0.2978	0.7324	0.1523
0.0	0.0032	-0.0172	0.0152	0.0077	0.0586	-0.1639	0.9844

Energy in cm^{-1}	^4G	$^2H(11)^a$	$^2H(21)^a$	^2I	^4I
33675.6	0.1146	0.8292	0.4060	0.3664	0.0123
20371.8	-0.0697	-0.3447	-0.1150	0.9289	0.0166
21373.4	0.9645	-0.2140	0.1538	0.0177	0.0159
15703.7	-0.2276	-0.3826	0.8884	-0.0508	0.0998
1866 .1	0.0071	0.0373	-0.0947	-0.0151	0.9947

Table 5.1 (continued)

Energy in cm^{-1}	^2I	^4I	^2K
29711.2	0.9947	0.0166	0.1011
18761.1	-0.0998	-0.0664	0.9928
3852.6	-0.0232	0.9977	0.0644

Energy in cm^{-1}	^4I	^2K	^2L
29119.8	-0.0163	0.2128	0.9770
20755.8	-0.1165	0.9700	-0.2132
5915.4	0.9931	0.1173	-0.0090

Energy in cm^{-1}	^2L
30605.6	1.000

a. In a multielectron system as for the rareearths, the basis states $SLJJ_z$ involve more than one 'term' having the same S and L values. The states are classified according to the seven dimensional rotation group R_7 and its sub-group G_2 using group theoretical techniques. In the f^3 configuration, the states with the same S and L differ in the quantum numbers which characterize the irreducible representations of G_2. These quantum numbers are shown in brackets.

alid for the calculation of the radiative transition rate of the level L hich is a mixture of five J levels - J = 1/2, 3/2, 5/2, 11/2 and 15/2[1]. There s no J mixing in the case of levels K and R. Each of the levels K and R has wo Stark components which are separated by ~ 40 cm^{-1}. There is no a priori reason to believe that both the components have equal transition probabilities for transitions to lower levels. Hence the assumption (1) is valid and assumption (2) is not strictly valid for levels K and R. The calculated values can still be expected to be in close agreement with the observed values as has been observed in other systems by many workers[3,4].

The intermediate coupling wavefunctions for $PbMoO_4:Nd^{3+}$ have been obtained by Minhas[5] by diagonalizing the Hamiltonian of the free ion which includes beside the Coulomb interaction and spin-orbit interaction terms, the configurational interaction. Since the wavefunctions show small variation from host to host, the same are used to calculate the transition rates of Nd^{3+} in LaF_3[6,7*]. The wavefunctions for different J levels of Nd^{3+} are shown in Table 5.1.

The matrix elements of the $\underline{U}$ matrix are first calculated using the above wavefunctions. These are given by

$$\langle f^n(\alpha SL)\, J \| \underline{U}^{\lambda} \| f^n(\alpha' S'L')J' \rangle = \sum C(\alpha SL)C'(\alpha' S'L') \times \langle f^n\, \alpha\, SLJ \| \underline{U}^{\lambda} \| f^n\, \alpha' S'L'J' \rangle \qquad (5.4)$$

---

* The positions of the centres of gravity of the crystal field levels of a rare earth ion in a crystal do not differ much from one crystal to another since the crystal field interaction is weak. A good fit with the centres of gravity of the crystal field levels in different crystals can be obtained by small changes in the parameters F_2, F_4, F_6, ξ, α, β, Y(22,1) and Y(22,3) which characterize the positions of the energy levels in a crystal.

Table 5.2

Reduced Matrix Elements of U Matrix for Transitions from Level R(3/2)

Lower Level	U_2^{2+}	U_4^{2+}	U_6^{2+}
Z(15/2)	0	0.235010	0.058370
Y(13/2)	0	0.145165	0.408664
X(11/2)	0	0	0.015455
W(9/2)	0	0	0.027556

\+ - Here and in subsequent tables 5.3 to 5.8,

U_x^2 (x = 2,4 and 6) are the elements of U matrix given by

$$U_x^2 = \langle f^N(\alpha SL)J \,||\, \underset{\sim}{U}^x \,||\, f^N(\alpha'S'L')J' \rangle^2$$

Table 5.3

Reduced Matrix Elements of U Matrix for Transitions from Level K(3/2)

Lower Level	U^2_2	U^2_4	U^2_6
Z (15/2)	0	0.006053	0.001208
Y (13/2)	0	0.030597	0.001056
X (11/2)	0	0	0.001829
W (9/2)	0	0	0.003511
R (3/2)	0	0	0
S (5/2)	0.007852	0.008567	0
S (9/2)	0	0.030154	0.064769
A (3/2)	0.014270	0	0
A (7/2)	0.004520	0.003202	0
B (9/2)	0	0.032412	0.052782
C (11/2)	0	0.000280	0.102877
D (5/2)	0.064302	0.000088	0
D (7/2)	0.009867	0.002959	0
E (7/2)	0.007808	0.010509	0
F (9/2)	0	0.056218	0.064885
G (15/2)	0	0	0.335212
G (9/2)	0	0.139030	0.137860

Table 5.4

Reduced Matrix Elements of U Matrix for Transition from Level L (1/2)

Lower Level	U^2_2	U^2_4	U^2_6
Z (15/2)	0	0.361777	0
Y (13/2)	0.018897	0	0
X (1/2)	0.013987	0	0
W (9/2)	0	0	0
R (3/2)	0.000041	0	0
S (5/2)	0.055448	0	0
S (9/2)	0	0.015479	0
A (3/2)	0.088360	0	0
A (7/2)	0	0.182188	0
B (9/2)	0	0.036728	0
C (11/2)	0.001371	0	0
D (5/2)	0.326119	0	0
D (7/2)	0	0.018700	0
E (7/2)	0	0.007785	0
F (9/2)	0	0.000120	0
G (15/2)	0	0	0
G (9/2)	0	0.001130	0

Table 5.5

Reduced Matrix Elements of U Matrix for Transitions from Level L (3/2)

Lower Level	U_2^2	U_4^2	U_6^2
Z (15/2)	0	0.267452	0.016666
Y (13/2)	0	0.408688	0.002636
X (11/2)	0	0	0.024826
W (9/2)	0	0	0.008624
R (3/2)	0.046376	0	0
S (5/2)	0.060691	0.204079	0
S (9/2)	0	0.028688	0.004820
A (3/2)	0.213522	0	0
A (7/2)	0.079793	0.016928	0
B (9/2)	0	0.181263	0.001724
C (11/2)	0	0.047342	0.011362
D (5/2)	0.810622	0.000815	0
D (7/2)	0.540389	0.049212	0
E (7/2)	0.174924	0.021274	0
F (9/2)	0	0.000181	0.091548
G (15/2)	0	0	0.001432
G (9/2)	0	0.001109	0.034816

Table 5.6

Reduced Matrix Elements of U Matrix for Transitions from Level L (5/2)

Lower Level	U^2_2	U^2_4	U^2_6
Z (15/2)	0.000107	0.077517	0.025431
Y (13/2)	0	0.330964	0.019454
X (11/2)	0	0.658878	0.000053
W (9/2)	0	0	0.038843
R (3/2)	0.015683	0.172281	0
S (5/2)	0.210868	0.035514	0
S (9/2)	0.238226	0.193321	0.022107
A (3/2)	0.364042	0.002098	0
A (7/2)	0.163727	0.069765	0.000054
B (9/2)	0.083073	0.213106	0.001512
C (11/2)	0	0.001783	0.025935
D (5/2)	0.024648	0.000045	0
D (7/2)	0.159229	0.065364	0.039525
E (7/2)	0.108398	0.006185	0.106823
F (9/2)	0.488063	0.004580	0.153776
G (15/2)	0	0	0.004980
G (9/2)	0.104801	0.000002	0.056833

Table 5.7

Reduced Matrix Elements of the U Matrix for Transitions from Level L (11/2)

Lower Level	U_2^2	U_4^2	U_6^2
Z (15/2)	0.000009	0.023428	0.012961
Y (13/2)	0.000408	0.000480	0.000597
X (11/2)	0.000215	0.008380	0.000862
W (9/2)	0.002089	0.002473	0.002906
R (3/2)	0	0.000032	0.004094
S (5/2)	0	0.001043	0.004965
S (9/2)	0.183304	0.218633	0.401612
A (3/2)	0	0.004804	0.000439
A (7/2)	0.004387	0.014901	0.006100
B (9/2)	0.041242	0.040065	0.009703
C (11/2)	0.001131	0.000017	0.072092
D (5/2)	0	0.000142	0.002471
D (7/2)	0.032672	0.089895	0.067410
E (7/2)	0.015225	0.047380	0.050825
F (9/2)	0.000181	0.012152	0.016509
G (15/2)	0.269737	0.004652	0.168627
G (9/2)	0.058168	0.002408	0.149186

Table 5.8

Reduced Matrix Elements of U Matrix for Transitions from Level L (15/2)

Lower Level	U^2_2	U^2_4	U^2_6
Z (15/2)	0	0.025690	0.015981
Y (13/2)	0.000342	0.005155	0.004105
X (11/2)	0.000100	0.007668	0.002950
W (9/2)	0	0.003388	0.005269
R (3/2)	0	0	0.010576
S (5/2)	0	0	0.000175
S (9/2)	0	0.399605	0.181585
A (3/2)	0	0	0.001916
A (7/2)	0	0.002290	0.044763
B (9/2)	0	0.234357	0.170173
C (11/2)	0.003053	0.151578	0.324103
D (5/2)	0	0	0.005683
D (7/2)	0	0.019678	0.348455
E (7/2)	0	0.004159	0.156987
F (9/2)	0	0.166273	0.115140
G (15/2)	0.062162	0.276361	0.109309
G (9/2)	0	0.164353	0.281113

Table 5.9

Average Frequencies of Different Transitions and Refractive Indices of LaF_3 for the Corresponding Radiation

Terminating Level	Originating Level: L			K			R		
	(cm^{-1})	n_e	n_o	(cm^{-1})	n_e	n_o	(cm^{-1})	n_e	n_o
Z (15/2)	28342	1.619	1.628	26189	1.615	1.623	11417	1.594	1.59
Y (13/2)	26436	1.615	1.623	24283	1.612	1.619	9515	1.592	1.58
X (11/2)	24448	1.612	1.619	22295	1.608	1.614	7564	1.590	1.58
W (9/2)	22373	1.608	1.614	20220	1.605	1.610	5810	1.588	1.58
R (3/2)	16924	1.600	1.603	14771	1.598	1.599			
S (5/2)	15926	1.599	1.601	13773	1.596	1.597			
S (9/2)	15763	1.599	1.601	13610	1.596	1.597			
A (3/2)	14891	1.598	1.599	12738	1.595	1.595			
A (7/2)	14891	1.598	1.599	12738	1.595	1.595			
B (9/2)	13643	1.596	1.597	11490	1.594	1.593			
C (11/2)	12489	1.595	1.595	10336	1.593	1.591			
D (5/2)	11082	1.593	1.592	8929	1.591	1.588			
D (7/2)	11082	1.593	1.592	8929	1.591	1.588			
E (7/2)	9298	1.592	1.589	7145	1.590	1.586			
F (9/2)	8877	1.591	1.588	6684	1.589	1.584			
G (15/2)	7285	1.590	1.586	5132	1.588	1.582			
G (9/2)	7285	1.590	1.586	5132	1.588	1.582			

where

$$\langle f^n \alpha\ SLJ \| \underset{\sim}{U}^{\lambda} \| f^n\ \alpha'S'L'J' \rangle = (-1)^{S+L'+J+\lambda}\ \delta(SS')$$

$$\times\ [(2J+1)(2J'+1)]^{\frac{1}{2}} \begin{Bmatrix} J & J' & \lambda \\ L' & L & S \end{Bmatrix} \langle f^n \alpha\ SL \| \underset{\sim}{U}^{\lambda} \| f^n\ \alpha'S'L' \rangle \quad (5.5)$$

The $C(\alpha SL)$ and $C(\alpha'S'L')$ are the intermediate coupling coefficients and $\langle f^n \alpha\ SL \| \underset{\sim}{U}^{\lambda} \| f^n\ \alpha'S'L' \rangle$ are the matrix elements of the reduced $\underset{\sim}{U}^{\lambda}$ matrix.

The matrix elements of the reduced matrices are taken from the tables of Nielsen and Koster[8] and the 6j symbols are taken from Rotenberg et.al[9].

The results are tabulated in Tables 5.2-5.8. Each table gives the U matrix elements for transitions to all the J levels below the originating J level. Also, there are five tables corresponding to the level L. The matrix elements for the level R(J = 3/2) and the level K (J = 3/2) are shown in Tables 5.2 and 5.3 respectively*.

The parameters Ω_λ for $LaF_3:Nd^{3+}$ have been reported by Krupke[3] from the measurements of line intensities and the total absorption spectrum. The values of the parameters are

$$\Omega_2 = (0.35 \pm 0.14) \times 10^{-20}, \quad \Omega_4 = (2.57 \pm 0.36) \times 10^{-20} \text{ and}$$

$$\Omega_6 = (2.50 \pm 0.33) \times 10^{-20}$$

---

* Here, and in subsequent discussion, the angular momenta J of the levels are shown in parenthesis.

The correction factor χ for the refractive index n of the medium is given by

$$\chi = \chi_{md} = n^3 \quad \text{for magnetic dipole transitions}$$

$$\text{and} \quad \chi = \chi_{ed} = \frac{n(n+1)^2}{9} \quad \text{for electric dipole transitions} \qquad (5.6)$$

The refractive indices of LaF_3 have been measured[10] as a function of wavelength and are given by the relations

$$n_e = 1.5833 + \frac{77.85}{\lambda_{WL}-1346.5} \quad \text{and} \quad n_o = 1.57376 + \frac{153.137}{\lambda_{WL}-686.2} \qquad (5.7)$$

where λ_{WL} is given in Å. The values of the refractive indices calculated from (5.7) for various λ_{WL} are tabulated in Table 5.9 for convenience.

Using the reduced matrix elements of U matrix, the Ω_λ's and average n from Table 5.9 the transition probabilities for electric dipole transitions for the levels L, K and R are calculated. The results are tabulated in Tables 5.10 for all the three levels.

5.1.3b Magnetic Dipole Transitions

The expressions for the matrix elements of the operator M for a transition from the initial level $|(\alpha SL)J\rangle$ to the level $|(\alpha'S'L')J'\rangle$ are given in (2.13-2.15)[4]. The transition probability for magnetic dipole transitions is calculated from equation (5.3) using these expressions. The calculations show that for all the three levels L, K and R the contributions of

Table 5.10

Radiative Transition Probabilities

Determining Level	Originating Level						
	R	K	L(1/2)	L(3/2)	L(5/2)	L(11/2)	L(15/2)
	All in sec^{-1}						
(15/2)	731	232	29475	11555	2776	489	420
(13/2)	787	810	170	13595	7711	12	76
(11/2)	11	35	100	632	11486	81	69
(9/2)	8	50	0	168	495	37	42
(3/2)	-	0	0	53	969	10	21
(5/2)	-	43	105	1474	297	14	0
(9/2)	-	403	208	225	1109	1423	970
(3/2)	-	7	137	165	196	10	3
(7/2)	-	14	2067	158	350	41	65
(9/2)	-	214	321	798	658	80	436
(11/2)	-	187	1	196	60	78	391
(5/2)	-	11	204	255	5	2	3
(7/2)	-	5	86	281	192	122	205
(7/2)	-	7	21	61	113	45	53
(9/2)	-	60	0	104	169	11	81
(15/2)	-	74	0	0	2	45	64
(9/2)	-	62	2	22	31	34	71
Total radiative transition probability of the originating level	1537	2214	32897	29742	26619	2534	2970

Table 5.11

Magnetic Dipole Transition Probabilities

Terminating Level	Originating Level L(1/2)	L(3/2)	L(5/2)	L(11/2)
	All in sec^{-1}			
R (3/2)	0.023	0.0470		
A (3/2,7/2)	0.177	0.500	0.0	
S (5/2,9/2)		0.143	0.05	0.285
D (5/2,7/2)		0.119	0.23	
Z (15/2)				0.964

magnetic dipole transitions to the total rate of radiative transitions is very small. Table 5.11 gives the calculated transition rates for some of the magnetic dipole transitions.

5.1.3c Total Radiative Transition Probabilities

The total transition probability for radiative transitions from a particular level is the sum of the transition probabilities for transitions to different terminating levels from it. The following are the calculated radiative transition rates (Table 5.10)

$$R(3/2) = 1537 \pm 260 \text{ sec}^{-1},\ K(3/2) = 2214 \pm 360 \text{ sec}^{-1},$$

$$L(3/2) = 29742 \pm 4200 \text{ sec}^{-1},\ L(5/2) = 26619 \pm 3800 \text{ sec}^{-1},$$

$$L(1/2) = 32897 \pm 4600 \text{ sec}^{-1},\ L(11/2) = 2534 \pm 400 \text{ sec}^{-1}, \text{ and}$$

$$L(15/2) = 2970 \pm 540 \text{ sec}^{-1}$$

The uncertainity in the calculated values of the transition rate is due to the uncertainity in the reported values of Ω_λ's which are experimentally determined.

The reported total decay rate from level R of Nd^{3+} in LaF_3 is 1430 sec^{-1} at liquid nitrogen temperature for a concentration of 0.1% by wt[14]. This decay rate includes a small contribution from the multiphonon transitions (see sec.5.1.4). Since at low concentration, the observed decay rate is the sum of

the rates of radiative and multiphonon transitions, the observed decay rate from level R is mostly the radiative transition rate. The calculated radiative transition rate of (1537 ± 260) sec^{-1} from level R is, thus, comparable to the observed decay rate.

Fluorescence decay time could not be measured from level K of Nd^{3+} in $LaF_3:Dy^{3+}$ because of insufficient signal strength. No fluorescence was observed from level R of Nd^{3+} in this crystal.

Most of the fluorescence from the level L originates from the Stark components L_2 and L_3[1]*. SLJ assignment has not been done for these Stark components as the level L is a mixture of five J levels. The relative positions of the J levels in the ascending order of energy as obtained from the diagonalization of the energy matrix is as follows: the lowest is the J=3/2 level followed by J=5/2, 11/2, 1/2 and 15/2 in order. J-J mixing is not considered in the calculation of the matrix elements.

The observed decay rate from L_2 and L_3 at liquid nitrogen temperature is 3.45×10^4 sec^{-1}. This includes the contribution from multiphonon transitions which is expected to be 1.15×10^4 sec^{-1} (see sec. 5.1.4). The calculated radiative transition rate from the lowest J levels - J=3/2 and J=5/2 are $(2.97 \pm 0.42) \times 10^4$ sec^{-1} and $(2.66 \pm 0.38) \times 10^4$ sec^{-1} respectively. The average radiative transition rate is $(2.82 \pm 0.49) \times 10^4$ sec^{-1}. The estimated multiphonon transition rate when added to this rate will result in a decay rate which is comparable to the observed decay rate. This is discussed in more detail in section 5.1.4.

* L_1, the lowest energy absorption band observed in the region 28000-30000 cm^{-1} at liquid nitrogen temperature is possibly due to the transition from the excited Stark component Z_2 of the ground level Z to the Stark component L_2 (hot transition).

5.1.4 Multiphonon Relaxation

The multiphonon relaxation of the excited electronic states has been observed for a number of ions in lanthanum halide crystals. This relaxation is the result of the ion-lattice interaction. The spontaneous emission of the lattice phonons takes place during the transition of the ion. The rate of relaxation increases with temperature due to the stimulated emission of phonons.

The rate of spontaneous emission of phonons has been observed to depend exponentially on the energy separation of the levels. It is characteristic of the lattice and is independent of the ion. For a separation of energy $\Delta\varepsilon$, the spontaneous emission probability of the phonons W is given by[12]

$$W = Ce^{-\alpha\Delta\varepsilon} \qquad (5.8)$$

where C and α are constants characteristic of the lattice. The rates calculated from this equation are found to be within a maximum of $\pm$ 50% of the experimentally observed values in most of the cases. The relation (5.8) has been experimentally established for LaF_3 lattice by Riseberg and Moos[12] and the plot of W, the spontaneous emission rate of the phonons as a function of the energy gap has been given. For the levels L, K and R of Nd^{3+} in LaF_3, the rates of the spontaneous emission of phonons estimated from this plot are 1.15×10^4 sec^{-1}, 1.65×10^3 sec^{-1} and $\sim 10^2$ sec^{-1} respectively.

The decay rate of fluorescence at low concentration has been measured only for the level L. The observed decay rate is $(3.45 \pm 0.11) \times 10^4$ sec^{-1} at liquid nitrogen temperature. A decay rate of 1430 sec^{-1} at liquid nitrogen

temperature has been reported by Asawa and Robinson[11] for the level R at a concentration of 0.1% by wt. The calculated radiative transition probabilities are $(2.82 \pm 0.49) \times 10^4$ sec^{-1} for the level L and 1537 ± 260 sec^{-1} for the level R. The multiphonon transition rate can be obtained from the observed decay rate at low concentration by substracting the calculated radiative transition rate. This comes out to be $(0.63 \pm 0.60) \times 10^4$ sec^{-1} for the level L. This is within the limits of the estimated multiphonon transition rate of $(1.15 \pm 0.58) \times 10^4$ sec^{-1}* from level L. The calculated radiative transition rate and the observed decay rate of the level R are of the same magnitude. Hence it has not been possible to calculate the multiphonon transition rate from the observed decay rate. This can be expected since the estimated multiphonon transition rate for the level R ($\sim$100 sec^{-1}) is small in comparison to the observed decay rate (1430 sec^{-1}).

5.1.5 Temperature Variation of the Multiphonon Transition Rate

The decay rate of the level L has been observed to vary with temperature. The multiphonon transition rate calculated from the observed decay rates of level L are shown in Table 5.12.

The rate of multiphonon transition varies with temperature due to the stimulated emission of phonons from phonon modes which are thermally excited. An analytic expression for the temperature dependence of the transition rate has been obtained by Fong et.al[13] in the framework of the first order

* Here, the spontaneous emission probability of the phonons and the multiphonon transition rate at liquid nitrogen temperature are taken to be the same. The actual calculation shows that the rate at liquid nitrogen temperature is higher than the spontaneous emission probability of phonons by a factor of 1.02 for a 6th order process (p=6) and by a factor of 1.05 for a 7th order process (p = 7).

Table 5.12

Calculated Multiphonon Transition Rates of Level L

Radiative Relaxation Rate of Level L = $(2.82 \pm 0.49) \times 10^4$ sec^{-1}		
Temperature in °K	Observed total decay rate in 10^4 sec^{-1}	Multiphonon relaxation rate in 10^3 sec^{-1}
77	$3.451 \pm \begin{matrix}0.110\\0.101\end{matrix}$	$6.31 \pm \begin{matrix}6.0\\5.91\end{matrix}$
160	$3.662 \pm \begin{matrix}0.521\\0.403\end{matrix}$	$8.42 \pm \begin{matrix}10.11\\8.93\end{matrix}$
196	$4.120 \pm \begin{matrix}0.168\\0.157\end{matrix}$	$13.0 \pm \begin{matrix}6.53\\6.47\end{matrix}$
223	$4.726 \pm \begin{matrix}0.309\\0.274\end{matrix}$	$19.0 \pm \begin{matrix}7.99\\7.64\end{matrix}$
273	$6.190 \pm \begin{matrix}0.558\\0.505\end{matrix}$	$33.7 \pm \begin{matrix}10.48\\9.54\end{matrix}$
308	$6.826 \pm \begin{matrix}0.431\\0.382\end{matrix}$	$40.06 \pm \begin{matrix}9.21\\8.72\end{matrix}$

perturbation theory using the time correlation function representation for the transition rate. The expression is given in (2.32). For transitions between two multiplets, this expression is averaged over all thermally accessible states. The level L of Nd^{3+} is a multiplet with overlapping Stark components of five J levels. The observed absorption spectrum shows only 6 components[1] while the expected number of components is 20 (2 for J = 3/2, 3 for J = 5/2, 6 for J = 11/2, 1 for J = 1/2 and 8 for J = 15/2)*. In the absence of the complete information about the Stark components of the level L, the experimental observations could not be explained on the basis of the model proposed by Fong[13].

A qualitative explanation of the temperature dependence of the rate can still be given on the basis of this model and the importance of the contribution from the low energy phonons to the relaxation rate can be brought out. The multiphonon transition rate $W_{\alpha\alpha'}$, between the levels α and α' at a temperature T is given by[13]

$$W_{\alpha\alpha'}(T) = W_{\alpha\alpha'}(T=0)\,(1+n_m)^p \exp(-\tfrac{1}{2} L_m g_m^2 n_m) \qquad (5.9)$$

where $W_{\alpha\alpha'}(T=0)$ is the spontaneous emission rate of the phonons, $n_m = (\exp(h w_m/kT)-1)^{-1}$ is the occupancy number of the phonons in the effective (mediating) mode w_m, p is the number of phonons required to conserve the energy of transition and $L_m g_m^2$ is the coupling parameter. This expression for W can be derived from (2.32) for $n_m \ll 1$+.

* In the absorption spectrum of $LaF_3:Nd^{3+}$[10] absorption bands have been observed at liquid nitrogen temperature[1]. Four of these have been identified as transitions from the higher Stark components of the ground level $Z(^4I_{9/2})$ (hot transitions). Some of these may also be Stark components of the level L.

+ In the temperature region of interest ($kT < 210\ cm^{-1}$), $n_m < 1$ for p=6 ($w_m = 325\ cm^{-1}$), p=7 ($w_m = 275\ cm^{-1}$) and p=8($w_m = 240\ cm^{-1}$).

The information about the lattice phonon frequency distribution and the ion phonon coupling strength is obtained from the infrared, Raman and vibronic spectra. The infrared[14] and Raman[15] spectra for LaF_3 have been studied and the phonon frequencies are reported. The vibronic spectrum of $LaF_3:Pr^{3+}$ has been reported by Yen et.al[16]. The intensity of the vibronic sidebands is proportional to the product of the mode density and the coupling strength of the various phonons. The distribution of the intensity over various sidebands has been experimentally found to be similar for different impurity ions in the same lattice[17,18]. Assuming this to be true for LaF_3 also, it can be expected that the lattice phonons with energy in the region 200-250 cm^{-1} have large density and are strongly coupled to the ion. The phonon cut off frequency for LaF_3 is $\sim$360 cm^{-1}[16].

The coupling parameter $L_m g_m^2$ has been experimentally observed to be small ($\sim$0.15-0.2) in the case of Lanthanum halides[13]. Since $n_m < 1$ the equation (5.9) can be approximated to

$$W_{\alpha\alpha'}(T) = W_{\alpha\alpha'}(T=0)(1+n_m)^p \qquad (5.10)$$

This is the rate of emission of phonons at a temperature T in the model proposed by Kiel[12].

The energy gap between the L and K multiplets of $LaF_3:Nd^{3+}$ is 1935 cm^{-1}. The lowest order process consistent with the energy conservation is given by p=6 with the effective phonon energy of 324cm^{-1}. The calculated multiphonon transition rate for p=6 is shown in Figure 5.1. It can be seen from the figure that the calculated rates are smaller than the observed rates at all temperatures

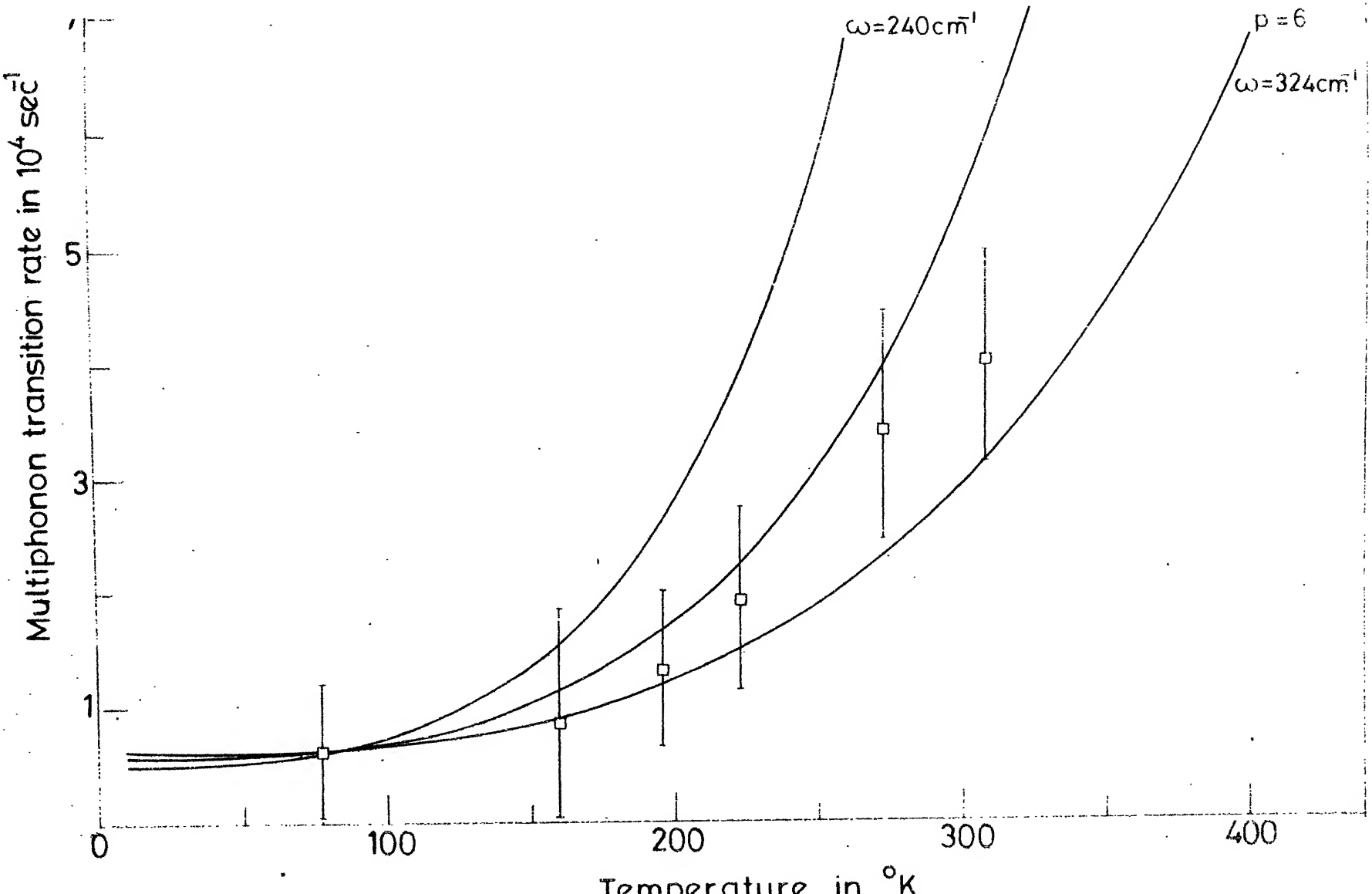

Fig.5.1 Temperature dependence of the multiphonon transition rate from level L_1 (Nd^{3+}) in LaF_3Nd^{3+}. The solid curves are calculated from equation 5.9 for 6th order, 7th order and 8th order processes.

indicating contributions from the higher order processes which have a steeper temperature dependence. The multiphonon transition rates for the 7^{th} and 8^{th} order processes are shown in Figure 5.1 for comparison. The 8^{th} order process corresponds to the effective phonon mode with energy in the range of 200 cm^{-1}-250 cm^{-1}. These are the strongly coupled modes.

A better fit with the experimental results can be obtained by considering the thermalization of the originating and terminating Stark multiplets since, the thermal average of the individual rates is less than the multiphonon transition rate calculated for the lowest Stark component of the originating level using equation (5.10).

In conclusion,it can be said that the above analysis of the temperature dependence of the multiphonon transition rate of level L is at best an explanation of the qualitative features of the observed dependence. There is, nevertheless, a clear indication of the importance of the contribution from low energy phonons to the relaxation process. A similar result has been reported for the multiphonon relaxation in $Y_3Al_5O_{12}$ and $YAlO_3$[18].

Temperature variation of the decay times of levels K and R has been studied in the 2% LaF_3Nd^{3+} system. The decay times of these levels have not been observed to vary much. The observed decay rate of 8.4×10^3 sec^{-1} at liquid nitrogen temperature from the level K is larger than the sum of the calculated radiative transition rate of 2.2×10^3 sec^{-1} and the estimated multiphonon transition rate of 1.65×10^3 sec^{-1} indicating contributions from other relaxation processes. Ion pair transitions are possible from this level to the lower levels contributing significantly to the relaxation rate. In the case of

the level R, the relaxation at high concentrations is predominantly due to ion pair transitions to the level W^{11} (see sec. 5.1.7). These ion pair transitions also can contribute to the temperature dependence of the decay rate. It is thus, not possible to conclude about the multiphonon transition rates from the measured decay rates of the levels K and R in the 2% $LaF_3:Nd^{3+}$ system, in the absence of the information about the ion pair transition rates from these levels.

5.1.6 Ion-Ion Interaction Relaxation

The observed relaxation rates from level L of Nd^{3+} in $LaF_3:Nd^{3+}$ is larger than what is observed in $LaF_3:Dy^{3+}$ at all temperatures indicating thereby that relaxation mechanismsother than the radiative and multiphonon transitions are operative. The concentration quenching of fluorescence is a well understood process[19]. In the absence of ion pair levels for possible energy exchange, the migration of the excitation energy to the quenching centers occurs where the energy transfer takes place. The lattice defects or the other impurity ions present in the crystal act as quenching centers. When the ion pair transitions are possible, the resultant rate of decay depends on the relative rates of the energy migration and the ion pair transitions[20]. The variations in the decay times due to different ion pairs is averaged out and the decay is a single exponential in the case of fast diffusion. The decay is nonexponential with a rapid fall in the excited ion population in the beginning followed by a slow decay when the rate of diffusion is not large.

For multipolar interactions, assuming no diffusion, the decay function is given by[21]

$$\Phi(t) = \Phi(0) \exp\left\{ -t/\tau_o - K(t/\tau_o)^{3/S} \right\} \qquad (5.11)$$

where $\Phi(0)$ is the initial excitation and τ_o is the intrinsic decay rate of the level. S indicates the different multipolar interactions - dipole-dipole (S=6), dipole-quadrupole (S=8) and quadrupole-quadrupole (S=10). The constant K is given by

$$K = \frac{4}{3} \Gamma(1 - 3/S) N_a R_o^3 \qquad (5.12)$$

where $\Gamma(x)$ is the gamma function with argument x, N_a is the acceptor concentration and R_o is the critical transfer distance $(C \tau_o)^{1/S}$ defined as that separation at which the probability for energy transfer between the donor-acceptor pair is equal to the intrinsic decay rate τ_o^{-1}, C being the interaction constant.

This equation is modified when the diffusion of the excitation energy is possible. The solution for the decay function including diffusion and donor-acceptor energy transfer via dipole-dipole coupling is given by[20]

$$\Phi(t) = \Phi(0) \exp\left\{ - t/\tau_o - \frac{4}{3} \pi^{3/2} A_t^{\frac{1}{2}} \left(\frac{1+10.87x+15.5x^2}{1+8.743x}\right) \right\} \qquad (5.13)$$

where $A = N_a C^{\frac{1}{2}}$ and $x = Bt^{2/3} = DC^{-1/3}t^{2/3}$, D being the diffusion constant for energy migration.

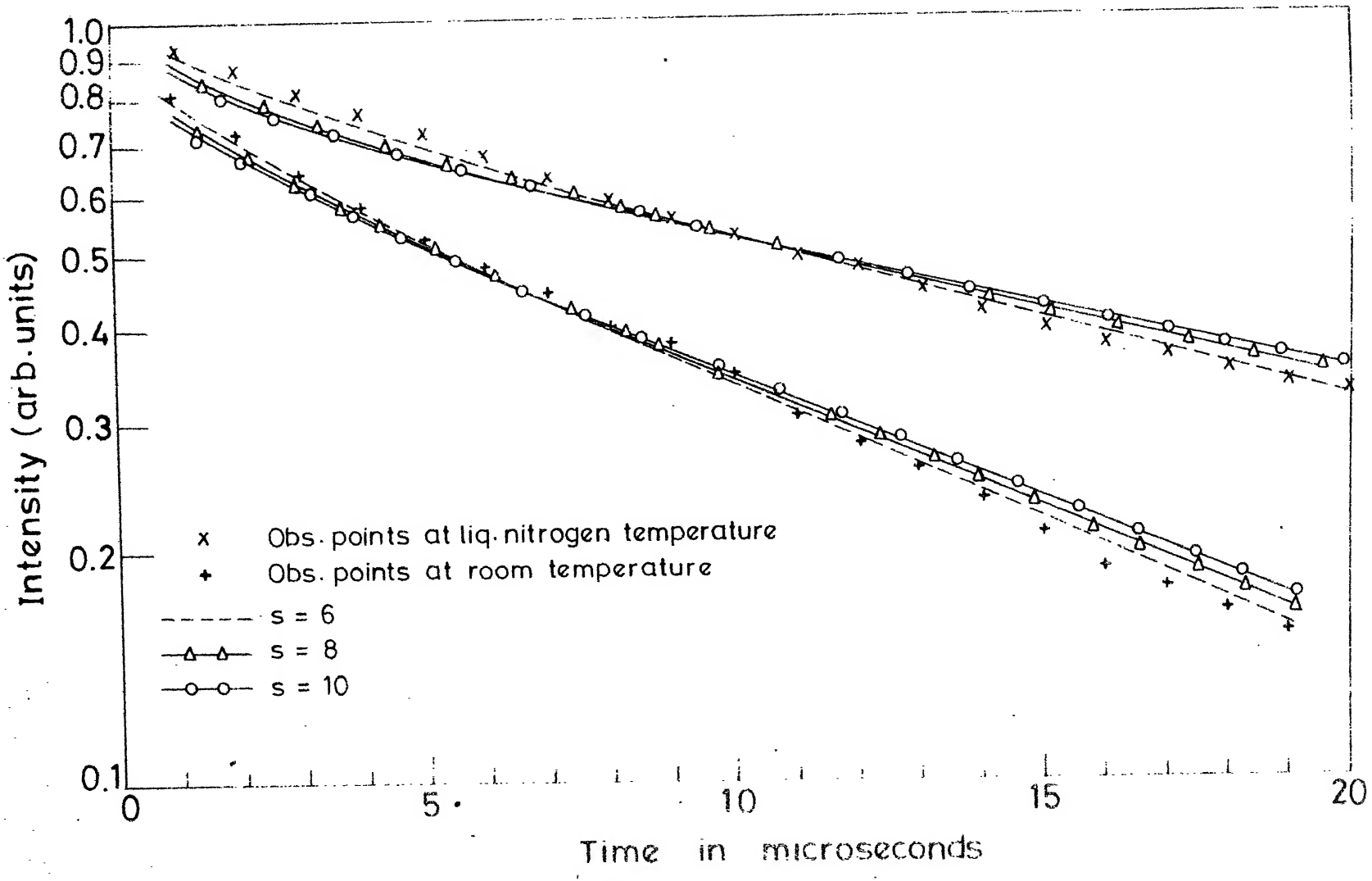

Fig. 5.2 Time dependence of the fluorescence from the level l_1 of Nd^{3+} in LaF_3. Dashed curves are calculated from equation(5.11) for different values of s.

The decay of fluorescence from level L of Nd^{3+} in LaF_3 is nonexponential. The semilog plot of the intensity with time is shown in Figure 5.2. The plot shows a faster decay in the beginning followed by a slow decay which approaches an exponential after $\sim$5 μsec. This suggests that the ion-ion interactions contribute to the relaxation from the level L. The reported positions of the Stark multiplets of Nd^{3+} in LaF_3[1] indicate a number of ion pair transitions from level L (see sec. 5.1.7).

The observed decay function is fitted to the equation (5.11) for S=6, 8 and 10. The calculated decay functions are shown in Figure 5.2. The agreement between the calculated and observed decay functions is better for S=6 than for S=8 or 10. The ion-ion interaction is, thus, predominantly via dipole-dipole coupling of the ions. The diffusion of the excitation energy is also likely as the donors and acceptors are Nd^{3+} ions. The rate of diffusion is not large. This can be seen from the small deviation of the calculated decay function from the observed decay function when t is sufficiently large. The decay rate due to diffusion $1/\tau_D$ can be calculated from the observed decay functions. $1/\tau_D$ is given by[22,23]

$$1/\tau_D = 11.404\, N_a D^{3/4} C^{1/4} \qquad (5.14)$$

where N_a is the acceptor concentration, D is the diffusion constant for the energy migration and C is the interaction constant.

The constants C and D are obtained by fitting the observed decay function shown in Figure 5.2 to the equation (5.13). The values of the constants are

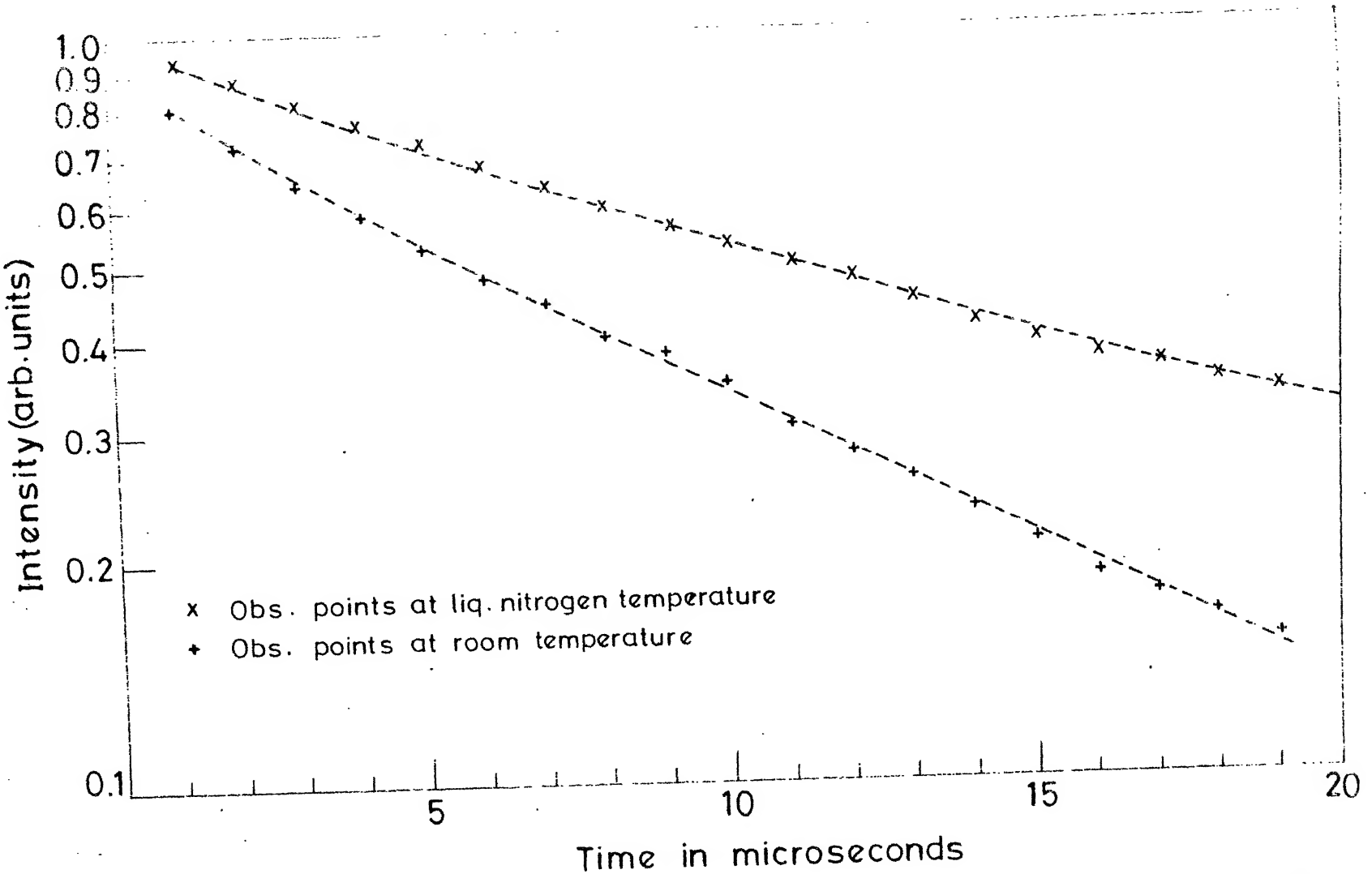

Fig. 5.3 Time dependence of the fluorescence from the level L of Nd^{3+} in LaF_3. The dashed curves are calculated from equation (5.13).

$$C = 7.8 \times 10^{-39}\ cm^6/sec \quad \text{and} \quad D = 7.9 \times 10^{-12}\ cm^2/sec$$

for the acceptor concentration $N_a \sim 2 \times 10^{20}/cm^3$ at liquid nitrogen temperature. The calculated and observed decay functions are shown in Figure 5.3.

The decay rate $1/\tau_D$ comes out to be

$$1/\tau_D = 11.404\ N_a\ D^{3/4}\ C^{1/4} = 3190\ sec^{-1}$$

This is small in comparison to the intrinsic decay rate of $3.45 \times 10^4\ sec^{-1}$ at liquid nitrogen temperature.

A similar result is obtained for the decay function of the same transition at room temperature (fig. 5.2 and 5.3). The values of the parameters C and D are

$$C = 7.4 \times 10^{-39}\ cm^6/sec \quad \text{and} \quad D = 1.5 \times 10^{-11}\ cm^2/sec$$

and $1/\tau_D = 5009\ sec^{-1}$ at room temperature.

The constant C depends on the overlap integral of the donor emission and the acceptor absorption spectra. and the intrinsic decay time of the donor ion. It can thus be expected to be dependent on temperature. The diffusion constant D also depends on the temperature through the linewidths of transitions and the transition probabilities[20].

The critical transfer distance $(C\tau_o)^{1/6}$ for the dipole-dipole coupling defined as that distance at which the probability of energy transfer between a donor-acceptor pair is equal to the intrinsic decay rate τ_o^{-1}, comes out to be

7.8Å at liquid nitrogen temperature and 6.9Å at room temperature. This distance is smaller than the average distance $d(\sim N_a^{-1/3})$ of 17Å between the neodymium ions. The ion-ion interaction is thus weak. This is also evident from the observed decay functions in which the nonexponentiality is less pronounced.

A detailed analysis of the decay functions with temperature is not possible due to the experimental uncertainties. The nonexponential region occurs within the first 5 microseconds. It is difficult to obtain many data points in this region. This, together with the inaccuracy in the measurement of the points, limits the scope of the experiment. The estimate of the order of magnitude of the quantities C and D can be made, at best.

Fluorescence from the level K is observed to decay as a sum of many exponentials. The intensity goes through a maximum of time t_{max}. The rate of decay of the 'tail' is $\sim 8 \times 10^3$ sec^{-1}. Ion pair transitions are possible from this level (see sec. 5.1.7). The nonexponential nature of the decay has not been observed from this level. This may be due to the slow pumping of the level K by the upper level L resulting in a multiexponential decay of the level K, thereby masking the nonexponential nature of the decay. Another reason could be fast diffusion of the excitation energy. The different transition rates due to the different ion pairs are averaged out and the decay is a single exponential.

Decay of fluorescence from level R is also multiexponential going through a maximum at t_{max}. The rate of decay of the 'tail' is $\sim 2 \times 10^3$ sec^{-1}. Ion pair relaxation is possible from this level and has been extensively studied by many workers in different lattices[11,25]. The concentration and temperature

quenching of fluorescence from this level in LaF_3 has been reported by Asawa and Robinson[11]. The single exponential decay of the level is attributed to the possibility of fast energy diffusion. Nonexponential decay of R level has been observed in silicate glasses, in which energy migration is small[24].

5.1.7 The Ion Pair Levels

The probable energy levels and transitions for ion pair transitions are obtained from fluorescence and absorption spectra[1]. The energy level diagram of $LaF_3:Nd^{3+}$ is shown in Figure 4.1. The following pairs of levels can be identified as possible levels for ion pair transitions from the reported positions of the energy levels.

(i) $L \longrightarrow K$, $Z \longrightarrow Y$

(ii) $L \longrightarrow A$, $Z \longrightarrow B$

(iii) $K \longrightarrow B$, $Z \longrightarrow R$

(iv) $L \longrightarrow D$, $Z \longrightarrow R$

(v) $L \longrightarrow C$, $Z \longrightarrow S$

(vi) $K \longrightarrow A$, $Z \longrightarrow S$

Some of the possible transitions are shown in Table 5.13.

The first three pairs are the resonant pairs. The last 3 are the non-resonant pairs requiring emission or absorption of phonons to conserve the energy. Of all the lattice phonons, the optical phonons are strongly coupled to the ions in comparison to the acoustic phonons[26]. Transitions involving the optical phonons are more probable. The phonon cut off frequency of LaF_3

Ion-pair Levels	Down Transition	Up Transition	Energy Difference	
$L \rightarrow K$, $Z \rightarrow Y$	$L_2(28339\ cm^{-1}) - K_2(26404\ cm^{-1})$	$Z_2(45\ cm^{-1}) - Y_1(1984\ cm^{-1})$	$+4\ cm^{-1}$	Resonant
		$Z_3(139\ cm^{-1}) - Y_3(2073\ cm^{-1})$	$-1\ cm^{-1}$	"
		$Z_4(291\ cm^{-1}) - Y_6(2225\ cm^{-1})$	$-1\ cm^{-1}$	"
	$L_5(28544\ cm^{-1}) - K_2(26404\ cm^{-1})$	$Z_2(45\ cm^{-1}) - Y_5(2190\ cm^{-1})$	$+1\ cm^{-1}$	"
	$L_5(28544\ cm^{-1}) - K_1(26364\ cm^{-1})$	$Z_2(45\ cm^{-1}) - Y_6(2225\ cm^{-1})$	$-4\ cm^{-1}$	"
$L \rightarrow B$, $Z \rightarrow A$	$L_2(28339\ cm^{-1}) - B_3(14891\ cm^{-1})$	$Z_2(139\ cm^{-1}) - A_2(13591\ cm^{-1})$	$+4\ cm^{-1}$	"
	$L_2(28339\ cm^{-1}) - B_5(14958\ cm^{-1})$	$Z_4(291\ cm^{-1}) - A_3(13671\ cm^{-1})$	$-1\ cm^{-1}$	"
		$Z_4(291\ cm^{-1}) - A_4(13677\ cm^{-1})$	$+5\ cm^{-1}$	"
	$L_3(2837\bullet\ cm^{-1}) - B_1(14835\ cm^{-1})$	$Z_3(139\ cm^{-1}) - A_3(13677\ cm^{-1})$	$-3\ cm^{-1}$	"
		$Z_3(139\ cm^{-1}) - A_4(13677\ cm^{-1})$	$+3\ cm^{-1}$	"
	$L_2(28370\ cm^{-1}) - B_2(14860\ cm^{-1})$	$Z_1(0\ cm^{-1}) - A_1(13515\ cm^{-1})$	$+5\ cm^{-1}$	"
	$L_4(28524\ cm^{-1}) - B_2(14860\ cm^{-1})$	$Z_2(45\ cm^{-1}) - A_5(13710\ cm^{-1})$	$+1\ cm^{-1}$	"
		$Z_2(45\ cm^{-1}) - A_6(13714\ cm^{-1})$	$+5\ cm^{-1}$	"
	$L_4(28524\ cm^{-1}) - B_3(14891\ cm^{-1})$	$Z_2(45\ cm^{-1}) - A_4(13677\ cm^{-1})$	$-1\ cm^{-1}$	"
	$L_4(28524\ cm^{-1}) - B_5(14566\ cm^{-1})$	$Z_3(139\ cm^{-1}) - A_5(13710\ cm^{-1})$	$5\ cm^{-1}$	"
	$L_3(28544\ cm^{-1}) - B_1(14835\ cm^{-1})$	$Z_1(0\ cm^{-1}) - A_5(13710\ cm^{-1})$	$1\ cm^{-1}$	"

Ion-pair Levels	Down Transition	Up Transition	Difference	
		Z_1(0 cm^{-1}) — A_6(13714 cm^{-1})	5 cm^{-1}	Resonant
	L_5(28544 cm^{-1}) — B_5(14958 cm^{-1})	Z_1(0 cm^{-1}) — A_2(13591 cm^{-1})	5 cm^{-1}	"
K → B, Z → R	K_2(26404 cm^{-1}) — B_2(14860 cm^{-1})	Z_1(45 cm^{-1}) — R_1(11592 cm^{-1})	3 cm^{-1}	"
L → D, Z → R	L_2(28339 cm^{-1}) — D_1(17304 cm^{-1})	Z_1(0 cm^{-1}) — R_2(11634 cm^{-1})	-557 cm^{-1}	Nonresonant 2 phonon assisted.
	L_5(28544 cm^{-1}) — D_3(17364 cm^{-1})	Z_3(139 cm^{-1}) — R_1(11592 cm^{-1})	-273 cm^{-1}	Nonresonant 1 phonon assisted.
	L_3(28370 cm^{-1}) — D_4(17512 cm^{-1})	Z_2(45 cm^{-1}) — R_1(11592 cm^{-1})	-690 cm^{-1}	Non resonant 2 phonon assisted.
L → C, Z → S	L_2(28339 cm^{-1}) — C_1(15998 cm^{-1})	Z_1(0 cm^{-1}) — S_1(12596 cm^{-1})	-255 cm^{-1}	Non resonant 1 phonon assisted.
	L_4(28524 cm^{-1}) — C_3(16045 cm^{-1})	Z_3(139 cm^{-1}) — S_2(12615 cm^{-1})	- 3 cm^{-1}	Resonant
	L_5(28544 cm^{-1}) — C_1(15998 cm^{-1})	Z_4(291 cm^{-1}) — S_1(12596 cm^{-1})	241 cm^{-1}	Nonresonant 1 phonon assisted.
	L_2(28339 cm^{-1}) — C_4(16059 cm^{-1})	Z_1(0 cm^{-1}) — S_8(12842 cm^{-1})	-562 cm^{-1}	Nonresonant 2 phonon assisted
K → A, Z → S	K_1(26364 cm^{-1}) — A_1(13515 cm^{-1})	Z_2(45 cm^{-1}) — S_1(12596 cm^{-1})	298 cm^{-1}	Nonresonant 1 phonon assisted
	K_1(26364 cm^{-1}) — A_6(13714 cm^{-1})	Z_2(45 cm^{-1}) — S_5(12694 cm^{-1})	+ 1 cm^{-1}	Resonant
	K_2(26404 cm^{-1}) — A_3(13631 cm^{-1})	Z_3(139 cm^{-1}) — S_1(12596 cm^{-1})	316 cm^{-1}	Nonresonant 1 phonon assisted
	K_2(26404 cm^{-1}) — A_5(13710 cm^{-1})	Z_1(0 cm^{-1}) — S_5(12694 cm^{-1})	1 cm^{-1}	Resonant

is $\sim$ 360 cm^{-1}. Phonon assisted ion pair transitions are thus possible for mismatch of energy $\gtrsim$ 250-300 cm^{-1}. The ion pair transitions for pair (4) occur through the assistance of 2 phonons. Transition between the pairs (5) and between the pairs (6) are possible by the assistance of a single phonon. The rate of phonon assisted transitions are much smaller than the multiphonon transitions for the same energy mismatch and, the dependence of the rate on the temperature is similar[27].

The maximum mismatch of energy for the resonant ion pair transitions (table 5.13) is 5 cm^{-1}. The reported absorption spectrum in the region of 28000-29000 cm^{-1} is accurate to within $\pm$ 5 cm^{-1}. The observed lines in the fluorescence spectrum are broader than the slitwidth used (30 μ)[28]. This corresponds to a minimum inaccuracy of $\pm$ 5 cm^{-1}. The energy mismatch of the ion pair transitions is, thus, within the experimental inaccuracy and a possibility of near matching of the levels exists. Better matching can be obtained at higher temperature due to the increase in the line width. The population of Z_4 and Z_5 is very small at liquid nitrogen temperature but increases with temperature. Contribution to the ion pair relaxation rate increases from these levels at higher temperature.

An indirect evidence of the ion pair relaxation can be obtained by studying the decay from the lower levels. The ion pair transitions affect the branching ratios of the originating level, if it is one of the ion pair levels. The decay functions of the lower levels depend on the decay times of the pumping levels and the branching ratios*. This can be illustrated by a simple example of a 4 level system.

---

* The branching ratio β_{ij} for transitions from level i to level j is difined as $\beta_{ij} = W_{ij} / \sum_j W_{ij}$ where W_{ij} is the probability for transitions to level j.

Consider a four level system with the level 3 relaxing radiatively to all the 3 levels and nonradiatively through multiphonon transitions to level 2, the level 2 relaxing radiatively to levels 1 and 0 and nonradiatively to level 1 and level 1 relaxing radiatively to level 0. No ion pair transitions are assumed to be present.

The rate equations for this system can be written as

$$\begin{aligned} \dot{n}_3 &= -w_3 n_3 \\ \dot{n}_2 &= \varphi_{32} w_3 n_3 - w_2 n_2 \\ \dot{n}_1 &= \varphi_{31} w_3 n_3 + \varphi_{21} w_2 n_2 - w_1 n_1 \end{aligned} \tag{5.15}$$

with the initial condition $n_3 = N$, $n_2 = 0$ and $n_1 = 0$ at $t = 0$. Here n_1, n_2, n_3 are the populations and w_1, w_2 and w_3 are the total decay rates of the levels 1, 2 and 3 respectively. φ_{ij} is the branching ratio of the decay rate for transitions from level i to level j.

The solutions of the equations (5.15) are

$$n_3 = N \exp(-w_3 t), \quad n_2 = \frac{\varphi_{32} N w_3}{(w_3 - w_2)} \left[\exp(-w_2 t) - \exp(-w_3 t)\right]$$

and

$$\begin{aligned} n_1 = {} & \frac{\varphi_{31} w_3 N}{(w_3 - w_1)} (e^{-w_1 t} - e^{-w_3 t}) + \frac{\varphi_{32} \varphi_{21} w_2 w_3 N}{(w_3 - w_1)(w_2 - w_1)} e^{-w_1 t} \\ & + \frac{\varphi_{21} \varphi_{32} w_2 w_3 N}{(w_2 - w_3)(w_2 - w_1)} e^{-w_2 t} - \frac{\varphi_{21} \varphi_{32} w_2 w_3 N}{(w_2 - w_3)(w_3 - w_1)} e^{-w_3 t} \end{aligned} \tag{5.16}$$

The population of level 2 increases in the beginning reaching a maximum at time t_{max} and then decays with the intrinsic decay rate of the level. The t_{max} is given by

$$t^2_{max} = \frac{\ln (w_3/w_2)}{w_3 - w_2} \tag{5.17}$$

The decay of population of level 1 depends on the decay time of intermediate level 2 and the branching ratios. In the limiting case when w_2 is very large,

$$n_1 = \left(\frac{\varphi_{31}\ w_3 N}{w_3 - w_1} + \frac{\varphi_{21}\ \varphi_{32} w_3 N}{w_3 - w_1}\right) (e^{- w_1 t} - e^{- w_3 t}) \tag{5.18}$$

The equation (5.18) shows that the level 1 decays as though no intermediate level is present. The branching ratio is different. The t_{max} depends on w_1 and w_3 only and is given by

$$t'_{max} (w_2 \longrightarrow \infty) = \frac{\ln (w_3/ w_1)}{w_3 - w_1} \tag{5.19}$$

For $w_2 > w_3$ and $w_2, w_3 > w_1$, the t_{max} is larger than $t'_{max} (w_2 \longrightarrow \infty)$. Typical decay curves of level 1 for different w_1, w_2 and w_3 are shown in Figure 5.4. In the other limit when $w_2 \simeq w_3 \simeq w$, the solution of n_1 is given by

$$n_1 = \frac{\varphi_{31}\ w\ N}{w - w_1} (e^{- w_1 t} - e^{-wt}) + \frac{\varphi_{21}\ \varphi_{32}\ N w^2}{(w - w_1)^2}$$

$$x \left(e^{- w_1 t} - \{(w - w_1)\ t + 1\}\ e^{-wt} \right) \tag{5.20}$$

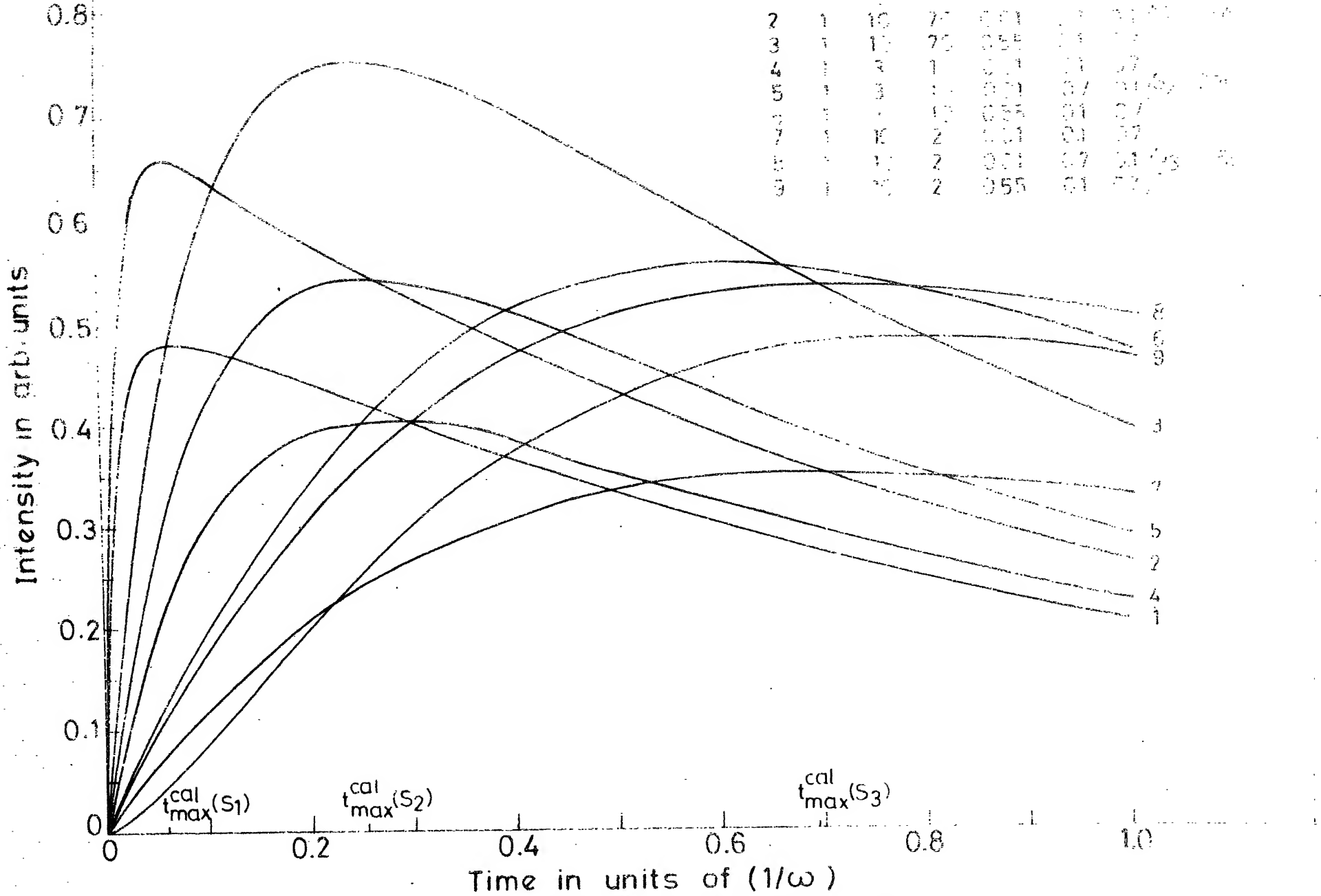

Fig. 5.4 Decay functions of the level I for different branching ratios

Here also, t'_{max} is greater than t'_{max} ($w_2 \to \infty$). Thus the effect of intermediate levels is to increase the t_{max}.

Consider now the case of strong ion-ion interactions in this system with the ion pair transitions taking place between the levels (3,0) and (2,1). The decay of the level 3 is nonexponential. In the limit of the Perrin's model, the effect of the ion-ion interactions is to populate levels 1 and 2 immediately on excitation of the level 3. The initial conditions for the system are

$$n_3 = N_3^0, \quad n_2 = N_2^0 \quad \text{and} \quad n_1 = N_1^0 \quad \text{at} \quad t = 0$$

The solutions for the rate equations (5.15) are

$$n_3 = N_3^0 \exp(-w_3 t)$$

$$n_2 = \left(N_2^0 + \frac{\varphi_{32} w_3 N_3^0}{w_3 - w_2}\right) \exp(-w_2 t) - \frac{\varphi_{32} w_3 N_3^0}{w_3 - w_2} \exp(-w_3 t)$$

and

$$n_1 = \left(\frac{\varphi_{31} w_3 N_3^0}{w_3 - w_1} + \varphi_{21} N_2^0 + N_1^0\right) e^{-w_1 t} - \frac{\varphi_{31} w_3 N_3^0}{w_3 - w_1} e^{-w_3 t} \qquad (5.21)$$

$$- \frac{\varphi_{21} w_2}{w_2 - w_1} \left(N_2^0 + N_3^0 \frac{\varphi_{32} w_3}{w_2 - w_3}\right) e^{-w_2 t}$$

The t_{max}, in this case, is given by

$$t_{max} = \frac{\ln\left(w_3 (\varphi_{32} w_3 N_3^0 / w_3 - w_2) / w_2 (N_2^0 + \varphi_{32} w_3 N_3^0 / w_3 - w_2)\right)}{w_3 - w_2} \qquad (5.22)$$

Table 5.14

The Observed and Calculated* t_{max} Values for L $\rightarrow$ R and K $\rightarrow$ R Transitions

Temperature	Observed t_{max}	Calculated t_{max}	
		t_{max}^{cal} for L $\rightarrow$ R	t_{max}^{cal} for K $\rightarrow$ R
77°K	30 μ sec	64.8 μ sec	215.7 μ sec
308°K	20.5 μ sec	43.9 μ sec	213.1 μ sec

Table 5.15

The Observed and Calculated* t_{max} Values for L $\rightarrow$ K Transitions

Temperature	Observed t_{max}	Calculated t_{max}^{cal}
77°K	31 μ sec	42.5 μ sec
308°K	27.5 μ sec	28.3 μ sec

* The decay rates used for the calculations are

	77°K	308°K
L	5×10^4 sec^{-1}	8.915×10^4 sec^{-1}
K	8.436×10^3 sec^{-1}	9.316×10^3 sec^{-1}
R	2.195×10^3 sec^{-1}	1.930×10^3 sec^{-1}

Similarly for t^1_{max} when $w_2 \to \infty$

$$t^1_{max} = \frac{\ln(w_3(\varphi_{31} w_3 N^o_3/(w_3 - w_1) + \varphi_{21} N^o_2 + N^o_1)/ w_1(\varphi_{31} w_3 N^o_3/(w_3 - w_1)))}{w_1 - w_3}$$

The additional populations N^o_1 and N^o_2 of the levels 1 and 2 reduce the t_{max}. The decrease in the t_{max}, thus, indicates possible ion-ion interaction relaxation.

Of the three fluorescing levels of Nd^{3+}, t_{max} is observed for K and R levels (table 5.14 and 5.15). The level K is populated by multiphonon and ion pair transitions from level L. The R level is populated by multiphonon and radiative transitions from levels L and K. Ion pair transitions are possible from level L to the levels A and B which relax by multiphonon transitions to the level K. To calculate the decay function of the level R, rate equations have to be solved in terms of the different branching ratios and the decay times of intermediate levels. The problem becomes intractable as (1) the decay of the level L is not a single exponential and (2) none of the intermediate levels fluoresce, with the result that branching ratios for the individual levels cannot be determined experimentally.

A qualitative explanation for the observed t_{max} of R level can be given in terms of the ideal 4 level system described above. The R level is assumed to have a single exponential decay. The level is populated by radiative and multiphonon transitions from many levels above it. Consider the two extreme cases - (1) Radiative transitions are the only possible transitions to the R level from levels K and L. The calculated t_{max}^{RT} for direct pumping through

radiative transition are 64.8 μsec for L → R transitions and 215.7 μsec for K → R transitions at liquid nitrogen temperature. Since the value of t_{max} due to K → R transitions is much larger than due to L → R transitions, the lower limit on t_{max}^{cal} is 64.8 μsec. (2) No radiative transitions to the level R are possible. Relaxation of the upper levels is by multiphonon transitions. In the case of the fast relaxation of the intermediate levels between L and R, the t_{max}^{MPT} is the same as t_{max}^{cal}. The effect of the intermediate levels is to increase the t_{max}. The estimated rates of multiphonon transitions for the intermediate levels is given in Table 5.16. These rates are calculated from the plot of multiphonon transition rates Vs energy gap[12]. The table clearly suggests that, because of the low multiphonon transitions rate of K and I levels, the t_{max}^{MPT} is larger than the t_{max}^{cal}. In the intermediate cases, the resulting t_{max}^{cal} depends on the different branching ratios and decay rates of the intermediate levels. The lower limit of t_{max}^{cal} is still what is obtained by assuming that all the intermediate levels relax very fast.

The observed t_{max}^{obs} are tabulated in Table 5.14. These are smaller than the t_{max}^{cal}. A decrease in t_{max} is possible if the lower levels have an initial population, or, if the lower levels are populated by some other mechanism with a rate faster than the rate of decay of the initial fluorescing level. In the case of the ideal 4 level system, it has been shown that ion-ion interaction transitions can populate the lower levels at a very fast rate resulting in the decrease of t_{max}. A similar mechanism is operative in this case also. The ion pair transitions are possible from the level L. The pair transition L → A, Z → B is the most probable transition to populate the level R. The levels

Table 5.16

Estimated Multiphonon Transition Rates

Originating Level	Energy gap in cm^{-1}	Transition rate in sec^{-1}
L	1935	1.15×10^4
K	2373	1.65×10^3
I	1469	2.25×10^5
H	194	$\gg 10^7$
G	1324	5×10^5
F	246	$\gg 10^7$
E	1548	1.5×10^5
D	1201	1×10^6
C	1040	2.25×10^6
B	1121	1.6×10^6
A	611	$> 10^7$
S	962	3.6×10^6
R	5041	$< 10^2$
W	1537	1.5×10^5
X	1696	7.5×10^4
Y	1484	2×10^5

A and B relax very fast to level R by multiphonon transitions. The large difference between the t_{max} and t_{max}^{obs} and the weak transitions observed from level L to level R suggest the possibility of the ion pair process being the dominant mechanism of populating the R level. This is in contrast to the dominance of multiphonon transitions observed in populating the level R of Nd^{3+} in $YAlO_3$[18]. The phonon cut off frequency of the lattice ($\sim$700 cm^{-1}) and the energy of the strongly coupled phonons (450-500 cm^{-1}) are larger in $YAlO_3$ than in LaF_3. The energy gaps between the levels L, K and I, on the other hand, are smaller. The multiphonon transition rates are very large for these levels in comparison to the rates in LaF_3. The dominance of the multiphonon transitions in the populating mechanism of the lower level can be expected in $YAlO_3$.

A similar decrease of t_{max} has been observed for the level K (table 5.15). The decrease in t_{max} is not as remarkable as in the case of level R. The difference in the observed and the calculated values of t_{max} can be attributed to the possible ion pair transitions from level L ($L \rightarrow K$, $Z \rightarrow Y$) though, the multiphonon transitions from level L contribute significantly to the K level population. The ion pair relaxation of the level K itself can be another reason. The decay due to ion pair transitions is nonexponential for negligible diffusion. This decay can be approximated to a sum of a number of exponentials, the lower limit on the decay rate being the intrinic decay rate. Each of these exponentials gives rise to a different t_{max}. The upper limit of the t_{max} is obtained for the decay with the slowest decay rate. The cumulative effect of all the exponential decays is to reduce t_{max}.

5.1.8 Fluorescence Mechanism of $LaF_3:Nd^{3+}$

The levels L, K and R are the only levels which are observed to fluoresce on excitation with nitrogen laser at 77°K. The laser radiation at 29656 cm^{-1} (3371Å) excites the neodymium ions in the ground level Z to the phonon coupled Stark components of the level L. The Stark component L_{10} (29551 cm^{-1}) of the level L observed in the absorption spectrum at liquid nitrogen temperature[1] is the closest to this energy of 29656 cm^{-1} requiring excitation of the lattice phonons around 105 cm^{-1} which is within the phonon spectrum of LaF_3.

The ions from level L relax mostly by radiative transitions to lower levels when the concentration of Nd^{3+} is small. The calculated radiative transition rates (Table 5.10) and the estimated multiphonon transition rates (Table 5.16) show that a maximum of ~ 30% of the ions reach level K by multiphonon transitions.* Of these, ~ 12% of the ions reach level I by multiphonon transitions while the rest decay by radiative transitions. The level I is separated from the next level H by 1469 cm^{-1} which is very large for efficient multiphonon relaxation. The level can, thus, be expected to fluoresce. No fluorescence has been observed from levels below level K in $LaF_3:Dy^{3+}$ in which the concentration of Nd^{3+} is ~0.02%. The possible reasons are

a. the concentration of the neodymium is too low for detectable fluorescence from levels below K,

b. the radiative transition rates of the levels below K are smaller than the corresponding multiphonon transition rates resulting in a predominant multiphonon relaxation, or

c. the branching ratios of the radiative transitions to the lower levels which give rise to fluorescence in the region 3400Å-9000Å (the region which has been investigated) are small.

* This number is obtained from the ratio of the estimated multiphonon transition rate of 1.15×10^4 sec^{-1} to the total decay rate of 3.45×10^4 sec^{-1} observed at liquid nitrogen temperature. The ratio is smaller if the calculated multiphonon transition rate of 0.63×10^4 sec^{-1} is considered. When the decay rate is not measured, as in case of level K, the sum of the calculated

The absence of fluorescence from the level R rules out the possibility (b), since all the ions from level I would eventually reach level R and the level R relaxes mostly by radiative transitions at low concentrations of neodymium.

When the concentrations of neodymium is high, as in the 2% $LaF_3:Nd^{3+}$ crystal, the ions from level L relax by ion pair and radiative transitions. The level K is populated more by multiphonon transitions than by ion pair transitions from level L. The observed decay rates and the estimated multiphonon transition rates indicate that 20% of the ions reach level K by multiphonon transitions of which $\lesssim$ 4% reach level I. This population ($\lesssim$ 4% of the total excited ion population) is much smaller in relative units compared to the population reaching level I ($\sim$ 20% of the total excited ion population) when the neodymium concentration is small. The absence of fluorescence from the levels I, G and E, which have smaller multiphonon transition rates compared to other levels, is possibly due to (b) or (c) or both, stated above. The level R is populated by radiative transitions from level L and by multiphonon transitions from level S. The ion pair transitions from level L populate the levels A and B which relax very fast, the minimum decay rate being the multiphonon transition rate of $\sim 10^6$ sec^{-1} from these levels. The levels A, B and S can be expected to have multiphonon transition rates which are at least comparable to the radiative transition rates. This is evident from the observation of smaller values of t_{max} for the fluorescence from level R, than what are expected assuming the absence of ion pair transitions from levels K or L. The observed values for t_{max} has been explained in terms of the rate of increase of the population of level R by fast multiphonon transitions from level S which is in turn populated

by fast multiphonon transitions from level A (see sec. 5.1.7). The level R is, thus, populated by fast multiphonon transitions from levels A and B through level S.

5.2.1 Lifetimes of Dy^{3+}

Two levels of Dy^{3+} - a level at 29500 cm^{-1} and the level $^4F_{9/2}$ ($\sim$21000 cm^{-1}) have been observed to fluoresce on excitation with nitrogen laser (fig. 4.4). The decay times of the level at 29500 cm^{-1} are not measured as the transitions from this level are weak. Temperature variation of the decay rate from the level $^4F_{9/2}$ has been studied. The variation in the decay rate is small. The decay function is a single exponential with t_{max} being less than the rise time of the detecting system ($\sim$5 μsec.).

The level $^4F_{9/2}$ is separated from the next level $^6F_{3/2}$ by $\sim$ 7500 cm^{-1}[29]. The expected multiphonon transition rate is very small. The observed decay rate is, thus, the sum of the radiative transition rate and ion-ion interaction transition rate, if any. The radiative transition rate could not be calculated for this system as the values of the parameters Ω_λ's are not reported. The ion pair transitions are possible from the level $^4F_{9/2}$ to the lower levels (see Table 5.17). This can only be confirmed by the measurement of decay rates with varying concentrations.

The absence of t_{max} indicates that the level is pumped by mechanisms whose rate is faster than $\sim 1 \times 10^6$ sec^{-1}. The maximum energy gap in the energy levels of Dy^{3+} above the level $^4F_{9/2}$ is 1500 cm^{-1}. The expected multiphonon transition rate for this gap is 2×10^5 sec^{-1}. The level $^4F_{9/2}$ is most

Table 5.17

Resonant Ion Pair Transitions in $LaF_3:Dy^{3+}$

Down Transitions	Up Transitions	Difference in Energy
29526 cm^{-1} — 23501 cm^{-1}	$^6H_{15/2}$(0 cm^{-1}) — $^6H_{11/2}$(6024 cm^{-1})	+ 1 cm^{-1}
— 23550 cm^{-1}	$^6H_{15/2}$(0 cm^{-1}) — $^6H_{11/2}$(5977 cm^{-1})	- 1 cm^{-1}
$^4F_{9/2}$(21141 cm^{-1}) — $^6F_{3/2}$ (13284 cm^{-1})	$^6H_{15/2}$(69cm^{-1}) — $^6H_{9/2}$(7931 cm^{-1})	- 5 cm^{-1}
$^4F_{9/2}$(21218 cm^{-1}) — $^6F_{3/2}$ (13284 cm^{-1})	$^6H_{15/2}$(0 cm^{-1}) — $^6H_{9/2}$(7931 cm^{-1})	+ 3 cm^{-1}
$^4F_{9/2}$(21218 cm^{-1}) — $^6F_{3/2}$ (13271 cm^{-1})	$^6H_{15/2}$(69cm^{-1}) — $^6H_{9/2}$(8011 cm^{-1})	+ 5 cm^{-1}

probably not populated by the multiphonon transitions from the upper levels. The possibility of ion pair transitions from the level at 29526 cm^{-1} to levels higher than the $^4F_{9/2}$ exists (Table 5.17). These levels relax very fast ($\gtrsim 10^6$ sec^{-1}) by multiphonon transitions to the $^4F_{9/2}$ thereby decreasing t_{max}.

5.3.1 Conclusion

The relaxation mechanism of the excited states of Nd^{3+} and Dy^{3+} in LaF_3 lattice have been studied by measuring the decay rates of the fluorescence excited by a pulsed nitrogen laser at six different temperatures. The energy levels studied are the L, K and R levels of Nd^{3+} and the level $^4F_{9/2}$ of Dy^{3+}.

The rate of decay from the level L is dependent on the temperature as well as the concentration. The decay time decreases with an increase in temperature and/or concentration. The decay function is a single exponential for Nd^{3+} in LaF_3:Dy^{3+} system and is nonexponential in the 2% LaF_3:Nd^{3+} system. This suggests the possibility of multiphonon and radiative relaxation being operative in both the systems with the ion-ion interaction relaxation contributing significantly only at higher concentrations. The other two levels K and R also relax by all the three processes though the rate of multiphonon transitions from level R is negligible in comparison to the total decay rate.

The radiative transition rates are calculated for all the three levels using Judd-Ofelt's theory[30]. The estimated rates of multiphonon transitions are obtained from the empirical relation between the transition rate and the energy gap, established for LaF_3 by Riseberg and Moos[12]. The total calculated decay rate (multiphonon and radiative transition rates) for the level R is in

agreement with the observed value. The fluorescence decay rates have not been measured for the K level at low concentration. No reported values of the decay rates from level K are available for a comparison with the calculated values. In the case of the level L, which is a mixture of five J levels, the application of the Judd-Ofelt's theory is not strictly valid as the J level mixing is not negligible. Still, the calculated decay rate has been found to be in agreement with the observed value. The difference between the two rates can be accounted for by the assumptions made in the theory and the uncertainity in the values of Ω_λ's.

The temperature variation of the multiphonon transition rate of the level L cannot be explained in terms of the models proposed by Fong[13] or Risberg and Moos[12]. The phonon mode with a frequency which is close to the cut off frequency of the phonon spectrum of the lattice, has been observed by them, to contribute significantly to the relaxation. This is not so in the present case. The calculated multiphonon transition rate from the level L is less than the observed rate for a lowest order process with the highest phonon energy, consistent with the energy conservation principle, even without taking into the consideration the thermalization of the Stark multiplets, which reduces the transition rate. The contribution to relaxation from higher order processes with lesser phonon energies is, thus, not insignificant.

The ion-ion interactions contribute significantly to the relaxation of all the three levels L, K and R in $LaF_3:Nd^{3+}$. The cross relaxation ($R \rightarrow W$, $Z \rightarrow Y$) of the level R has been studied in many hosts including LaF_3[11,24,25]. The exact nature of the ion-ion interaction in LaF_3 is not known.

The contribution to the relaxation by different ion pairs is averaged out by fast migration[11] of the excitation energy as is evident from the single exponential decay. Ion pair transitions are possible from the other two levels K and L. The decay function is observed to be nonexponential in the case of level L. The ion-ion interactions for this level are mostly dipole-dipole in nature. Migration of an excitation energy is small.

An indirect evidence of the ion pair transitions from the level L has been obtained by studying the decay functions of the levels K and R. The fluorescence intensity of these levels goes through a maximum in time which is characteristic of indirectly pumped levels. The observed values for t_{max} are less than the estimated lower limits on t_{max} obtained from the multiphonon transition rates and the calculated radiative transition rates. Decrease in t_{max} is possible when the rate of pumping of the level is faster than the multiphonon and radiative transition rates. The ion pair transitions from the level L to the lower levels can explain the increase in the pumping rate of the levels R and K.

Fluorescence has been observed to decay exponentially from the $^4F_{9/2}$ level of Dy^{3+} in LaF_3. The decay rate does not vary much with temperature. This level is separated from the next lower level by $\sim$ 7500 cm^{-1}. The multiphonon transition rate is thus negligible. The level decays mostly by radiative and ion pair transitions. The fluorescence mechanism of this level is not very clear as the observed t_{max} is very small compared to the estimated value.

5.3.2 Comments for Further Work

Most of the work presented in this thesis has been done on the samples of $LaF_3:Nd^{3+}$ at six temperatures in between room temperature and liquid nitrogen temperature. It is suggested that the measurements be made on more number of samples with the concentration of Nd^{3+} varying from a very low value of 0.01% by wt. to a very high value of 15% - 20% by wt. This will establish the radiative and the multiphonon transition rates from the level K. The MPTR* for the level L has been calculated from the observed decay rate and the calculated radiative transition rates. A better method is to measure the multiphonon quantum efficiency at different temperatures for the levels and thus establish the multiphonon transition rates. The contribution due to the phonon-assisted ion pair transitions and the temperature dependent resonant ion pair transitions can be separated from the total decay rate at higher concentrations. The dominant mechanism of the ion pair transitions from the level L can be established by studying the decay rate at different concentrations and temperatures. The initial rapid fall in the intensity which occurs within the first 5 μsec. is to be followed carefully for this. The study of the variation of the t_{max} of the lower levels with concentration and temperature can provide additional information.

In the case of $LaF_3:Dy^{3+}$ also, the measurement of the decay time has to be made on more number of samples at different temperatures. The level $^4F_{9/2}$ is ideal for the study of ion pair transitions and energy migration in LaF_3 as the multiphonon decay rates are negligible. The radiative transition rate can be obtained from the measurement of the decay rate with low concentration

---

* MPTR - Multiphonon Transition Rates.

samples. The phenomenological parameters required for the calculation of the radiative transition rates are not reported. They can be calculated from the observed absorption and fluorescence spectra of $LaF_3:Dy^{3+}$ reported by Fry et.al[29].

REFERENCES

1. Kumar, U.V., Jagannath, H., Ramachandra Rao, D., and Venkateswarlu, P. - Ind. J. of Phys. 50, 90 (1976).

2. Partlow, W.D., and Moos, H.W., - Phys. Rev. 157, 252 (1967).

3. (a) Krupke, W.F. - Phys. Rev. 145, 325 (1966).

   (b) Krupke, W.F. - IEEE J. Quantum Electronics QE 7, 153 (1971).

4. (a) Weber, M.J. - Phys. Rev. 157, 262 (1968).

   (b) Weber, M.J., Matsinger, B.H., Donlan, V.L., and Surratt, G.T. - J. Chem. Phys. 57, 562 (1972).

5. Minhas, I.S. - Ph.D. thesis, Indian Institute of Technology Kanpur, India (1972).

6. Narayana, P.A. - Can. J. Phys. 47, 2753 (1969).

7. Wong, E.Y. - J. Chem. Phys. 35, 544 (1961).

8. Nielsen, C.W., and Koster, G.F. - Spectroscopic Coefficients for the p^n, d^n and f^n Configurations (The MIT Press, Cambridge, Mass., 1963).

9. Rotenberg, M., Bivens, R., Metropolis, N., and Wooten, J.K. - The 3-j and 6-j Symbols (MIT Press, Cambridge, Massachusetts, 1964).

10. Wirick, M.P. - App. Optics 5, 1966 (1966).

11. Asawa Cook, and Robinson, M.T. - Phys. Rev. 141, 251 (1966).

12. Riseberg, L.A., and Moos, H.W. - Phys. Rev. 174, 429 (1968).

13. (a) Fong, F.K., Naberhuis, S.L., and Miller, M.M. - J. Chem. Phys. 56, 4020 (1972).

   (b) Wassam, W.A., and Fong, F.K. - J. Chem. Phys. 58, 956 (1973).

14. Rast, H.E., Casper, H.H., Miller, S.A., and Buchanan, R.A. - Phys. Rev. 171, 1051 (1968).

15. Bauman, R.P., and Porto, S.P.S. - Phys. Rev. 161, 842 (1967).

16. Yen, W.M., Scott, W.C., and Schalow, A.L. - Phys. Rev. A271, 136 (1964).

17. Cohen, E., Riseberg, L.A., and Moos, H.W. - Phys. Rev. 175, 521 (1968).

18. Weber, M.J. - Phys. Rev. B8, 54 (1973).

19. Dexter, D.L., and Schulman, H.H. - J. Chem. Phys. 22, 1063 (1954).

20. Weber, M.J. - Phys. Rev. B4, 2932 (1971).

21. Inokuti, M., and Hirayana, F. - J. Chem. Phys. 43, 1978 (1965).

22. Wright, J.C. - Private Communication.

23. Van der Ziel, J.P., Kopf, L., and Van Uitert, L.G. - Phys; Rev. B6, 615 (1972).

24. Chrysochoos, J. - J. Chem. Phys. 61, 4596 (1974).

25.(a) Liao, P.F., and Weber, H.P. - J. App. Phys. 45, 2931 (1974).

(b) Singh, S., Miller, D.C., Potowics, J.R., and Shick, L.K. - J. App. Phys. 46, 1191 (1975).

26. Imbusch, G.F. - Phys. Rev. 153, 326 (1967).

27. Yamada, N., Shionaya, S., and Kushida, T. - J. Phys. Soc. Japan 32, 1577 (1972).

28. Kumar, U.V. - Ph.D Thesis, Indian Institute of Technology Kanpur, India (1975).

29. Fry, J.L., Caspers, H.H., Rast, H.E., Miller, S.A., and Freasier, B. - J. Chem. Phys. 48, 2342 (1968).

30.(a) Judd, B.R. - Phys. Rev. 127, 750 (1962).

(b) Ofelt, G.S. - J. Chem. Phys. 37, 511 (1962).

CHAPTER VI

FLUORESCENCE SPECTRUM OF $CaF_2:Dy^{3+}$

6.1 Introduction

The luminescence spectrum of trivalent dysprosium in CaF_2 has been studied by many workers[1-7]. The dysprosium ion occupies the site of calcium in the lattice. In the absence of other impurities, the excess positive charge on the Dy^{3+} ion is balanced by an extra F^- ion. The relative position of the F^- ion with respect to the Dy^{3+} ion decides the site symmetry of the Dy ion as cubic, tetragonal, trigonal or orthorhombic. The number of Stark components of the different 'free ion' levels and the separations between them depend on the site symmetry. Different centers are found to predominate in the luminescence spectra depending on the concentration of dysprosium and on the method of excitation[5,6,10,11].

The first attempt to identify the centers was by Rabbiner[1] who studied the luminescence spectra of crystals grown in a reducing atmosphere. On the basis of the number of Stark components observed, he concluded that the spectrum

is mainly due to cubic centers. The three subgroups observed, have been explained by Rabbiner[1] as due to transitions from the Stark levels of $^6F_{11/2}$ to those of $^6H_{15/2}$, $^6H_{13/2}$ and $^6H_{11/2}$ respectively from cubic centers. However, later work of other authors - Voronko et.al[2], Kiss and Staebler[3], Merz and Pershan[4] and Luks et.al[5] has indicated that the spectrum obtained by Rabbiner is not due to cubic centers. The absorption, luminescence and excitation spectra was studied by Voronko et.al[2]. The presence of three centers none of which is cubic, is indicated in their studies. The centers were denoted as Type I, Type II and Type III. One of the three centers (Type III) has been found to dominate in crystals containing oxygen as an additional impurity. Subsequently Kiss and Staebler[3] and Merz and Pershan[4] have obtained the luminescence spectrum due to cubic centers in thermoluminescence of X-ray irradiated crystals. Luks et.al[5] have investigated the luminescence spectrum of $CaF_2:Dy^{3+}$ in the region 5700Å-4800Å at room temperature, liquid nitrogen temperature and liquid helium temperature. Spectra due to four different centers have been observed. These have been isolated by studying the after glow times of luminescence which are different for different centers. An energy level scheme involving transitions from the Stark levels of $^6F_{11/2}$ to those of $^6H_{15/2}$ and $^6H_{13/2}$ has been proposed for three of the four centers[5].

Luminescence of Dy^{3+} in the systems MeF_2 (Me = Ca, Cd, Ba and Sr) has been studied by Al'tshuler et.al[6]. The spectrum due to cubic centers has been found to be similar in all the hosts. This is confirmed by studying the after glow times. The upper free ion level from which the luminescence originates has been identified to be $^4F_{9/2}$ and not $^6F_{11/2}$. The lower free ion levels

involved are $^6H_{15/2}$, $^6H_{13/2}$ and $^6H_{11/2}$. An energy level diagram showing the levels - $^6H_{15/2}$, $^6H_{13/2}$, $^6H_{11/2}$ and $^4F_{9/2}$ and the involved transitions for cubic centers is given[6]. A similar identification has been possible for the orthorhombic centers[6]. It may be noted here that transition identified as belonging to orthorhombic centers by Altshuler et.al[6] are the same as those originally attributed by Luks et.al[5] to rhombic centers. Crystal field parameters have been calculated[6] from the observed spectra for cubic and orthorhombic centers.

Transitions from $^4F_{9/2}$ level to other levels ($^6H_{9/2}$, $^6F_{11/2}$), ($^6H_{7/2}$, $^6F_{9/2}$), $^6H_{5/2}$ and $^6F_{7/2}$ are also possible. These have been observed in the case of LaF_3 and other hosts[8,9] but are not reported in CaF_2:Dy^{3+}. We have now observed the transitions from $^4F_{9/2}$ level to ($^6H_{9/2}$, $^6F_{11/2}$) and ($^6H_{7/2}$, $^6F_{9/2}$) levels in the luminescence spectrum of CaF_2:Dy^{3+} excited by nitrogen laser (3371Å). Most of the observed transitions (see Figs. 6.5 and 6.6) have been found to be transitions between the levels of tetragonal centers. An attempt is made here to obtain the position of the Stark components of $^6H_{11/2}$, ($^6H_{9/2}$, $^6F_{11/2}$) and ($^6H_{7/2}$, $^6F_{9/2}$) levels from the observed spectrum.

6.2 Experimental Details

CaF_2:Dy (0.01%, 0.03%, 0.09%, 0.27%, 0.54% and 1% by wt) crystals were grown by Bridgeman's method in a vacuum furnace at Bhabha Atomic Research Centre, Bombay, India.* The crystals are found to contain Nd^{3+} as an additional impurity in very small quantities (~10 ppm). The spectrum of Nd^{3+} predominates in the region 3400Å-4200Å in the crystals with low concentration of Dy^{3+}.

* The author has grown these crystals in association with his colleague Mr. A.Sivaram and Dr. S. Muralidhara Rao, Health Physics Division, BARC in a vacuum furnace built by Dr. S. Muralidhara Rao.

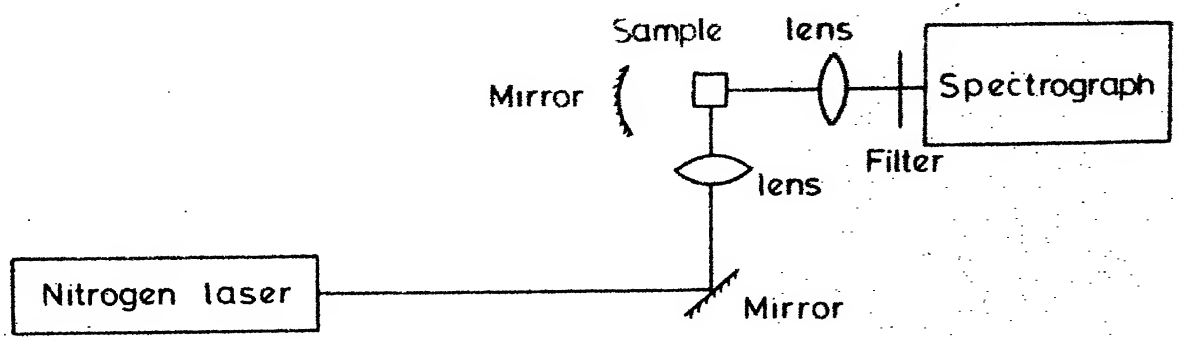

Fig. 6.1 Optical arrangement for photographing the spectrum.

Nitrogen laser is used as the source of radiation. The optical arrangement is shown in Figure 6.1. The fluorescence output is collected in a direction perpendicular to the incident beam and is focussed on the entrance slit of the spectrograph. A Carl Zeiss Q-24 UV spectrograph and a 3 prism glass spectrograph are used to photograph the spectrum in the region 3400Å-9000Å. The dispersion of the spectrograph varies with the region - from 47Å/mm at 4500Å to 220Å/mm at 9000Å. A slitwidth of 30 μ is used in all the regions. This corresponds to a spectral width of ~ 1.5Å (7 cm^{-1}) at 4500Å and ~ 6.5Å (8 cm^{-1}) at 9000Å. Eastman Kodak spectrographic plates (103 a-O, N and F) are used to record the spectra. Cesium and potassium lamps (Osram) are used for obtaining the standard spectra in the region 5250Å-9000Å. Iron arc is used as a standard for the region below 5250Å (not shown in the figure). The plates are measured on a Carl Zeiss model B, Abbe comparator which has a least count of 1 μ. The estimated error in the measurements is about ± 1Å.

6.3 Results and Discussion

Five groups of fluorescence are observed in $CaF_2:Dy^{3+}$ at liquid nitrogen temperature and are shown in Figures 6.2 and 6.3. On comparison with the fluorescence spectrum[8] of $LaF_3:Dy^{3+}$ at liquid nitrogen temperature, the following assignments can be made:

1. $^4F_{9/2} - {}^6H_{15/2}$ (~21000 cm^{-1})
2. $^4F_{9/2} - {}^6H_{13/2}$ (~17400 cm^{-1})
3. $^4F_{9/2} - {}^6H_{11/2}$ (~15000 cm^{-1})
4. $^4F_{9/2} - {}^6H_{9/2}, {}^6F_{11/2}$ (~13200 cm^{-1})
5. $^4F_{9/2} - {}^6H_{7/2}, {}^6F_{9/2}$ (~11800 cm^{-1})

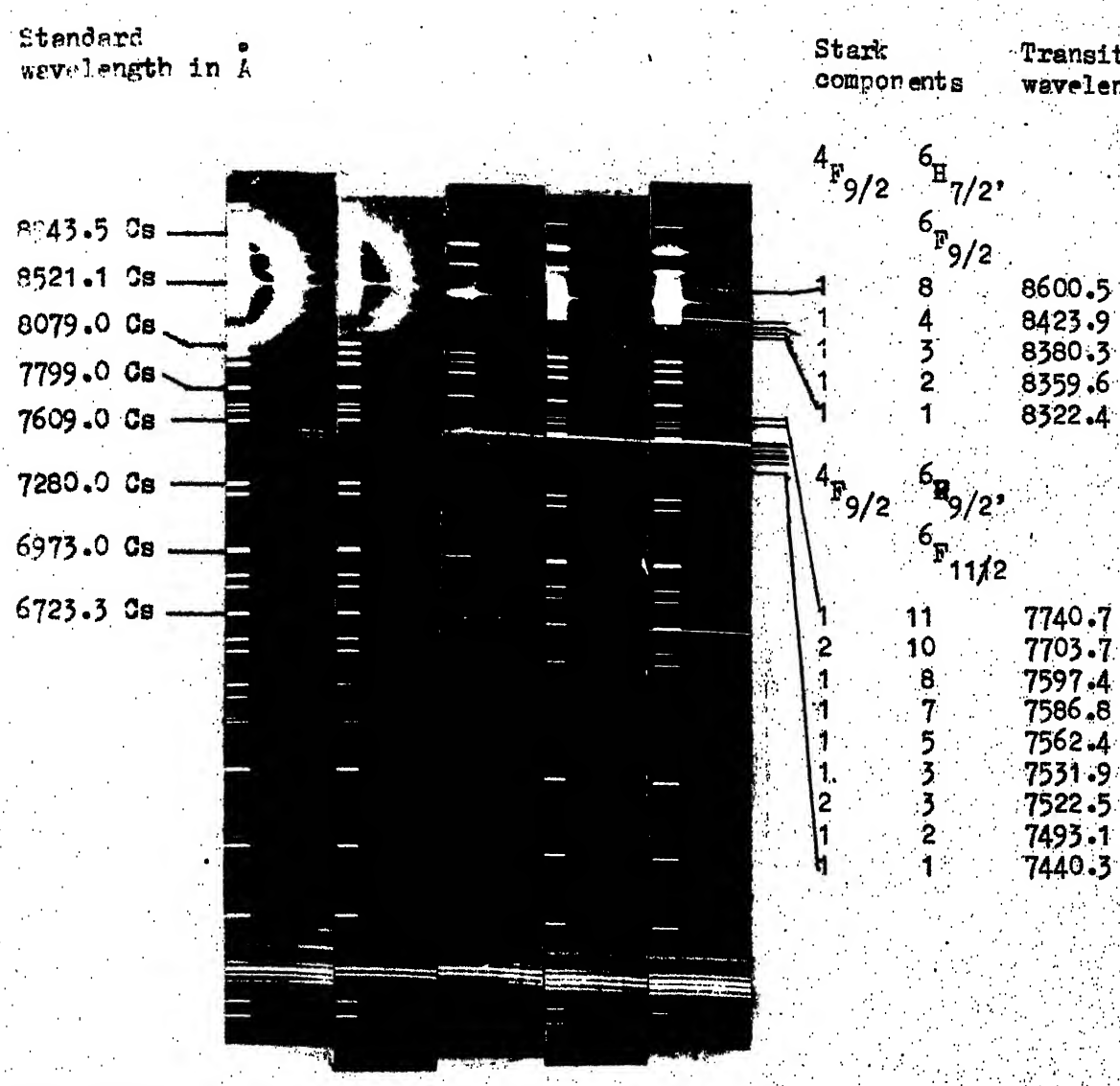

Fig. 6.3 - Fluorescence spectrum of $CaF_2:Dy^{3+}$ at 77°K.

$^4F_{9/2} - {}^6H_{7/2}$, $^6F_{9/2}$ and $^4F_{9/2} - {}^6F_{11/2}$, $^6H_{9/2}$ groups.

The wavelengths of the observed spectrum are tabulated in Table 6.1 . The mean values shown in the table are obtained by taking the average of the measured wavelengths for the same transition but for different concentrations of Dy^{3+} in the crystal. The errors in the values are mainly due to the width of the lines. The observed lines are broader than the slit width used (30 μ). The variation in the measured values of wavelength for the same transition in different crystals are thus, within the experimental inaccuracy.

It can be seen from the Figures 6.2 and 6.3 that there is some variation in the relative intensities of different transitions in the same group as the concentration of the impurity ion is changed. This is particularly so for the transitions 6716.6Å, 6695.4Å, 6572.2Å of the group $^4F_{9/2} - {}^6H_{11/2}$. The intensity variation of the transitions with the concentration of the impurity ion has been observed earlier[10,11]. This has been ascribed to the transitions between the levels of different centers. The dependence of the relative intensities of the transition on the concentration is different for different centers[10,11] (fig. 6.4). A complete analysis of the intensity variation is possible only when the transition under consideration is isolated i.e. no overlapping of transitions occurs. This necessitates the use of a spectrograph with higher dispersion. The analysis of the intensity variation has not been done as the spectra were recorded on a spectrograph with low dispersion.

The analysis is based on the observed luminescence spectrum and the energy level structure proposed by Luks and his coworkers[5,6,10], for the transitions involving $^6H_{15/2}$ and $^6H_{13/2}$ for the lower level. The upper level of fluorescence in $^4F_{9/2}$ and not $^6F_{11/2}$, as pointed out by Altshuler et.al[6]

$CaF_2:Dy^{3+}$ 1% by wt.	$CaF_2:Dy^{3+}$ 0.54% by wt.	$CaF_2:Dy^{3+}$ 0.27% by wt.	$CaF_2:Dy$ 0.09% by wt.	$CaF_2:Dy^{3+}$ 0.03% by wt.	$CaF_2:Dy^{3+}$ 0.01% by wt.	Average wave length in Å	Energy in cm^{-1}
All wavelengths in A							
4696.6 w		4697.0 w				4696.8	21285
4704.9 w		4704.3 w				4704.6	21250
4715.6 w		4716.4 w	4714.8 m			4715.9	21199
4721.7 w		4721.4 m	4721.4 m			4721.5	21174
4733.3 w		4732.7 m	4732.3 w			4732.8	21123
4745.3 w		4744.1 m	4744.8 w			4744.7	21070
4750.7 S		4750.0 Vs	4750.2 Vs			4750.3	21045
4757.1 w		4756.6 m	4757.5 w			4757.1	21015
4762.4 m		4762.0 S	4762.1 S			4762.2	20993
4766.3 m		4766.1 S	4767.0 m			4766.5	20974
4780.5 m		4779.2 S	4779.1 m			4779.6	20916
4786.8 m		4786.6 S	4786.6 m			4786.7	20885
4792.8 m		4792.8 S	4793.1 S			4792.9	20858
4917.7 S		4917.7 S	4916.0 Vw			4917.1	20332
5677.6 w	5675.2 w	5676.0 m	5677.1 S	5675.8 w		5676.4	17612
5685.9 S	5687.7 S	5687.9 S	5690.1 S	5687.5 w		5687.8	17577
5707.9 S	5707.2 S	5708.1 S	5708.9 m	5707.9 m		5707.9	17515
5721.7 S	5720.5 S	5720.5 S	5721.6 S	5720.1 m		5720.9	17475
5734.0 S	5732.2 S	5732.3 S	5732.7 S	5731.6 m		5732.6	17439
5745.5 S	5744.8 S	5746.2 S	5747.4 S	5744.3 m		5745.6	17400
5762.7 w	5762.3 m	5762.4 m	5761.9 w	5762.3 w		5762.3	17349
5782.4 S	5782.0 S	5781.8 S	5782.4 S	5781.3 S		5782.0	17290
5813.9 S	5812.0 S	5810.4 m	5812.5 m	5812.0 w		5812.2	17200
5822.3 S	5822.0 S	5822.4 S	5822.1 S	5823.4 m		5822.4	17170

$aF_2:Dy^{3+}$ % by wt.	$CaF_2:Dy^{3+}$ 0.54% by wt.	$CaF_2:Dy^{3+}$ 0.27% by wt.	$CaF_2:Dy$ 0.09% by wt.	$CaF_2:Dy^{3+}$ 0.03% by wt.	$CaF_2:Dy^{3+}$ 0.01% by wt.	Average wave length in Å	Energy in cm^{-1}
← All wavelengths in A →							
	5858.5 w	5859.8 w	5865.0 w			5861.1	17057
			6400.2 m	6402.9 m	6402.9 m	6402.0	15616
	6572.2 S	6574.4 S	6573.1 S	6573.2 w	6573.6 w	6573.6	15209
		6584.1 w	6583.2 w			6583.7	15185
		6621.8 w	6622.2 w			6622.0	15097
	6643.3 w	6644.7 w	6644.1 w	6641.2 w		6643.3	15049
	6655.7 S	6656.1 S	6657.9 S	6658.4 m	6655.6 m	6656.7	15010
	6678.8 m	6680.7 w	6682.3 w		6679.7 w	6678.3	14970
	6694.8 S	6695.6 S	6695.9 S	6695.3 w	6695.2 m	6695.4	14932
	6716.6 S	6717.2 S	6717.9 S		6714.3 Vw	6716.5	14885
7439.1 S	7439.5 m	7442.5 S	7439.7 S	7440.5 m		7440.3	13437
7492.3 S	7491.5 m	7495.3 S	7492.8 m	7493.6 m		7493.1	13342
7521.3 S	7523.6 w					7522.5	13290
7531.8 S	7530.9 m	7534.0 S	7531.5 S	7531.4 S		7531.9	13273
7546.2 m	7545.4 w	7549.3 m	7546.1 w	7547.1 w		7546.8	13247
7561.7 S	7562.0 m	7564.1 m	7562.2 S	7561.8 m		7562.4	13220
7573.0 m	7574.5 m	7575.7 m	7574.0 m	7572.8 m		7574.0	13199
7585.6 Vs	7586.2 S	7589.1 S	7586.6 S	7586.6 m		7586.8	13177
7596.3 Vs	7596.3 S	7599.2 S	7597.9 m	7597.5 w		7597.4	13159
7618.9 w	7619.3 Vw	7621.8 w	7619.8 w	7621.4 w		7620.2	13119
7634.0 w	7634.9 w	7639.2 w	7637.8 w	7633.2 w		7635.8	13093
7704.0 S	7704.7 w	7703.8 Vw	7705.9 Vw	7700.0 Vw		7703.7	12977
7739.1 S	7741.9 m	7741.2 Vw				7740.7	12915
8320.6 m	8322.1 m	8323.2 m	8323.0 m	8322.9 m		8322.4	12012
8358.7 m	8360.2 m	8360.6 m	8358.3 m	8359.9 m		8359.6	11959

$CaF_2:Dy^{3+}$ by wt.	$CaF_2:Dy^{3+}$ 0.54% by wt.	$CaF_2:Dy^{3+}$ 0.27% by wt.	$CaF_2:Dy$ 0.09% by wt.	$CaF_2:Dy^{3+}$ 0.03% by wt.	$CaF_2:Dy^{3+}$ 0.01% by wt.	Average wave Length in Å	Energy in cm^{-1}
All wavelengths in Å							
78.2 w	8381.7 w	8379.9 m	8380.1 w	8381.5 w		8380.3	11929
21.6 S	8422.9 S	8426.0 m	8425.0 w			8423.9	11868
99.6 m	8503.8 w	8505.3 w	8501.4 w			8502.5	11753
21.0 w		8526.4 w	8528.1 Vw			8525.2	11727
81.2 w	8584.9 w	8583.7 Vw	8576.7 Vw	8589.4 Vw		8581.2	11650
99.8 S	8601.4 m	8601.4 Vw	8599.3 Vw			8600.5	11624

Note to the Table 6.1:

The letters Vs, S, m, w, Vw stand for very strong, strong, medium, weak, very weak intensities.

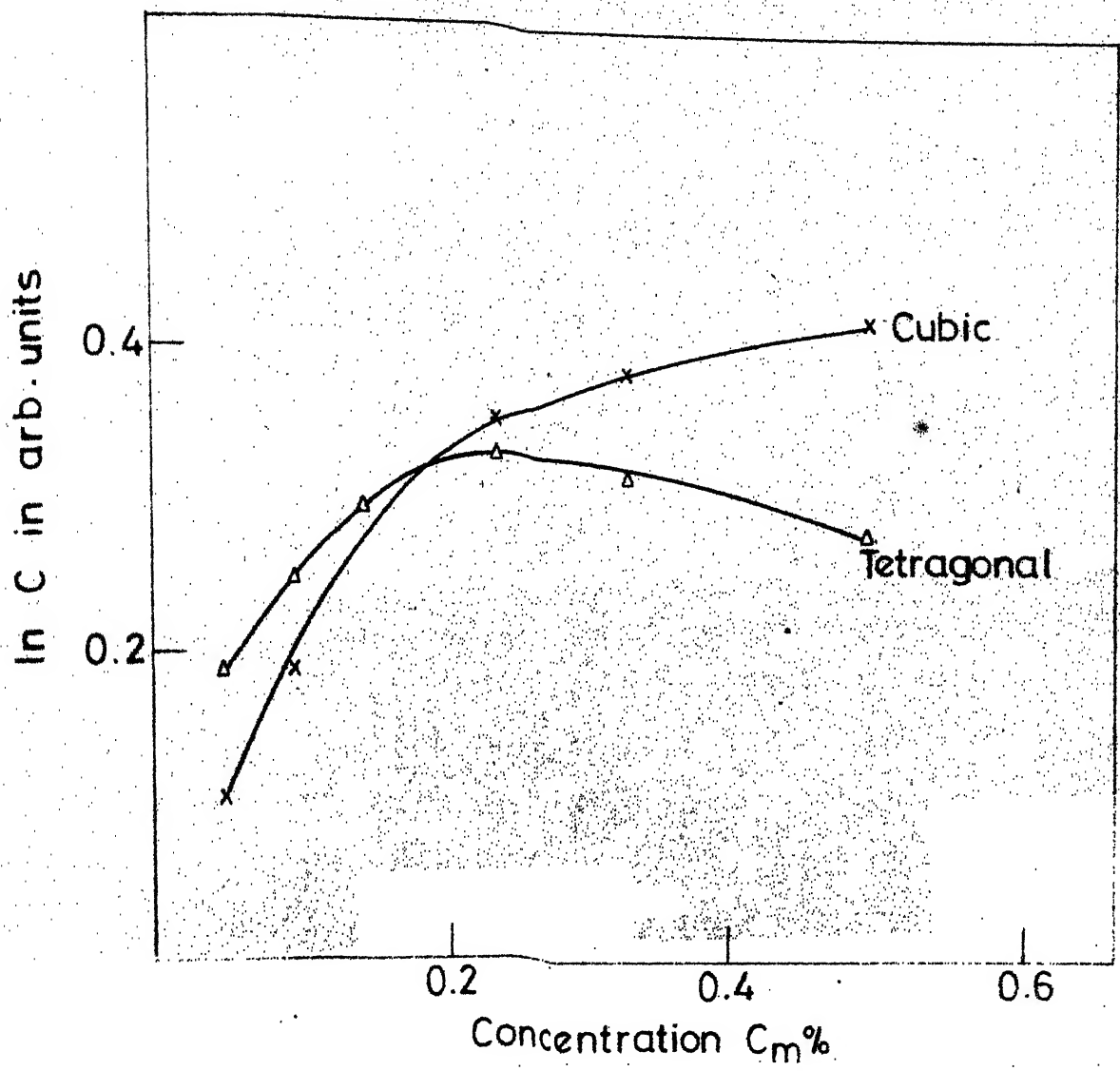

Fig. 6.4 The dependence of the number C of cubic and tetragonal Dy^{3+} centers in CaF_2 crystals (in relative units) on the activator concentration in the mixture (ref. 10).

and Antipin et.al[10]. No information on the absorption spectrum of $CaF_2:Dy^{3+}$ is available in the literature. Attempts to obtain the absorption spectrum did not succeed. The average wavelength and wavenumbers of the fluorescence lines obtained in this work along with the data of Luks and his coworkers are given in Tables 6.3 and 6.5 for comparison. A comparative study of the present data and luminescence data observed by Luks et.al[5] along with the work of Antipin et.al[10] on tetragonal centers of Dy^{3+} in CaF_2 shows that most of the transitions given in the Table 6.1 belong to the tetragonal sites. Transitions due to other sites are very few in number and are not taken into consideration for analysis.*

The method of approach to the analysis is as follows. The groups $^4F_{9/2} - {}^6H_{15/2}$ and $^4F_{9/2} - {}^6H_{13/2}$ have been observed[5] earlier at liquid helium temperature. The originating Stark components and the ground Stark multiplet separations have been established. Assuming the ground level separations, the possible positions of the upper level Stark components are determined by adding the energy of the observed transitions to the ground level Stark separations. The positions of the Stark components of the levels $^6H_{11/2}$, $(^6H_{9/2}, {}^6F_{11/2})$ and $(^6H_{7/2}, {}^6F_{9/2})$ are determined by substracting the observed transitions $^4F_{9/2} - {}^6H_{11/2}$, $^4F_{9/2} - (^6H_{9/2}, {}^6F_{11/2})$ and $^4F_{9/2} - (^6H_{7/2}, {}^6F_{9/2})$ from the position of the Stark components of $^4F_{9/2}$.

---

* The following fluorescing transitions belonging to the cubic centers as reported earlier by Luks and his coworkers[5] and by Altshuler et.al[6], have also been observed by us.

4917.1Å, 4786.7Å and 4757.1Å in the $^4F_{9/2} \longrightarrow {}^6H_{15/2}$ group of transitions 5782.1Å in the $^4F_{9/2} \longrightarrow {}^6H_{13/2}$ group of transition, and 6717.2Å 6680.6Å, 6622Å and 6608.7Å in the $^4F_{9/2} \longrightarrow {}^6H_{11/2}$ group of transition.

Some of these transitions may be overlapping with the transitions between the levels of tetragonal centers.

6.4 Group $^4F_{9/2}$ — $^6H_{15/2}$ ($\sim$ 21000 cm^{-1})

Thirteen transitions of this group have been observed in the present case. This group has been observed earlier by Luks et.al[5] and Al'tshuler et.al[6] for different centers - cubic, tetragonal, trigonal and orthorhombic. A comparison of the observed spectrum with the reported spectra indicates that observed transitions 21070 cm^{-1}, 21045 cm^{-1}, 21015 cm^{-1}, 20993 cm^{-1}, 20974 cm^{-1}, 20916 cm^{-1}, 20885 cm^{-1} and 20858 cm^{-1} can be assigned as the transitions between the levels $^4F_{9/2}$ and $^6H_{15/2}$ of the tetragonal center, the fluorescing Stark components of $^4F_{9/2}$ being 21070 cm^{-1} and 21045 cm^{-1}. The transitions from these two Stark components to the Stark multiplet of $^6H_{15/2}$ are stronger compared to the other transitions. The lowest Stark components of $^6H_{15/2}$ at 0 and 6 cm^{-1} are very close in energy. Transitions to these components from the Stark components 21045 cm^{-1} and 21070 cm^{-1} of $^4F_{9/2}$ are not observed separately as the minimum width of the lines is of the same order. The remaining five transitions 21285 cm^{-1}, 21250 cm^{-1}, 21299 cm^{-1}, 21174 cm^{-1} and 21123 cm^{-1} are assigned to the Stark components of the levels $^4F_{9/2}$ of the tetragonal center assuming the presence of two more Stark components at 21285 cm^{-1} and 21250 cm^{-1} (see figs. 6.5 and Table 6.2). These Stark components are more than 200 cm^{-1} above the lowest Stark component 21045 cm^{-1} and hence, are not probably active at 4.2°K. The energy level diagram proposed by Luks et.al[5] for tetragonal centers is based on the luminescence spectrum observed at 4.2°K. No reference to these levels at 21285 and 21250 cm^{-1} was, thus, possible in their energy level structure.

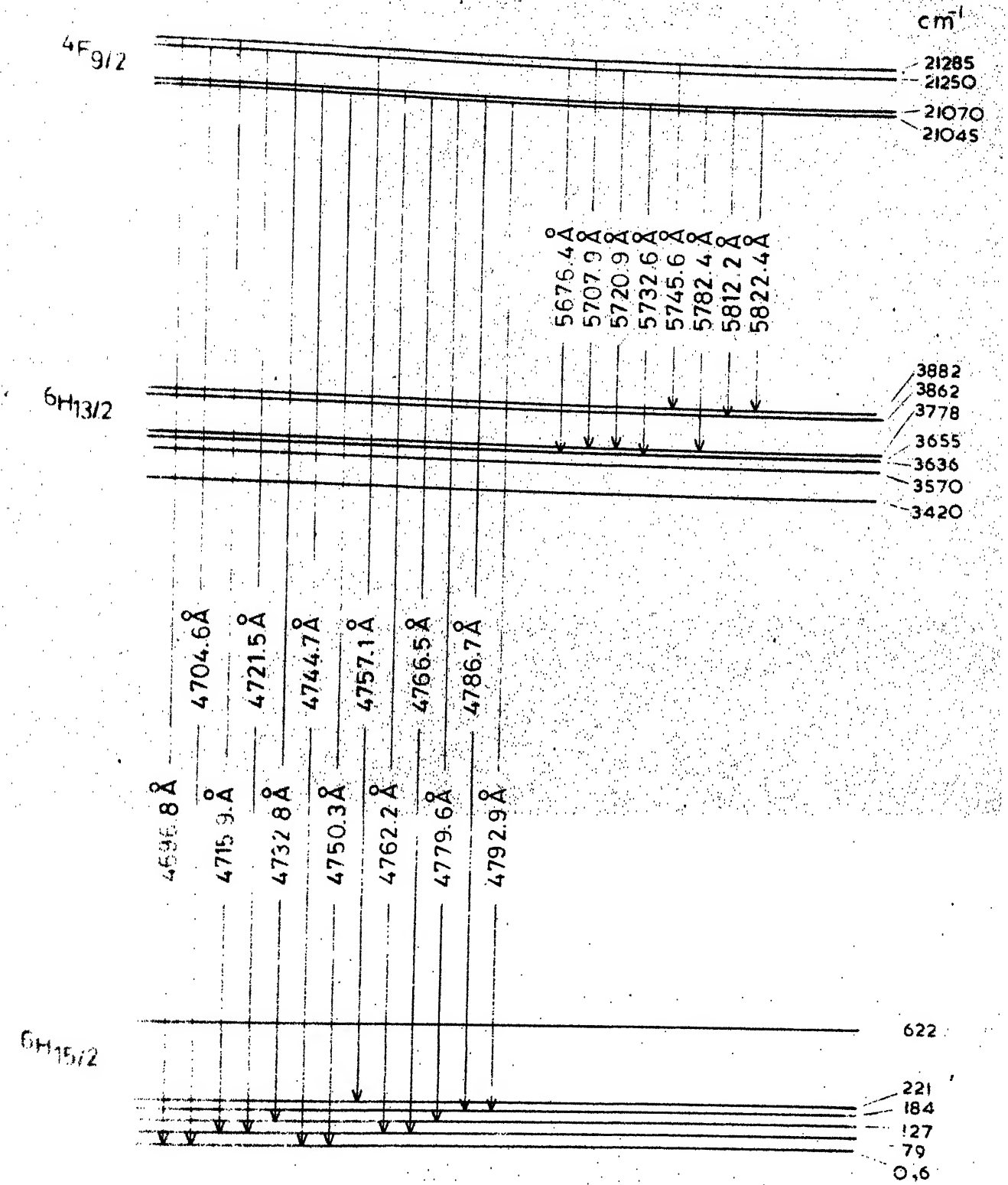

Fig. 6.5 Partial energy level diagram of $CaF_2:Dy^{3+}$ for tetragonal centers showing the observed fluorescence transition groups $^4F_{9/2} - {}^6H_{15/2}$ and $^4F_{9/2} - {}^6H_{13/2}$.

Table 6.2

'Summation' Matrix for the transition $^4F_{9/2} - {}^6H_{15/2}$

$^6H_{15/2}$ Stark components →	$^6H_{15/2}$ (1)	$^6H_{15/2}$ (2)	$^6H_{15/2}$ (3)	$^6H_{15/2}$ (4)	$^6H_{15/2}$ (5)	$^6H_{15/2}$ (6)	$^6H_{15/2}$ (7)
Observed Transitions in cm^{-1}	0	6	79	127	184	221	622
← All in cm^{-1} →							
21285	21285	21291	21364	21412	21469	21506	21907
21250	21250	256	329	377	434	471	872
21199	21199	205	278	326	383	420	821
21174	21174	180	253	301	358	395	796
21123	21123	129	202	250	307	344	745
21070	21070	076	149	197	254	291	692
21045	21045	051	124	172	229	266	667
21015	21015	021	094	142	199	236	637
20993	20993	20999	21072	120	177	214	615
20974	20974	980	21053	101	158	195	596
20916	20916	922	20995	21043	100	137	538
20885	20885	891	964	21012	069	106	507
20858	20858	864	937	20985	21042	079	480

Table 6.3

Transition Assignments in the Fluorescence Group $^4F_{9/2} - {}^6H_{15/2}$

Luks et.al[5] Tetragonal Center (Å)	Present data			Transition Assignments[a,b]
	Relative Intensity[c]	(Å)	(cm^{-1})	
	w	4696.8	21285	$^4F_{9/2}(4) \cdots {}^6H_{15/2}(1)$
	w	4704.6	21250	$^4F_{9/2}(3) - {}^6H_{15/2}(1)$
	w	4715.9	21199	$^4F_{9/2}(4) - {}^6H_{15/2}(3)$
	m	4721.5	21174	$^4F_{9/2}(3) - {}^6H_{15/2}(3)$
	m	4732.8	21123	$^4F_{9/2}(3) - {}^6H_{15/2}(4)$
4744.5	m	4744.7	21070	$^4F_{9/2}(2) - {}^6H_{15/2}(1)$
4750.6	vs	4750.3	21045	$^4F_{9/2}(1) - {}^6H_{15/2}(1)$
4751.9				$(^4F_{9/2}(1) - {}^6H_{15/2}(2)$
	m	4757.1	21015	$^4F_{9/2}(3) - {}^6H_{15/2}(6)$
4762.3	s	4762.2	20993	$^4F_{9/2}(2) - {}^6H_{15/2}(3)$
4768.4	s	4766.5	20974	$^4F_{9/2}(1) - {}^6H_{15/2}(3)$
4773.3				$(^4F_{9/2}(2) - {}^6H_{15/2}(4))$
4779.3	s	4779.6	20916	$^4F_{9/2}(1) - {}^6H_{15/2}(4)$
4786.3	s	4786.7	20885	$^4F_{9/2}(2) - {}^6H_{15/2}(5)$
4792.5	s	4792.9	20858	$^4F_{9/2}(1) - {}^6H_{15/2}(5)$
4801.0				$(^4F_{9/2}(1) - {}^6H_{15/2}(6))$
4888.9				$(^4F_{9/2}(2) - {}^6H_{15/2}(7))$
4895.2				$(^4F_{9/2}(1) - {}^6H_{15/2}(7))$

Notes to Table 6.3:

(a) 1, 2, 3 and 4 in parenthesis with $^4F_{9/2}$ stand for the Stark components at 21045, 21070, 21250 and 21285 cm^{-1} respectively.

(b) 1, 2, 3, 4, 5 and 6 in parenthesis with $^6H_{15/2}$ stand for the Stark components at 0, 6, 79, 127, 184, 221 and 622 cm^{-1} respectively. The assignments given in parenthesis ( ) are of Luks et. al, and they are not observed in the present case.

(c) The relative intensities listed are from the spectrum taken in the present work with 0.09% concentration of Dy^{3+} by weight in $CaF_2:Dy^{3+}$. The letters w, m, s and vs stand for weak, medium, strong and very strong intensities.

The summation matrix obtained by summing the energy (in cm^{-1}) of the observed fluorescing transitions and the energy of the Stark components of the terminating level $^6H_{15/2}$ is shown in Table 6.2. This matrix gives the energy of the possible originating Stark components. The table clearly shows that most of the transitions originate from 21045 cm^{-1}, 21070 cm^{-1} and 21250 cm^{-1} and 21285 cm^{-1}. The transition assignment for the 13 fluorescence lines are given in Table 6.3 and also shown in Figure 6.5.

6.5 Group $^4F_{9/2} \rightarrow {}^6H_{13/2}$ ($\sim$ 17400 cm^{-1})

Eleven transitions have been observed in this group. The summation matrix is shown in Table 6.4. The positions of the Stark components of $^6H_{13/2}$ are taken from the energy level structure proposed by Luks et.al[5] for tetragonal centers. Assignments of the transitions for 8 of the 11 fluorescing lines observed in this group are given in Table 6.5 and the transitions are marked in Figure 6.5. The remaining three lines 17577 cm^{-1}, 17347 cm^{-1} and 17057 cm^{-1} may have to be explained by taking the lattice phonons into consideration or they may belong to other possible centers of Dy^{3+}.

6.6 Group $^4F_{9/2} \rightarrow {}^6H_{11/2}$ (~15000 cm^{-1})

Nine transitions have been observed in this group. This group of transitions has not been observed earlier for the tetragonal sites. The positions of the Stark components of the $^6H_{11/2}$ are obtained by substracting the energy of the observed transitions from the energy of the originating Stark components.

Table 6.4

'Summation' Matrix for the transitions $^4F_{9/2} - {}^6H_{13/2}$

$^6H_{13/2}$ Stark Components → / Observed Transition in cm^{-1}	$^6H_{13/2}(1)$	$^6H_{13/2}(2)$	$^6H_{13/2}(3)$	$^6H_{13/2}(4)$	$^6H_{13/2}(5)$	$^6H_{13/2}(6)$	$^6H_{13/2}(7)$
	3420	3570	3636	3655	3778	3862	3882
	← All in cm^{-1} →						
17612	21032	21182	21248	21267	21390	21474	21494
17577	20997	21147	213	232	355	439	459
17515	20935	21085	151	170	293	377	397
17475	20895	21045	111	130	253	337	357
17439	20859	21009	075	094	217	301	321
17400	20820	20970	036	055	178	262	282
17349	20769	919	20985	21004	127	211	231
17290	20719	860	926	20945	21068	152	172
17200	20620	770	836	855	20978	21062	082
17170	20590	740	806	825	948	21032	052
17057	20477	627	693	712	835	20919	20939

Table 6.5

Transition Assignments in the Fluorescence Group $^4F_{9/2}$ — $^6H_{13/2}$

Luks et.al[5] Relative Tetragonal Centers Intensities	Present work		Transition Assignments[a,b]
Å	Å	cm^{-1}	
5672.5			($^4F_{9/2}(1)$ — $^6H_{15/2}(1)$)
m	5676.4	17612	$^4F_{9/2}(3)$ — $^6H_{13/2}(3)$
S	5687.8	17577	
S	5707.9	17515	$^4F_{9/2}(4)$ — $^6H_{13/2}(5)$
5711.1			($^4F_{9/2}(1)$ — $^6H_{13/2}(1)$)
S	5720.9	17475	$^4F_{9/2}(3)$ — $^6H_{13/2}(5)$
S	5732.6	17439	$^4F_{9/2}(2)$ — $^6H_{13/2}(3)$
5742.6			($^4F_{9/2}(1)$ — $^6H_{13/2}(3)$)
S	5745.6	17460	$^4F_{9/2}(4)$ — $^6H_{13/2}(7)$
5748.7			($^4F_{9/2}(1)$ — $^6H_{13/2}(4)$)
m	5762.3	17349	
5779.5			($^4F_{9/2}(1)$ — $^6H_{13/2}(5)$)
S	5782.4	17290	$^4F_{9/2}(2)$ — $^6H_{13/2}(5)$
5809.6			($^4F_{9/2}(2)$ — $^6H_{13/2}(6)$
m	5812.2	17200	$^4F_{9/2}(2)$ — $^6H_{13/2}(6)$
5815.7			($^4F_{9/2}(2)$ — $^6H_{13/2}(7)$
5817.9			($^4F_{9/2}(1)$ — $^6H_{13/2}(6)$
5824.9 S	5822.4	17170	$^4F_{9/2}(1)$ — $^6H_{13/2}(7)$
w	5861.1	17057	

Table 6.5

Transition Assignments in the Fluorescence Group $^4F_{9/2}$ — $^6H_{13/2}$

Luks et.al[5] Tetragonal Centers Å	Relative Intensities	Present work Å	Present work cm^{-1}	Transition Assignments[a,b]
5672.5				$(^4F_{9/2}(1) - {}^6H_{15/2}(1))$
	m	5676.4	17612	$^4F_{9/2}(3) - {}^6H_{13/2}(3)$
	S	5687.8	17577	
	S	5707.9	17515	$^4F_{9/2}(4) - {}^6H_{13/2}(5)$
5711.1				$(^4F_{9/2}(1) - {}^6H_{13/2}(1))$
	S	5720.9	17475	$^4F_{9/2}(3) - {}^6H_{13/2}(5)$
	S	5732.6	17439	$^4F_{9/2}(2) - {}^6H_{13/2}(3)$
5742.6				$(^4F_{9/2}(1) - {}^6H_{13/2}(3))$
	S	5745.6	17460	$^4F_{9/2}(4) - {}^6H_{13/2}(7)$
5748.7				$(^4F_{9/2}(1) - {}^6H_{13/2}(4))$
	m	5762.3	17349	
5779.5				$(^4F_{9/2}(1) - {}^6H_{13/2}(5))$
	S	5782.4	17290	$^4F_{9/2}(2) - {}^6H_{13/2}(5)$
5809.6				$(^4F_{9/2}(2) - {}^6H_{13/2}(6)$
	m	5812.2	17200	$^4F_{9/2}(2) - {}^6H_{13/2}(6)$
5815.7				$(^4F_{9/2}(2) - {}^6H_{13/2}(7)$
5817.9				$(^4F_{9/2}(1) - {}^6H_{13/2}(6)$
5824.9	S	5822.4	17170	$^4F_{9/2}(1) - {}^6H_{13/2}(7)$
	w	5861.1	17057	

Notes to Table 6.5

(a) 1, 2, 3 and 4 in parenthesis with $^4F_{9/2}$ stand for the Stark components at 21045, 21070, 21250 and 21285 cm^{-1} respectively.

(b) 1, 2, 3, 4, 5, 6 and 7 in parenthesis with $^6H_{13/2}$ stand for the Stark components at 3420, 3570, 3636, 3655, 3778, 3862 and 3882 cm^{-1} respectively. This assignment in parenthesis are those of Luks et.al for their observed bands.

(c) The relative intensities listed are from the spectrum taken in the present work with 0.09% concentration of Dy^{3+} by weight in $CaF_2:Dy^{3+}$. The letters S, w and m stand for strong, week and medium intensities.

For this, first, a difference matrix is constructed (Table 6.6). The elements of the difference matrix are the energy differences of the originating Stark components and the observed transitions. All possible pairs of the originating Stark components and the observed transitions are considered. Some of the matrix elements are the same (within experimental error) indicating coincidences of different lower Stark components.

As the transitions arising from the Stark component at 21045 cm^{-1} of $^4F_{9/2}$ are expected to be more intense compared to the transitions from the other Stark components, it may be suggested that the six Stark components of $^6H_{11/2}$ are at 5836, 5860, 5949, 6024, 6107 and 6160 cm^{-1}. These form the lower Stark components for eight of the nine fluorescence lines observed in the region 6400-6720Å. The assignments are given in Table 6.7 and the transitions are shown in Figure 6.6. The ninth line observed at 6402 cm^{-1} (15616 cm^{-1}) is somewhat far off from the other eight lines which lie in the region 6570-6720Å.* If however the tenth line at 15616 cm^{-1} is to be taken as corresponding to the same group of transitions as the other nine lines, a Stark component at 5428 cm^{-1} is to be postulated instead of probably the one at 5836 cm^{-1} suggested above.

6.7 Group $^4F_{9/2} \rightarrow {}^6H_{9/2}, {}^6F_{11/2}$ (~13200 cm^{-1})

A study of the optical absorption and fluorescence of $LaF_3:Dy^{3+}$ by Fry et.al[8] showed the existence of 11 energy levels in the region 7600-8100 cm^{-1} which are attributed to the overlapping group of Stark components of the levels

---

* It may be noted here that the fluorescence group of $LaF_3:Dy^{3+}$ arising from the transition $^4F_{9/2} \rightarrow {}^6H_{11/2}$ observed by Fry et.al[8] lies in the region 6580-6650Å, falling in the present region of observation of fluorescence in $CaF_2:Dy^{3+}$.

Table 6.6

Difference Matri. for the Transitions $^4F_{9/2} - {}^6H_{11/2}$

Relative Intensities* in $CaF_2:Dy^{3+}$ 0.09% by wt	$^4F_{9/2}$ Stark Components Observed Transitions in cm^{-1}	$^4F_{9/2}(1)$ 21045	$^4F_{9/2}(2)$ 21070	$^4F_{9/2}(3)$ 21250	$^4F_{9/2}(4)$ 21285
		All in cm^{-1} →			
s	14885	6160	6185	6365	6400
s	14932	6113	138	318	353
w	14970	6075	100	280	315
s	15018	6027	052	232	267
w	15049	5996	6021	201	236
w	15097	5948	5973	6153	188
w	15185	5860	5885	6065	100
s	15209	5836	861	6044	076
m	15616	5429	454	5634	5669

* The letters s, m and w stand for strong, medium and weak transitions.

Table 6.7

Transition Assignments for the Fluorescence Group $^4F_{9/2}$ — $^6H_{11/2}$

Relative Intensities[c]	Present work		Transition Assignments[a,b]
	Å	cm^{-1}	
m	6402.0	15616	($^4F_{9/2}(1)$ — $^6H_{11/2}(1)$)
S	6573.3	15209	($^4F_{9/2}(2)$ — $^6H_{11/2}(2)$)
		or	$^4F_{9/2}(1)$ — $^6H_{11/2}(1)$
w	6583.7	15185	$^4F_{9/2}(1)$ — $^6H_{11/2}(2)$
w	6622.0	15097	$^4F_{9/2}(1)$ — $^6H_{11/2}(3)$
w	6643.3	15049	$^4F_{9/2}(2)$ — $^6H_{11/2}(4)$
S	6656.7	15018	$^4F_{9/2}(1)$ — $^6H_{11/2}(4)$
w	6678.7	14970	$^4F_{9/2}(2)$ — $^6H_{11/2}(5)$
S	6695.4	14932	$^4F_{9/2}(1)$ — $^6H_{11/2}(5)$
S	6716.5	14885	$^4F_{9/2}(1)$ — $^6H_{11/2}(6)$

Notes to Table 6.7:

(a) 1, 2, 3 and 4 in parenthesis with $^4F_{9/2}$ stand for the Stark components at 21045, 21070, 21250 and 21285 cm^{-1} respectively.

(b) 1, 2, 3, 4, 5 and 6 in parenthesis with $^6H_{11/2}$ stand for the proposed Stark components at 5836, 5860, 5945, 6024, 6107 and 6160 cm^{-1} respectively. The alternative assignments are given in brackets ( ) if the first Stark component happens to be 5429 cm^{-1} instead of 5836 cm^{-1}.

(c) The relative intensities listed are from the spectrum taken in the present work with 0.09% concentration of Dy^{3+} by weight in CaF_2:Dy^{3+}. The letters S, m and w stand for strong, medium and weak intensities.

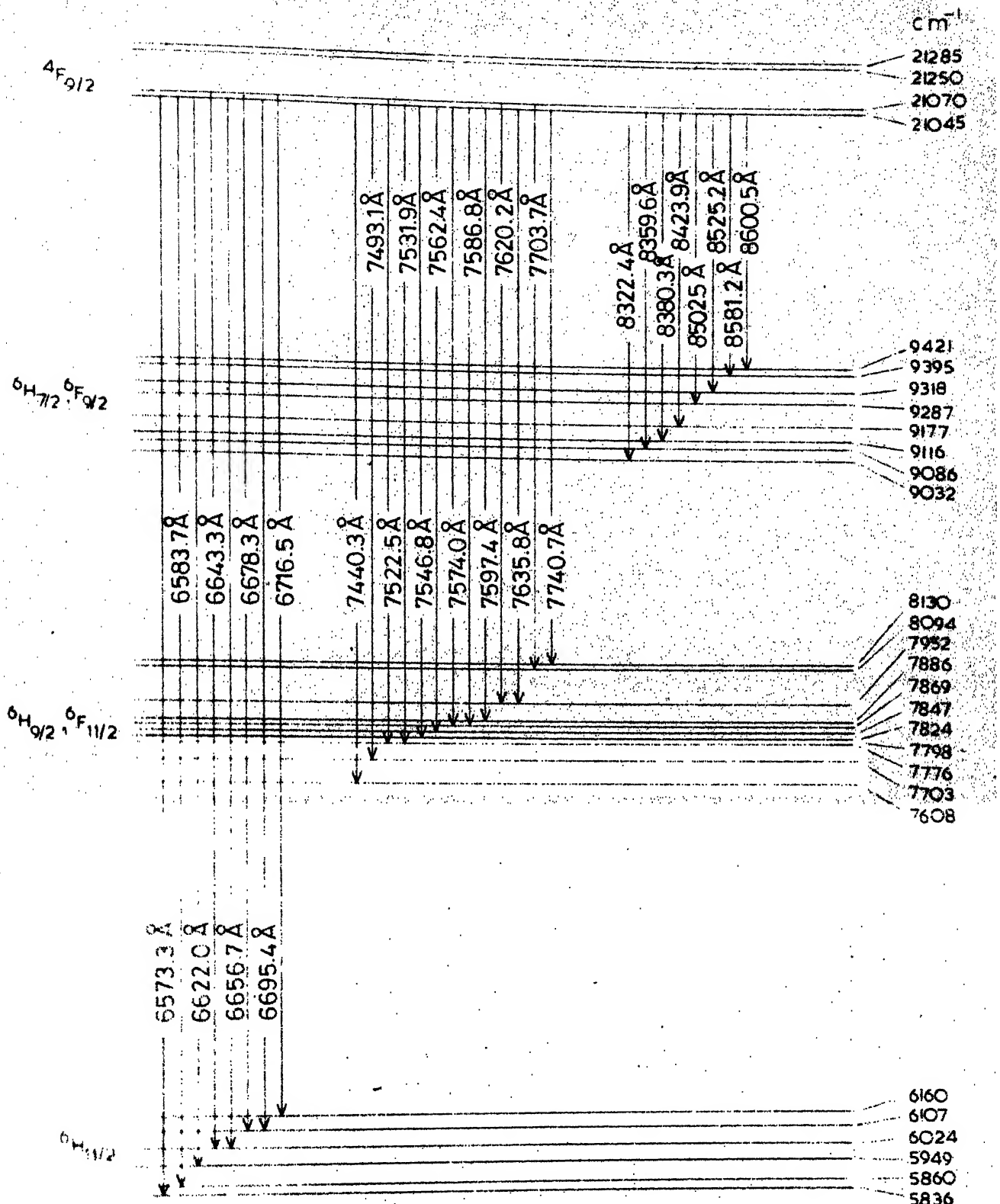

Fig.6.6 Partial energy level diagram of $CaF_2:Dy^{3+}$ for tetragonal centers showing the fluorescence transition groups. $^4F_{9/2} - {}^6H_{11/2}$, $^4F_{9/2} - {}^6H_{9/2}$, $^6F_{11/2}$ and $^4F_{9/2} - {}^6H_{7/2}$, $^6F_{9/2}$ at 77°K.

$^6H_{9/2}$ and $^6F_{11/2}$. The eleven fluorescence lines from $^4F_{9/2}$ to $^6H_{9/2}$, $^6F_{11/2}$ in $LaF_3:Dy^{3+}$ spectrum lie in the region 12900-13450 cm^{-1}. In the same region the fluorescence of $CaF_2:Dy^{3+}$ in the present work gives 14 transitions. The difference matrix for this group of lines is shown in Table 6.8, taking the four Stark components of $^4F_{9/2}$ at 21045, 21070, 21250 and 21285 cm^{-1} into consideration. A number of coincidences can be seen from the table. Assuming that fluorescence arises mostly from 21045 cm^{-1} at liquid nitrogen temperature and that the spread of energy levels of the group of $^6H_{9/2}$ and $^6F_{11/2}$ will be about the same as that in the $LaF_3:Dy^{3+}$, the following eleven terminating Stark components of $^6H_{9/2}$, $^6F_{11/2}$ for the fluorescence group are suggested; 7608, 7703, 7776, 7798, 7824, 7847, 7869, 7886, 7952, 8094 and 8130 cm^{-1}. The assignments for the 14 fluorescence lines observed are shown in Table 6.9 and the transitions are marked in Figure 6.6.

6.8 Group $^4F_{9/2}$ — $^6H_{7/2}$, $^6F_{9/2}$ (11800 cm^{-1})

Fry et.al[8] obtained in $LaF_3:Dy^{3+}$ single crystal at 4.2K, nine absorption lines in the region 8990-9450 cm^{-1}, the energies of which are taken to correspond the positions of the nine Stark components expected for the levels $^6H_{7/2}$ and $^6F_{9/2}$ of Dy^{3+}. These nine Stark components form the lower states of the nine fluorescence lines observed by them in the same crystal in the region 8280-8600Å, all arising from the upper level $^4F_{9/2}$ of Dy^{3+}. In the present work we have observed 8 fluorescence lines in the region 8320-8600Å for the $CaF_2:Dy^{3+}$ system at liquid nitrogen temperature. The wavelengths and

Table 6.8

Difference Matrix for the Transitions $^4F_{9/2} - {}^6H_{9/2}$, $^6F_{11/2}$

Relative Intensities in CaF_2 Dy^{3+} 0.09% by wt.	$^4F_{9/2}$ Stark Components Observed Transitions in cm^{-1}	$^4F_{9/2}(1)$	$^4F_{9/2}(2)$	$^4F_{9/2}(3)$	$^4F_{9/2}(4)$
		21045	21070	21250	21285
		← All in cm^{-1} →			
S	13437	7608	7633	7813	7848
m	13342	7703	728	908	943
	13290	7755	780	960	995
S	13273	7772	797	977	8012
w	13247	7798	823	8003	8038
S	13220	7825	850	8030	065
m	13199	7846	871	8051	086
S	13177	7868	893	8073	108
m	13159	7886	911	8091	126
w	13119	7926	951	8131	166
w	13093	7952	977	8157	192
Vw	12977	8068	093	273	308
	12915	8130	155	335	470

The letters S, m, w and Vw stand for strong, medium, weak and very weak transitions.

Table 6.9

Transition Assignments for the Fluorescence Group $^4F_{9/2}$ — $^6H_{9/2}$, $^6F_{11/2}$

Relative Intensity[c]	Present work		Transition Assignments[a,b]
	Å	cm^{-1}	
S	7440.3	13437	$^4F_{9/2}(1)$ — $^6H_{9/2}$, $^6F_{11/2}(1)$
m	7493.1	13342	$^4F_{9/2}(1)$ — $^6H_{9/2}$, $^6F_{11/2}(2)$
	7522.5	13290	$^4F_{9/2}(2)$ — $^6H_{9/2}$, $^6F_{11/2}(3)$
S	7531.9	13273	$^4F_{9/2}(1)$ — $^6H_{9/2}$, $^6F_{11/2}(3)$
w	7546.8	13247	$^4F_{9/2}(1)$ — $^6H_{9/2}$, $^6F_{11/2}(4)$
S	7562.4	13220	$^4F_{9/2}(1)$ — $^6H_{9/2}$, $^6F_{11/2}(5)$
m	7574.0	13199	$^4F_{9/2}(1)$ — $^6H_{9/2}$, $^6F_{11/2}(6)$
S	7586.8	13177	$^4F_{9/2}(1)$ — $^6H_{9/2}$, $^6F_{11/2}(7)$
m	7597.4	13159	$^4F_{9/2}(1)$ — $^6H_{9/2}$, $^6F_{11/2}(8)$
w	7620.2	13119	$^4F_{9/2}(2)$ — $^6H_{9/2}$, $^6F_{12/2}(9)$
w	7635.8	13093	$^4F_{9/2}(1)$ — $^6H_{9/2}$, $^6F_{11/2}(9)$
vw	7703.7	12977	$^4F_{9/2}(2)$ — $^6H_{9/2}$, $^6F_{11/2}(10)$
	7740.7	12915	$^4F_{9/2}(1)$ — $^6H_{9/2}$, $^6F_{11/2}(11)$

Notes to Table 6.9:

(a) 1, 2, 3 and 4 in parenthesis with $^4F_{9/2}$ stand for the Stark components at 21045, 21070, 21250 and 21285 cm^{-1} respectively.

(b) 1, 2, 3, 4, 5, 6, 7, 8, 9, 10 and 11 in parenthesis with $^6H_{9/2}$, $^6F_{11/2}$ stand for the proposed Stark components at 7608, 7703, 7776, 7798, 7824, 7847, 7869, 7886, 7952, 8094 and 8130 cm^{-1} respectively.

(c) The relative intensities listed are from the spectrum taken in the present work with 0.09% concentration of Dy^{3+} by weight in $CaF_2:Dy^{3+}$. The letters marked S, m, w and vw stand for strong, medium, weak and very weak intensities.

Table 6.10

Difference Matrix for the Transitions $^4F_{9/2} - {}^6H_{7/2}$, $^6F_{9/2}$

Relative Intensities in CaF_2 Dy^{3+} 0.09% by wt.	$^4F_{9/2}$ Stark Components / Observed Transitions in Cm^{-1}	$^4F_{9/2}(1)$	$^4F_{9/2}(2)$	$^4F_{9/2}(3)$	$^4F_{9/2}(4)$
		21045	21070	21250	21285
		← All in Cm^{-1} →			
m	12012	9032	9057	9237	9273
m	11959	9086	111	291	326
w	11929	9116	141	321	356
w	11868	9177	202	382	417
w	11758	9287	312	492	527
vw	11727	9318	343	523	558
vw	11650	9395	420	600	635
vw	11624	9421	446	626	661

* The letters m, w and vw stand for medium, weak and very weak intensities.

Table 6.11

Transition Assignments for the Fluorescence Group $^4F_{9/2} - {}^6H_{7/2}, {}^6F_{9/2}$

Relative Intensity	Present work		Transition Assignments[a,b]
	Å	cm^{-1}	
m	8322.4	12012	$^4F_{9/2}(1) - {}^6H_{7/2}, {}^6F_{9/2}(1)$
m	8359.6	11959	$^4F_{9/2}(1) - {}^6H_{7/2}, {}^6F_{9/2}(2)$
w	8380.3	11929	$^4F_{9/2}(1) - {}^6H_{7/2}, {}^6F_{9/2}(3)$
w	8423.9	11868	$^4F_{9/2}(1) - {}^6H_{7/2}, {}^6F_{9/2}(4)$
w	8502.5	11758	$^4F_{9/2}(1) - {}^6H_{7/2}, {}^6F_{9/2}(5)$
vw	8525.2	11727	$^4F_{9/2}(1) - {}^6H_{7/2}, {}^6F_{9/2}(6)$
vw	8581.2	11650	$^4F_{9/2}(1) - {}^6H_{7/2}, {}^6F_{9/2}(7)$
vw	8600.5	11624	$^4F_{9/2}(1) - {}^6H_{7/2}, {}^6F_{9/2}(8)$

Notes to Table 6.11:

(a) 1, 2, 3 and 4 in parenthesis with $^4F_{9/2}$ stand for the Stark levels at 21045, 21070, 21250 and 21285 cm^{-1} respectively.

(b) 1, 2, 3, 4, 5, 6, 7 and 8 in parenthesis with $^6H_{7/2}$, $^6F_{9/2}$ stand for the Stark levels at 9032, 9086, 9116, 9177, 9287, 9318, 9395 and 9421 cm^{-1} respectively.

(c) The relative intensities listed are from the spectrum taken in the present work with 0.09% concentration of Dy^{3+} by weight in $CaF_2:Dy^{3+}$. The letters m, w and vw stand for medium, weak and very weak intensities respectively.

wavenumbers of the system are given in Table 6.1. It is assumed that the transitions involved for this group would be $^4F_{9/2} - {}^6H_{7/2}$, $^6F_{9/2}$ as in the $LaF_3 : Dy^{3+}$ system. A difference matrix for the transitions observed is shown in Table 6.10 where a number of coincidences could be seen. However, following the results in the $LaF_3 : Dy^{3+}$, we suggest that 9032, 9086, 9116, 9177 , 9287, 9318, 9395 and 9421 cm^{-1} represent the positions of eight of the nine Stark components expected for the levels $^6H_{7/2}$ and $^6F_{9/2}$. The transitions involved are given in Table 6.11 and are also shown in Fig. 6.6.

6.9. Conclusion

Nitrogen laser excited fluorescence spectrum has been observed in $CaF_2 : Dy^{3+}$ in the region 4700-9000Å. The observed spectrum is mostly due to tetragonal centers. Fluorescence has been observed from two more Stark components at 21250 cm^{-1} and 21285 cm^{-1} of the level $^4F_{9/2}$ of Dy^{3+}. Three new groups of fluorescence transitions to the levels $^6H_{11/2}$, ($^6H_{9/2}$, $^6F_{11/2}$) and ($^6H_{7/2}$, $^6F_{9/2}$) have been observed. Tentative assignment of the Stark component positions of the levels $^6H_{11/2}$, ($^6H_{9/2}$, $^6F_{11/2}$) and ($^6H_{7/2}$, $^6F_{9/2}$) has been made.

REFERENCES

1. Rabbiner, N., - Phys. Rev. 132, 224 (1963).

2. Voron'ko Yu, K., Osiko, V.V., Udovenchik, V.T., and Fursikov, M.M. - Sov. Phys. Solid State 7, 204 (1965).

3. Kiss, Z.J., and Staebler, D.L. - Phys. Rev. Lett. 14, 691 (1965).

4. Merz, J.L., and Pershan, D.S. - Phys. Rev. 162, 217 (1967).

5. Luks, R.K., Saitkulov, I.G., and Stolov, A.L. - Sov. Phys. Solid State 11, 210 (1969).

6. Al'tshuler, N.S., Eremin, M.V., Luks, R.K., and Stolov, A.L. - Sov. Phys. Solid State, 11, 2921 (1970).

7. Nara, H., and Schlesinger, M. - Solid State Communications 9, 1247 (1971).

8. Fry, J.L., Caspers, H.H., Rast, J.E., Miller, S.A., and Freasier, B., - J. Chem. Phys. 48, 2342 (1968).

9. Dicke, G.H., and Singh, S. - J. Opt. Soc. Am. 46, 495 (1956).

10. Antipin, A.A., Davydova, M.P., Eremin, M.V., Luks, R.K., and Stolov, A.L. - Optics and Spectr. 33, 372 (1972).

11. Gilfanov, F.Z., Stolov, A.L., and Yakovleva, Zh.S. - Optics and Spectr. 24, 302 (1968).